Università degli Studi di Padova

Laurea Magistrale in Ingegneria Meccanica

Enrichment and Coupling of the Finite Element Method and Meshless Local Petrov Galerkin in Elastostatics

Laureando:
Andrea Zanette, 1035926

Relatori:
Ing. Massimiliano Ferronato
Ing. Carlo Janna

Università degli Studi di Padova

Department of Civil, Environmental and Architectural Engineering

February 2014 - July 2014

"Now we that are strong ought to bear the infirmities of the weak, and not to please ourselves."

Romans 15:1

The mathematical models in science and engineering mainly take the form of differential or integral equations. The rapid development of high speed computers, that nowadays appears to be unstoppable, has paved the way to the *simulation* of complicated systems, not otherwise possible. The basic idea in any numerical method for a differential equation is to discretize the given continuous problem with only finitely many unknowns, that can be solved using a computer. The *Finite Element Method* is currently the most popular and widely used method in structural engineering. The method is robust, well developed, and has lead an enormous impact on the scientific community. Nevertheless, in some problems it can suffer from the drawbacks associated with the use of meshes consisting of geometrically adjacent elements. Indeed, the problem of the mesh generation has become even more acute in recent years. Increased computational power has enabled scientists to tackle problems of increasing size and complexity. While computers have seen great advances, mesh generation has lagged behind. Many generation procedures often lack automation, requiring many man-hours, which are becoming far more expensive than computer hardware. In addition, they are are less reliable for complex geometry with sharp corners, concavity, or otherwise complex features. Since the application of computational methods to real world problems appears to be paced by mesh generation, alleviating this bottleneck can potentially impact several problems. To this aim, Meshless methods open a relatively new area of research, designed to help alleviate the burden of mesh generation. Despite their recent inception, there exists no shortage of formulations in the literature. Among the others, a Meshless scheme that attempts to entirely bypass the use of a conventional mesh, both for the interpolation of the unknown approximant and for the integration of the energy, is, for instance, the *Meshless Local Petrov Galerkin* method. The governing partial differential equations are discretized on scattered clouds of points, thus avoiding the need for any topologically connected data set. The price to pay is, however, the greater computational cost which reduces the range of practical applicability. While the relatively new Meshless procedures carry many other drawbacks, the Finite Element Method had gained, in the past, an impeccable reputation and it is therefore well trusted by practitioners. Eventually, a Meshless approach, which has however caught high academic consideration, has failed to replace the Finite Element Method as a general purpose tool for the solution of the differential equations in Elastostatics.

With an aim towards alleviating the need for remeshing, while still retaining the computational performance of the Finite Element Method, several authors have

already proposed to use a mixed Finite Elements and meshless interpolation. The goal is to emphasize the merit of each method: the Finite Element Method provides the bulk of the computational burden, while the particles, added a *posteriori*, enhance the solution, where it is deemed necessary. That is, as many particles as needed can be freely added in the computational domain, independently of the adjacent Finite Element mesh. Indeed, the proposed approach appears to be well suited for the following procedure:

- compute a solution by the use of the Finite Element Method,
- estimate the error a posteriori
- improve the solution by adding particles without any remeshing process.

Meshless methods, coupled with Finite Element Method, are ideal for such a procedure. Further, if the enriched region does not extend until the boundary of the computational domain, the impositions of the essential boundary conditions, which is otherwise not so straightforward, would be greatly simplified. In the present work, two types of enrichments, applied to an elastostatics problem, have been investigated. The first type, called *Fully Coupled Enrichment*, starts from a variational formulation of the elastostatics problem. The final discretized system of equations can be easily obtained as soon as both functional spaces, for FEM and MLPG trial functions, respectively, are considered together. It is quite intuitive that, by repeatedly increasing the dimension of the functional space, the solution can be greatly enhanced. In practice, the enrichment of the functional space is carried out without changing the underlying Finite Element mesh. Also, the two bases *interact* to provide a better solution, hence it is possible to think of the fully coupled enrichment as a *two-way* enrichment. A second, more versatile and less costly approach can be readily obtained by neglecting some terms in the final system of equations, hence obtaining the so called *Uncoupled Enrichment*. It will be shown that this is equivalent to having the elastostatics problem solved first and independently by, for instance, the Finite Element Method; and, at a second time, an a posteriori enrichment is carried out by solving a second problem, as small as the number of particles added. However, in the latter approach, the contribution of the Finite Element Method is not backwardly influenced and therefore the uncoupled enrichment may be considered as a *one-way* enrichment.

Contents

Acknowledgements

I ringraziamenti di questa Tesi iniziano con tre persone, Paola Enri e Gian. Abbiamo finito il Liceo insieme, ed insieme siamo scesi a Padova, per iniziare questa avventura universitaria. Memorabili quanto interminabili erano le briscole del primo anno. Con voi ho condiviso la maggior parte dei mercoledì padovani, andando alle varie feste, e creandole noi. I "Cocktail Parties" che seguivano con spensierata allegria i nostri compleanni non li potrò mai scordare. Abbiamo iniziato ad esploare i vari posti di Padova, e a conoscere nuove persone. Alle serate alla "Corte Sconta", ad un certo punto divenute fin quotidine, si é aggiunto Sandro, divenuto mio storico coinquilino di sempre, nonché preparato collega con cui affrontare le "scomode" difficoltà universitarie. Non é mai trascorsa una serata, nel nostro appartamento, che non fosse stata piena di allegria, e sei stato senza dubbio il miglior coinquilino di sempre (il cliente dell'Hotel Gerry non si offenda ora). Ringrazio nuovamente Paola ed Enri, a cui aggiungo Elisa, per avermi regalato la fiammante estate della libertà "da singles"; se fare presto voleva dire tornare alle cinque di notte, fare "davvero tardi" era sfiorare le quarantott'ore. Ringrazio anche gli altri miei amici del Liceo con cui sono stati condivisi bei momenti in questo periodo universitario, e in particolare "Fly". Un grazie anche a Giulia, per aver fatto apparire le feste ovunque camminavi, e per avermi salvato nella "foresta di Nottingham". Grazie anche ad Irene.

In questo periodo universitario ho avuto l'onore e la fortuna di essere uno studente del Prof. Ezio Stagnaro, che mi ha impartito i corsi di Algebra Lineare e Geometria, nonché di Algebra Commutativa (o Geometria Algebrica Affine). Il metodo d'indagine e ricerca che mi ha trasmesso non ha prezzo, e l'umiltà con cui si è posto ad insegnare, sempre facendo il "tifo" per noi studenti, hanno reso ancora più piacevole le Sue lezioni. Il Suo metodo di insegnamento dovrebbe essere di ispirazione per qualunque Istituizione di Didattica.

A questo punto sento di dover ringraziare F.M. Susin e sopratutto l'Ing. E. Benini, per aver supportato la mia applicazione al Von Karman Insitute for Fluid Dynamics. In this very diverse environment I meet the "two american folks", Shadeo Ramjatan and Daniel Hnatovic. You guys definitely made the atmosphere more lovely, and more lively. Daniel, you became my first "walk-around" friend, and we experienced fantastic adventures together. And thank you for constantly correcting me on my English. Sahaheo, your constant support and mindful suggestions were of great help to me, during my stay. We shared truly beautiful moments. I

have to thank you if I found myself involved, on the "professor side", in the VKI's Open-Day. This invaluable experience really went down in history. I will never forget our crazy "road-trips" ever. Many thanks to my advisor Lilla K. Koloszar and to my (maybe unofficial) supervisor Filip Ballien, for your great competence and ultimate patience. Bonetti and Resmini are also acknowledged.
E una volta tornato nel Bel Paese, questa periodo di Tesi, accompagnato dall' abbonamento ai Navigli; li, e alla Corte Sconta, e al Gozzi, e ai "weekend cosmopolita" a Lignano, e alle serate poker.. c'era sempre il Saggio, spalla universitaria ed extra-universitaria, mai mancata una volta. Hai più volte dimostrato di saperti fare carico di situazioni complicate e difficoltose, da vero fedele amico, ed instancabile supporter. Sei in cima alla mia lista delle persone su cui posso contare.
Tante altre persone mi hanno regalato bei momenti, tra cui mi sento di menzionare esplicitamente il Beli, Daiana, Carlo Emilio, Gamba, la Cugy, Alma, Chiara, e Serena.
Questi ringraziamenti giungono verso il termine passando per tre persone, Fandy, Debby, e Gerry. Fandy, dapprima mio collega, poi compagno di viaggio, quindi miglior amico. La tua profondità d'animo e di pensiero sono state illuminanti, nelle nostre giornate di "dialogo sopra i massimi sistemi", fornendomi preziosi consigli di vita.
Debby, dapprima mia collega, sempre hai fato il tifo per il tuo "bro", regalando saggi consigli "di mondo". Sei stata cara amica di "districazioni" universitarie e di mondane feste padovane, purtroppo bruscamente interrotte. Solo con una persona così speciale potevo sperare di superare tale difficoltà, riuscendo a rafforzare l'amicizia nostra più di prima.
Gerry, dapprima mio collega, poi divenuto il coinquilino "svanevole" che, da vero uomo di business, scese con la "ventiquattrore". Entrato a fare parte del mio mondo in un momento complesso, sei riuscito a svolgere un lavoro encomiabile. I consigli di una persona dotata di una così rara intelligenza umana illuminano e supportano in continuazione le mie decisioni, e sono per me fonte di stabilizzante certezza.
Queste tre persone sono entrate nella mia vita in occasioni allegre, in seguito hanno aggiunto molto con la loro profondità. Si sono sapute fare carico di situazioni spesso scomode, non lasciandosi trasportare dall'invidia, e fornendo un raro e prezioso aiuto concreto, rivelandosi valevoli punti di riferimento. A queste tre persone desidero dedicare questa Tesi, alle quali aggiungo mio Padre. Pronto a

fornire tutto l'aiuto di cui eri capace, hai fin troppo appoggiato ogni mia scelta; mentre mi hai lasciato la libertà di sbagliare responsabilmente, hai vegliato in silenzio sopra di me. Amico e compagno di avventure, l'essere la vera persona sui cui poter sempre contare per un aiuto concreto, ti rendono il Padre migliore del mondo. Grazie a tutta la mia famiglia, per esserci sempre stata in questi anni. Grazie Mamma per l'infinita pazienza; e alle due Nonne per i deliziosi manicaretti. E se anche questa Tesi giunge al suo termine, devo ringraziare il (now ex-) Department of Mathematical Models and Methods for Scientific Applications, un oasi felice in fatta di gente competente e preparata, che aggiunge umiltà ed allegria al lavoro quotidiano. Ringrazio in particolare il mio relatore Ing. Massimiliano Ferronato e co-relatore Ing. Carlo Janna, per avermi accettato nel vostro Dipartimento da "foresto meccanico", e per avermi proposto questa tanto ricercata Tesi di Laurea. Grazie per avermi dato la possibilità di affrontare questo argomento così affascinante, pieno di velleità matematiche; del quale argomento questa Tesi spero possa essere *an Introductory Survey*.

Dedicated to my three best friends,
Fandy, Debby, Gerry,
and ultimately to my Father

Chapter 1

A Theoretical Introduction

1.1 Elliptic PDE

This section outlines some theoretical results of the mathematical theory of numerical methods applied to an Elliptic PDE. The details, as well as the proofs, can be found in a mathematical text about Partial Differential Equations [14], [13].

Let $\mathcal{V}$ be a Hilbert space equipped with a scalar product[1] $(.,.)_{\mathcal{V}}$ and the corresponding euclidean norm[2] $||\cdot||_{\mathcal{V}}$. Let $a(.,.)$ be a bilinear form on $\mathcal{V}$ x $\mathcal{V}$ and L_f a linear form on $\mathcal{V}$ such that:

- $a(.,.)$ is *continuous*, i.e. $\exists \gamma > 0$ such that $\forall v, w \in \mathcal{V}$

$$|a(v,w)| \leq \gamma \, ||v||_{\mathcal{V}} ||u||_{\mathcal{V}}$$

- $a(.,.)$ is $\mathcal{V}$-*elliptic*, i.e. $\exists \alpha > 0$ such that $\forall v \in \mathcal{V}$

$$|a(v,w)| \geq \alpha \, ||v||^2_{\mathcal{V}}$$

- $L_f(v)$ is *continuous*, i.e. $\exists \beta > 0$ such that $\forall v \in \mathcal{V}$

$$|L_f(v)| \leq \beta \, ||v||_{\mathcal{V}}$$

[1] $(f,g) = \int_\Omega f(x)g(x)dx$
[2] $||f|| = (f,f) = \int_\Omega f^2(x)dx$

It is possible to prove [14] that the general variational problem (V): Find $v \in \mathcal{V}$ such that

$$a(u, v) \;=\; L_f(v)$$

has a *unique* solution $v^{sol} \in \mathcal{V}$.

It is also possible to prove [14] that when $a(.,.)$ is *symmetric* there exists an associated minimization problem. In the present Thesis, which relies on the Petrov-Galerkin procedure, $a(.,.)$ is non symmetric; hence a weighted residual variational formulation is used, with no associated minimization problem.
Let $\mathcal{V}_h$ be a *finite*-dimensional subspace of $\mathcal{V}$ of size n and let $(\phi_1, \ldots, \phi_n)$ be a basis for $\mathcal{V}_h$ so that *any* $v \in \mathcal{V}^h \subset \mathcal{V}$ has the unique representation

$$v = \sum_i \phi_i u_i$$

where $u_i \in \mathbb{R}$.
It is possible to formulate the discrete analog for the variational problem (V), namely: Find $u_h \in \mathcal{V}_h$ such that

$$a(u_h, v) \;=\; L_f(v), \quad \forall v \in \mathcal{V}$$

Further restricting the test function space to $\mathcal{V}_t^h$ leads to:

$$a(u_h, v_i) \;=\; L_f(v_i), \quad \forall v_i \in \mathcal{V}_t^h$$

It can be proved [14] that this is equivalent to set:

$$a(u_h, v_i) \;=\; L_f(v_i), \quad \forall v_i \in \{v_1, \ldots, v_n\}$$

where $\{v_1, \ldots, v_n\}$ is a basis of $\mathcal{V}_t^h$. Substitution of $v = \sum_i \phi_i \widehat{u}_i$ leads to:

$$\sum_j a\big(\phi_j, v_i\big)\widehat{u}_j \;=\; L_f(v_i)$$

which can conveniently be expressed in matrix form

$$\mathbf{K} \cdot \widehat{\mathbf{u}} \;=\; \mathbf{b} \tag{1.1}$$

If the problem is well posed, system 1.1 has a *unique* solution [14]. It is also possible

to prove [14] that the matrix $\mathbf{K}$ is symmetric and positive definite if $v_i \equiv \phi_i, \ \forall i$, that is, test and shape function are chosen to be the same for each node. This is usually the case for the Finite Element Method, but not that of Meshless Local Petrov Galerkin method.

1.2 The Theoretical Formulation of the Enrichment

This section provides a theoretical variational formulation of the enrichment of the Finite Element Method by the use of a Meshless technique. The formulation will later be developed for solving an elastostatics problem. It is noted that the only difference with respect to the standard Galerkin formulation, presented in the foregoing section, is that a distinction here is operated between the two functional spaces, while writing both the variational problem and the analog discrete problem.

Further, the idea of the uncoupled enrichment is introduced, with the aim at an even simpler and less costly alternative to enhance the solution. Moreover, if the enrichment is done in the interior of the computational domain, the prescription of the essential and the natural boundary conditions would be greatly simplified, as they have to be enforced only on FE in a strong way. A fictitious zero value is imposed at the boundary of the enriched region in this case to ensure compatibility. Further, as many particles as needed can be added where they are deemed necessary thus avoiding the burden of remeshing. The situation is more complex, if the enriched region crosses the boundary, as it is not easy to prescribe the essential boundary conditions in non-interpolating schemes. This will be addressed in the relevant section of the Thesis.

Now it will be outlined how it is possible to enhance the solution, either after the Finite Element Method problem has been solved, or at the same time, by enriching the functional space. Both methods will be fully developed throughout this Thesis, showing how the former approach can be easily obtained by neglecting some terms of the general equations.

Let $\mathcal{V}(\Omega)$ be an Hilbert space as before. The variational problem (V):

$$a(u, v) = L(v), \quad \forall v \in \mathcal{V}$$

can be written in the analog discrete form, i.e., by restricting the problem to the finite space $\mathcal{V}^h$. Now let $\mathcal{V}^h_{FE}$ be the finite element space for the trial function, and $\mathcal{V}^h_{ML}$ that of the Meshless trial function; let

$$\{\phi^{FE}_1, \ldots, \phi^{FE}_{n_{FE}}\} \quad \text{be a basis of} \quad \mathcal{V}^h_{FE}$$

$$\{\phi^{ML}_1, \ldots, \phi^{ML}_{n_{ML}}\} \quad \text{be a basis of} \quad \mathcal{V}^h_{ML}$$

If $\mathcal{V}^h_{FE} \cap \mathcal{V}^h_{ML} = \{\emptyset\}$ then it is easily seen that

$$\{\phi^{FE}_1, \ldots, \phi^{FE}_{n_{FE}}, \phi^{ML}_1, \ldots, \phi^{ML}_{n_{ML}}\} \quad \text{is a basis of} \quad \mathcal{V}^h = \mathcal{V}^h_{FE} \cup \mathcal{V}^h_{ML}$$

Hence,

$$\forall u^h \in \mathcal{V}^h, \quad u^h = \sum_i^n \phi^h u_i = \sum_i^{n_{FE}} \phi^{FE}_i u^{FE}_i + \sum_i^{n_{ML}} \phi^{ML}_i u^{ML}_i$$

where

$$\mathcal{V}^h = \mathcal{V}^h_{FE} + \mathcal{V}^h_{ML}$$

and also

$$u^{ML}_i, u^{FE}_i \in \mathbb{R}$$

are uniquely determined by u^h. According to a standard nomenclature, u^h will be called the *unknown approximant*.

The fictitious values u^{FE} and u^{ML} can be obtained by solving the discrete analog of the variational formulation by the convenient use of the basis of the functional space:

$$a(u^h, v) = L(v), \quad \forall v \in \mathcal{V}, \quad u^h \in \mathcal{V}^h$$

that is, by selecting appropriate test functions. For the Finite Element Method, they are such that

$$\mathcal{V}^{test}_{FE} = \mathcal{V}^h_{FE}$$

The MLPG test functions will belong to a different space that will be defined later

$$< v_i >= \mathcal{V}^{test}_{ML} \neq \mathcal{V}^h_{ML}$$

Now let

$$\{v_{1_{ML}}, \ldots, v_{n_{ML}}\} \quad \text{be a basis for} \quad \mathcal{V}^{test}_{ML}$$

Assuming that $\mathcal{V}_{FE}^{trial} \cap \mathcal{V}_{ML}^{trial} = \{\emptyset\}$ we restrict the space $\mathcal{V}$ for the test function:

$$\mathcal{V}^{test} = \mathcal{V}_{FE}^{test} + \mathcal{V}_{ML}^{test}$$

Finally the final system of discretized equations can be obtained:

$$\begin{cases} \sum_j^{n_{FE}} a(\phi_j^{FE}, v_i^{FE}) u_j^{FE} + \sum_j^{n_{FE}} a(\phi_j^{ML}, v_i^{FE}) u_j^{ML} & = L_{FE}(v_i^{FE}) \quad \forall i = 1, \dots, n_{FE} \\ \sum_j^{n_{ML}} a(\phi_j^{FE}, v_i^{ML}) u_j^{FE} + \sum_j^{n_{ML}} a(\phi_j^{ML}, v_i^{ML}) u_j^{ML} & = L_{ML}(v_i^{ML}) \quad \forall i = 1, \dots, n_{ML} \end{cases}$$

Note that the test functions originate from both the sets in standard FEM and MLPG. The finite element test functions are set to be the same as the respective shape functions, that is the traditional Ritz-Galerkin approach. On the contrary Meshless methods instead use a different space; other choices are of course possible but will not be investigated in the present Thesis. In a more compact notation it is possible to write the discretized problem as a system of equations:

$$\begin{cases} \mathbf{K}_{FE}\mathbf{u}_{FE} + \mathbf{K}_{MF}\mathbf{u}_{ML} & = \mathbf{b}_{FE} \\ \mathbf{K}_{FM}\mathbf{u}_{FE} + \mathbf{K}_{ML}\mathbf{u}_{ML} & = \mathbf{b}_{ML} \end{cases} \tag{1.2}$$

or equivalently:

$$\begin{bmatrix} \mathbf{K}_{FE} & \mathbf{K}_{MF} \\ \mathbf{K}_{FM} & \mathbf{K}_{ML} \end{bmatrix} \cdot \begin{bmatrix} \mathbf{u}_{FE} \\ \mathbf{u}_{ML} \end{bmatrix} = \begin{bmatrix} \mathbf{b}_{FE} \\ \mathbf{b}_{ML} \end{bmatrix}$$

where $\mathbf{K}_{FE}$ and $\mathbf{K}_{ML}$ are the FE and MLPG stiffness matrices, respectively, $\mathbf{K}_{FM}$ and $\mathbf{K}_{MF}$ the two coupling blocks; $\mathbf{b}_{FE}$ and $\mathbf{b}_{ML}$ are the forcing vectors, if any. Note that the integration domain can be restricted to a domain where both the trial and the test function are non vanishing.

In the most general formulations, both $\mathbf{K}_{FE}$ and $\mathbf{K}_{ML}$ blocks needs to be computed. However, $\mathbf{K}_{MF}$ or[3] $\mathbf{K}_{FM}$ blocks can be neglected. Indeed, neglecting the $\mathbf{K}_{MF}$ block or $\mathbf{K}_{FM}$ gives rise to the so called *uncoupled enrichment*. The system of equations now reads, in the first case:

$$\begin{bmatrix} \mathbf{K}_{FE} & \mathbf{0} \\ \mathbf{K}_{FM} & \mathbf{K}_{ML} \end{bmatrix} \cdot \begin{bmatrix} \mathbf{u}_{FE} \\ \mathbf{u}_{ML} \end{bmatrix} = \begin{bmatrix} \mathbf{b}_{FE} \\ \mathbf{b}_{ML} \end{bmatrix}$$

[3] this depends on the actual way in which boundary conditions are enforced, i.e., the size of the enriched region

or equivalently:

$$\begin{cases} \mathbf{K}_{FE}\mathbf{u}_{FE} & = \mathbf{b}_{FE} \\ \mathbf{K}_{FM}\mathbf{u}_{FE} + \mathbf{K}_{ML}\mathbf{u}_{ML} & = \mathbf{b}_{ML} \end{cases} \tag{1.3}$$

which can be seen as a two-step problem in which the FEM problem

$$\mathbf{K}_{FE}\mathbf{u}_{FE} = \mathbf{b}_{FE}$$

is solved first, and the MLPG, at second step, solves

$$\mathbf{K}_{ML}\mathbf{u}_{ML} = \mathbf{b}_{ML} - \mathbf{K}_{MF}\mathbf{u}_{FE}$$

where

$$\mathbf{K}_{MF}\mathbf{u}_{FE} = \sum_{j}^{n_{ML}} a(\phi_j^{FE}, v_i^{ML})u_j^{FE}$$

is the discrete analogs of

$$a(u^{FE}, v), \quad \forall v \in \mathcal{V}$$

Compared to the fully coupled enrichment, this approach has the following advantages:

- the computational overhead is less than that of a fully coupled procedure, since the problem is solved via a multistep algorithm
- the solver can take advantage of the symmetric positive definiteness of $\mathbf{K}_{FE}$
- a further refinement on the MLPG can be quickly accomplished, since only a small linear system $\mathbf{K}_{ML}\mathbf{u}_{ML} = \mathbf{b}_{ML} - \mathbf{K}_{MF}\mathbf{u}_{FE}$ has to be solved, while $\mathbf{K}_{FE}\mathbf{u}_{FE} = \mathbf{b}_{FE}$, that can be huge, is solved once and for all

Conversely, the method can be expected to suffer from the following disadvantages:

- the derived quantities are poorly represented

- the accuracy of the method is generally lower then that of the fully coupled enrichment

The last chapter will deal with numerical result and should give reason of the previous statements.

1.3 The Meshless Local Petrov Galerkin Discrete Functional Space $\mathcal{V}_{ML}^h$ for the Trial Functions

The Meshless shape functions, as used in the Meshless Local Petrov Galerkin formulation, typically exhibit quite a complex behavior, hence this section aims at showing how MLPG shape functions can be obtained. This section briefly introduces the *Least Squares Approximation* (LS), which is at the basis of further generalizations. This can be extended in order to obtain the *Weighted Least Squares Approximation* (WLSA) and hence the *Moving Least Squares Approximation* (MLS) methods used in MLPG. The basic linear systems of equations will be obtained for the global least squares, and the weighted, local least squares approximation of function values from scattered data. Bt scattered data we mean any arbitrary set of points in $\mathbb{R}^n$ which carring scalar quantities (i.e. a scalar field in n dimensional space), although this can be easily extended to the vector quantities actually used in the case of elastostatics. In contrast to the global nature of the least-squares fit, the weighted, local approximation is computed either at discrete points, or continuously over the parameter domain, resulting in the global WLS or in the local MLS approximation, respectively.

1.3.1 The Least Square

The moving least square approximation is the most basic non interpolating scheme and will be introduced in this Thesis only because it is the founding idea for the MLS method.
Consider N points located at positions x_i in $\mathbb{R}^n$. The aim is to obtain a function $f(x)$ that approximates the given scalar values f_i at points x_i in the least-squares

sense, that is, minimizing the functional

$$\mathcal{J}_{LS} = \sum ||f(x_i) - f_i||^2$$

where f is an arbitrary function that depends on some parameters. Those parameters are the values that minimize the functional written above. In this Thesis, f will be taken from the space of m-degree polynomials.
The generic polynomial can be written as $f(x) = \mathbf{b}(\mathbf{x})^T\mathbf{a}$, where $\mathbf{b}(\mathbf{x}) = [b_1(\mathbf{x}), ..., b_n(\mathbf{x})]^T$ is the polynomial basis vector and $\mathbf{a} = [a_1, ..., a_n]^T \in \mathbb{R}^n$ is the vector of coefficients that minimize the functional. It is anticipated that only a linear[4] basis will be employed in the MLPG formulation of the present Thesis, that is $\mathbf{b} = [1, x, y]^T$, yielding to three unknowns $\mathbf{a} = [a_0, a_x, a_y]$.
The functional can be minimized by setting the partial derivatives $\mathcal{J}_{LS}$ to zero, $\nabla\mathcal{J}_{LS} = 0$ where $\nabla = [\partial/\partial a_1, ..., \partial/\partial a_n]^T$.
This simple idea serves as the basis for the more refined MLS method. By taking partial derivatives with respect to the unknown coefficients $a_1, ..., a_n$, a linear system of equations is obtained. In matrix-vector notation, this can be written as

$$\sum_i 2\mathbf{b}(\mathbf{x}_i)[\mathbf{b}(\mathbf{x}_i)^T\mathbf{a} - f_i] =$$

$$2\sum_i [\mathbf{b}(\mathbf{x}_i)\mathbf{b}(\mathbf{x}_i)^T\mathbf{a} - \mathbf{b}(\mathbf{x}_i)f_i] = 0.$$

Dividing by 2 and rearranging we have

$$\sum_i \mathbf{b}(\mathbf{x}_i)\mathbf{b}(\mathbf{x}_i)^T\mathbf{a} = \sum_i \mathbf{b}(\mathbf{x}_i)f_i$$

which is solved as

$$\mathbf{a} = \sum_i \Big([\mathbf{b}(\mathbf{x}_i)\mathbf{b}(\mathbf{x}_i)^T]\Big)^{-1} \sum_i \mathbf{b}(\mathbf{x}_i)f_i.$$

If the square matrix

$$\sum_i [\mathbf{b}(\mathbf{x}_i)\mathbf{b}(\mathbf{x}_i)^T]$$

is nonsingular, the last equation provides the desired solution.

[4] for each direction, the problem being two-dimensional, i.e., $\mathbf{x} \in \mathbb{R}^2$

1.3.2 The Weighted Least Square

Now consider the weighted least squares formulation, of which the LS approach is a particular case. Consider the error functional

$$\mathcal{J}_{WLS} = \sum_i w\big(||\overline{\mathbf{x}} - \mathbf{x}_i||\big)||f(\mathbf{x}_i) - f_i||^2$$

for a *fixed* point $\overline{\mathbf{x}} \in \mathbb{R}^n$. This functional is similar to LS, only that now the error is weighted by $w(d_i)$ where d_i are the Euclidiean distances between $\overline{\mathbf{x}}$ and the positions of data points $\mathbf{x}_i$. Here it is remarked again that the minimization is done with respect to a point $\overline{\mathbf{x}}$ fixed in the space, and thus different choices of such a point will generally result in different minimizing parameters. The minimization process is nearly the same as the one shown before for LS, that is, by taking the partial derivatives with respect to the unknown coefficients:

$$\sum_i 2w(d_i)\mathbf{b}(\mathbf{x}_i)[\mathbf{b}(\mathbf{x}_i)^T\mathbf{a} - f_i] =$$

$$2\sum_i [w(d_i)\mathbf{b}(\mathbf{x}_i)\mathbf{b}(\mathbf{x}_i)^T\mathbf{a} - w(d_i)\mathbf{b}(\mathbf{x}_i)f_i] = 0.$$

Dividing by 2 and rearranging we obtain:

$$\sum_i w(d_i)\mathbf{b}(\mathbf{x}_i)\mathbf{b}(\mathbf{x}_i)^T\mathbf{a} = \sum_i w(d_i)\mathbf{b}(\mathbf{x}_i)f_i$$

which is solved as

$$\mathbf{a} = \sum_i \Big([w(d_i)\mathbf{b}(\mathbf{x}_i)\mathbf{b}(\mathbf{x}_i)^T]\Big)^{-1} \sum_i w(d_i)\mathbf{b}(\mathbf{x}_i)f_i.$$

The only difference with respect to LS is the presence of the weighting terms. Also, note that, for a fixed $\overline{\mathbf{x}}$, the coefficients are *constant* when evaluating f throughout the domain. Hence, if $\mathbf{b}(\mathbf{x})$ is a polynomial of degree m, f is still a polynomial of degree at most m. Note also, that the coefficients $\mathbf{a}$ in WLS are *local*, as they have to be recomputed for every $\overline{\mathbf{x}}$.

1.3.3 The Moving Least Square

Originally advanced for smoothing and interpolating data, the Moving Least Square method is recognized as a stable and accurate method for approximating scattered data [2]. The idea is to start with a weighted least squares formulation for an arbitrary fixed point $\overline{\mathbf{x}} \in \mathbb{R}^n$, and then *move* this point over the entire domain where the function f is evaluated. In other words, a weighted least squares fit is computed and evaluated for each point $\mathbf{x} = \overline{\mathbf{x}}$ where $f(\mathbf{x})$ is computed individually. It can be shown that the global function $f(\mathbf{x})$, is continuously differentiable if and only if the weighting functions are continuously differentiable. So instead of constructing the global approximation, a local polynomial fit is performed and evaluated continuously over the entire domain Ω, resulting in the MLS fit function. Note that, in contrast to the functions f obtained before, now f is (generally) no longer a polynomial if $\mathbf{b}(\mathbf{x})$ is a polynomial. It is intuitive that varying the weight function can directly influence the approximating nature of the MLS fit function, so attention must be paid to its accurate selection. Since MLPG relies on this approximating technique, it is easy to envision that the proper selection of the shape and size[5] of the weighting functions is far from being straightforward, and can significantly affect the results. This can be seen as a slight loss in generality of the approximation method as compared to LS, because the user has to make a wise choice of such weighting functions. Therefore, this can be an advantage, since the *behaviour* of MLS can be tweaked for the particular application, but, on the other side, a wrong choice may lead to poor results.
One might expect that also MLPG, which relies on this technique, and hence the coupling approach between FEM and MLPG, will share this feature.
Now the MLS approximation will be obtained in a suitable form for MLPG. In a similar fashion as LS and WLS, the purpose is to minimize some norm. However, it is possible to deliberately let the unknown coefficients $\mathbf{a}$ of the unknown trial function

$$u^h(\mathbf{x}) = \mathbf{a}(\overline{\mathbf{x}})^T \mathbf{b}(\mathbf{x})$$

vary as $\mathbf{x}$ is moved through the domain. In other words, when trying to compute $f(\mathbf{x}) = a(\overline{\mathbf{x}})^T b(\mathbf{x})$, a minimization is done in the WLS fashion *with respect to* $\mathbf{x}$, i.e., by setting $\overline{\mathbf{x}} = \mathbf{x}$, if one wants to retain the previous typeset. Again, when computing $f(\tilde{\mathbf{x}})$ with $\tilde{\mathbf{x}} \neq \mathbf{x}$ the MLS scheme requests that the unknown minimizing coefficients *be recalculated* again by minimizing the norm at $\tilde{\mathbf{x}}$. This is a much

[5] size here refers to the size of the domain where $w_i(x)$ does not vanish

more expensive approach, as the final system of equations for the approximation must be solved for *each* point $\mathbf{x} \in \Omega$. It might be expected that this adds a considerable overhead to the calculation of the shape functions in MLPG, and indeed this is very much what happens.

After this introduction, consider, with a notation that will be used later in MLPG, a sub-domain Ω_i, which is defined as the neighborhood of a point $\mathbf{x}_i$. This is denoted as the *domain of definition* of the MLS approximation for the trial function at $\mathbf{x}$, and is located in the problem domain Ω.

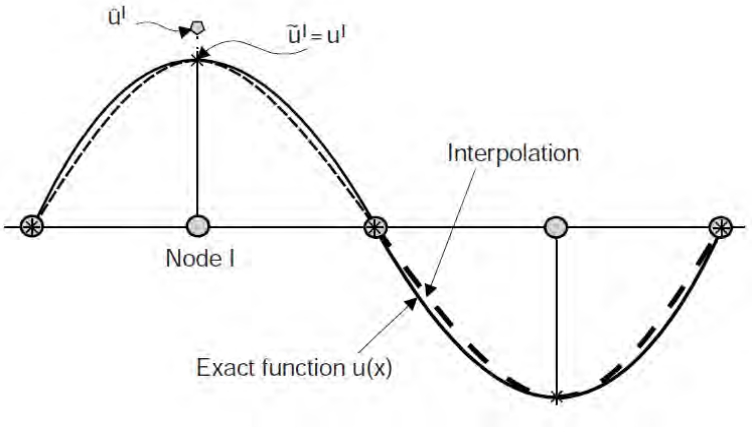

FIGURE 1.1: The MLPG approximation.

To *approximate* the distribution of the function u, over a number of randomly located nodes $\{\mathbf{x}_i |\ \mathbf{x}_i \in \Omega\}$, $i = 1, 2, ..., N$ the moving least squares approximant $u^h(\mathbf{x})$ of u, $\forall \mathbf{x} \in \Omega$, can be calculated, by minimizing

$$\mathcal{J}_{MLS} = \sum_i w\left(||\overline{\mathbf{x}} - \mathbf{x}_i||\right) \cdot \left(u^h_{\overline{\mathbf{x}}}(\mathbf{x}) - u_i^{fict}\right)^2$$

with $\overline{\mathbf{x}} = \mathbf{x}$, that is:

$$\mathcal{J}_{MLS} = \sum_i w\left(||\mathbf{x} - \mathbf{x}_i||\right) \cdot \left(\mathbf{b}(\mathbf{x})^T \mathbf{a}(\mathbf{x}) - u_i^{fict}\right)^2 =$$

which, in matrix form reads:

$$= \left[\mathbf{P} \cdot \mathbf{a}(x) - \mathbf{u}^{fict}\right]^T \cdot \mathbf{W} \cdot \left[\mathbf{P} \cdot \mathbf{a}(x) - \mathbf{u}^{fict}\right]$$

where,

$$\mathbf{P} \;=\; \left[\begin{array}{c} \mathbf{b}_1^T(\mathbf{x}) \\ \mathbf{b}_2^T(\mathbf{x}) \\ \ldots \\ \mathbf{b}_n^T(\mathbf{x}) \end{array}\right]_{n\,\mathrm{x}\,m} \qquad \mathbf{W} \;=\; \left[\begin{array}{ccc} w_1(\mathbf{x}) & \ldots & 0 \\ \ldots & \ldots & \ldots \\ 0 & \ldots & w_n(\mathbf{x}) \end{array}\right]_{n\,\mathrm{x}\,m}$$

and,

$$\mathbf{u}^{fict} \;=\; \left[u_1^{fict},\; u_2^{fict},\; \ldots,\; u_n^{fict}\right]$$

Here it should be noted that u_i^{fict} are the fictitious nodal values, and not the nodal values of the unknown trial function $u^h(\mathbf{x})$.
The stationarity of $\mathcal{J}_{MLS}$ with respect to the *function* $\mathbf{a}(\mathbf{x})$ leads to the following linear relation:

$$\frac{\partial \mathcal{J}_{MLS}}{\partial \mathbf{a}} = 2 \cdot \left[\mathbf{P} \cdot \mathbf{a}(\mathbf{x}) - \mathbf{u}^{fict}\right]^T \cdot \mathbf{W} \;=\; \mathbf{0}$$

or equivalently,

$$2 \cdot \sum_i w_i(||\mathbf{x} - \mathbf{x}_i||) \cdot \mathbf{p}(\mathbf{x}) \left(\mathbf{b}(\mathbf{x})^T \mathbf{a}(\mathbf{x}) - \mathbf{u}_i\right) = \mathbf{0}$$

Rearranging:

$$\underbrace{\sum_i \left(w_i(||\mathbf{x} - \mathbf{x}_i||) \cdot \mathbf{b}(\mathbf{x}_i)\,\mathbf{b}(\mathbf{x}_i)^T\right)}_{\mathbf{A}(\mathbf{x})} \mathbf{a}(\mathbf{x}) \;=\; \underbrace{\sum_i w_i(||\mathbf{x} - \mathbf{x}_i||)\,\mathbf{b}(\mathbf{x}_i)\,\mathbf{u}_i^{fict}}_{\mathbf{B}(\mathbf{x}) \cdot \mathbf{u}^{fict}} \tag{1.4}$$

with:

$$\mathbf{A}(\mathbf{x}) = \sum_i \left(w_i(||\mathbf{x} - \mathbf{x}_i||) \cdot \mathbf{b}(\mathbf{x}_i)\,\mathbf{b}(\mathbf{x}_i)^T\right) = \mathbf{P}^T\mathbf{W}\mathbf{P}$$

$$\mathbf{B}(\mathbf{x}) = \sum_i w_i(||\mathbf{x} - \mathbf{x}_i||)\,\mathbf{b}(\mathbf{x}_i)\,\mathbf{u}_i^{fict} = \mathbf{P}^T\mathbf{W}$$

The system 1.4 can be easily solved by inverting $\mathbf{A}(\mathbf{x})$, i.e.:

$$\mathbf{a}(\mathbf{x}) = \mathbf{A}^{-1}(\mathbf{x})\mathbf{B}(\mathbf{x})\mathbf{u}^{fict}$$

More explicitly:

$$\mathbf{a}\left(\mathbf{x}\right) = \underbrace{\sum_i \left(w_i\left(||\mathbf{x}-\mathbf{x}_i||\right)\cdot \mathbf{b}\left(\mathbf{x}_i\right)\mathbf{b}\left(\mathbf{x}_i\right)^T\right)^{-1}}_{\mathbf{A}(\mathbf{x})^{-1}} \underbrace{\sum_i w_i\left(||\mathbf{x}-\mathbf{x}_i||\right)\mathbf{b}\left(\mathbf{x}_i\right)\mathbf{u}_i^{fict}}_{\mathbf{B}(\mathbf{x})\cdot\mathbf{u}^{fict}}$$

Note that this expression is very similar to the WS obtained before, with the only difference that the weight function is chosen to be different for each interpolating node and its value varies as $\mathbf{x}$ moves in the domain. Hence $\mathbf{A}^{-1}(\mathbf{x})$ and $\mathbf{B}(\mathbf{x})$ will depend on $\mathbf{x}$ and ultimately $\mathbf{a} = \mathbf{a}(\mathbf{x})$.

Substitution of $\mathbf{a}$ into the original form of the unknown approximant $\mathbf{a}(\mathbf{x})^T\mathbf{b}(\mathbf{x})$ yields to:

$$u^h(\mathbf{x}) = \mathbf{b}(\mathbf{x})^T\mathbf{a}(\mathbf{x}) =$$

$$= \mathbf{b}^T(\mathbf{x}) \cdot \underbrace{\left(\sum_i \left(w_i\left(||\mathbf{x}-\mathbf{x}_i||\right)\cdot \mathbf{p}\left(\mathbf{x}_i\right)\mathbf{p}\left(\mathbf{x}_i\right)^T\right)^{-1} \sum_i w_i\left(||\mathbf{x}-\mathbf{x}_i||\right)\mathbf{p}\left(\mathbf{x}_i\right)\mathbf{u}_i^{fict}\right)}_{\mathbf{a}(\mathbf{x})}$$

or alternatively:

$$u^h(\mathbf{x}) = \mathbf{b}(\mathbf{x})^T\mathbf{a}(\mathbf{x}) = \mathbf{b}(\mathbf{x})\mathbf{A}(\mathbf{x})^{-1}\mathbf{B}(\mathbf{x})\mathbf{u}^{fict}$$

that gives a relation which may be written in the form of a linear combination of basis fucntions

$$\mathbf{u}^h(\mathbf{x}) = \mathbf{\Phi}(\mathbf{x})^T\mathbf{u}^{fict} = \sum_i \phi_i(\mathbf{x})u_i^{fict}$$

where $\mathbf{\Phi}^T$ reads:

$$\mathbf{\Phi}^T = \mathbf{b}(\mathbf{x})\mathbf{A}(\mathbf{x})^{-1}\mathbf{B}(\mathbf{x})$$

For a single node, the basis function Φ_I reads

$$\phi_I = \mathbf{b}^T(\mathbf{x}) \cdot \left(\sum_J \left(w_J \left(||\mathbf{x} - \mathbf{x}_J|| \right) \cdot \mathbf{p}\left(\mathbf{x}_J\right) \mathbf{p}\left(\mathbf{x}_J\right)^T \right)^{-1} w_I \left(||\mathbf{x} - \mathbf{x}_I|| \right) \mathbf{p}\left(\mathbf{x}_I\right) \right)$$

Note that the computation of ϕ_I for each sample point leads to the inversion of the matrix $\mathbf{A}(\mathbf{x})$. Thus, the MLS approximation is well defined only when the matrix $\mathbf{A}(\mathbf{x})$, which is a 3 x 3 matrix in this case, is non-singular. It can be seen that this is the case if and only if at least 3 non aligned nodes with non vanishing weight functions are non-zero at the point $\mathbf{x}$ under consideration. However, should the value of some of the respective weight functions be numerically small, the resulting matrix would be *numerically* close to being singular. Indeed, three conditions must be satisfied *at the same time* for at least three nodes:

- they have to be non-aligned
- their weight function has to be non vanishing
- their weight function has to be non numerically small

The last condition in fact implies the second, and should be interpreted with common sense. Note, that in general it is not required to perform any of these checks, as the weight functions have their radius big enough in order for the MLPG to deliver accurate results. In practice, checking that the three conditions above are satisfied is hardly ever requested. Also, it is seen that $\mathbf{A}(\mathbf{x})$ is ill-conditioned when the points are "clustered" together far from the origin; thus it is convenient to work in a local coordinate system normalized with respect to a significant size parameter; this can indeed be the size of the support of the nodal point, i.e., where w_I is non vanishing, as described below.
The support of each nodal point is usually taken to be a circle, centered at the node under consideration. The fact that the weight function is zero for any point not in the support of the nodal point I preserves the local character of the Moving Least Squares approximation, and ultimately will make the MLPG efficient, sparsifying

the resulting stiffness matrix. The smoothness of the shape functions is determined by that of the basis functions and of the weight functions. Here the basis functions are $\in C^{\infty}(\Omega)$, but the gaussian weight functions, which are the common and recommended choice, are, in general, not even $\in C^{1}(\Omega)$. The Gaussian weight function reads:

$$w_I(\mathbf{x}) = \begin{cases} \frac{e^{-\left(\frac{d}{c}\right)^2} - e^{-\left(\frac{r}{c}\right)^2}}{1 - e^{-\left(\frac{r}{c}\right)^2}} & \text{d} < \text{r} \\ 0 & \text{d} > \text{r} \end{cases}$$

where d is the usual euclidean distance, r is the user specified radius and c another user specified parameter to control the shape of the weight function. It can be seen that the derivative of the weight function is discontinuous where the analytical law changes, that is, at $d = r$. Note that this is a *radial function*, $w = w(d)$, and can be obtained by shifting the standard gaussian e^{-x^2} by $e^{-\left(\frac{r}{c}\right)^2}$ and normalizing it by $1 - e^{-\left(\frac{r}{c}\right)^2}$. Then, when $d > r$ simply set $w(\mathbf{x}) = w(r) = 0$ and this choice explains why w is non differentiable at $||\mathbf{x}|| = r$. In practice, however, to obtain a higher order of continuity a ratio of $\frac{r}{c} = 4$ is employed and, as a result, the function in Figure 1.2 is close to being differentiable[6]. Lower values of this ratio will not be able to attain the desired level of continuity, and, conversely, higher values will pose a major problem when integrating the shape function because it too rapidly vanishes inside its domain of definition. As a matter of fact, a ratio of $\frac{r}{c} = 4$ for the weight function in the shape function and $\frac{r}{c} = 1$ for the test function, which is chosen to be the weight function, is advised in MLPG, and are implicitly assumed in the numerical results. Changing these values even slightly can cause the accuracy of the method to deteriorate in some specific situations. This clearly points to a limitation of MLPG.

It is anticipated that the finite space of the trial function for MLPG, $\mathcal{V}^h_{ML}$ will be chosen such that:

$$\mathcal{V}^h_{ML} =< \phi_1, \ldots, \phi_n >$$

which is another way of saying $u^h(\mathbf{x}) = \sum_i \phi_i(\mathbf{x}) u_i^{fict}$.

It is seen that ϕ_I are linearly independent and thus form a basis of $\mathcal{V}^h_{ML}$.

[6] meaning that the a directional derivative of w at $x = r$ approaches 10^{-6} when $r = 1$

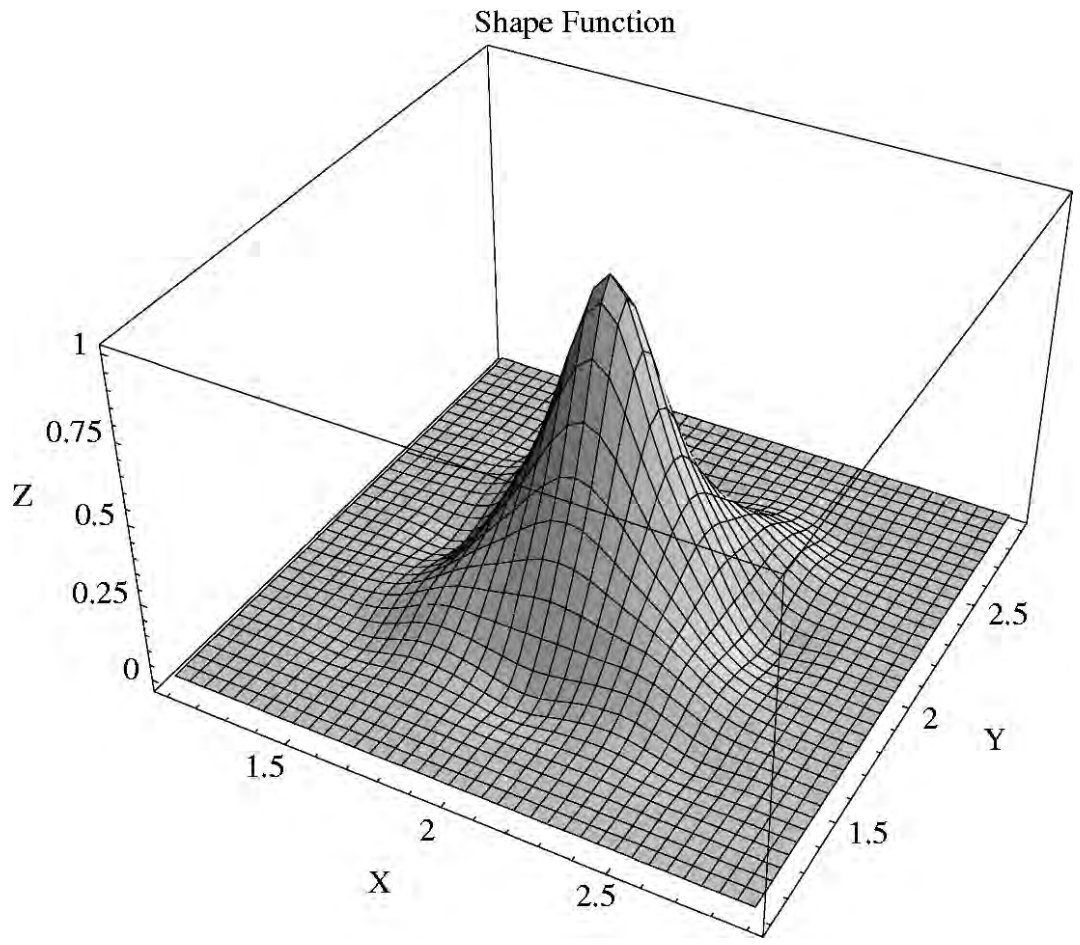

FIGURE 1.2: A Shape Function of the space $\mathcal{V}^h_{ML}$

Chapter 2

Enrichment Applied to the Elastostatic Problem

This chapter provides the bulk of the theory for a successful enrichment of the Finite Element Method with MLPG. The general framework developed in the present Thesis will be specified for FE and MLPG. The equations needed for coupling the two methods stems directly from the general approach, as soon as both functional spaces $\mathcal{V}_{FE}$, $\mathcal{V}_{ML}$ for FEM and MLPG, respectively, are considered together.

2.1 A Local Approach

In a conventional Galerkin Finite Element formulation, the *global* weak form is used to solve the boundary value problem numerically. However, the MLPG method starts from a *local* weak form.
In order to retain a common working approach while coupling both methods, the present development starts, as done by Atluri in MLPG [16], [8], from a local sub-domain, or a patch, $\{\Omega^I_{test}\}$ inside the global domain Ω. The final form of the equations will be developed sharing this starting point, and the differences between FEM and MLPG will be pointed out as they arise. Moreover, the final system of equations, encompassing the so called *coupling blocks*, will arise naturally from the calculations.

2.1.1 Global Domain Decomposition

Let $\{\Omega^I_{test}\}$ be a set of overlapping patches, which cover the global domain Ω, where $I(= 1, 2, \ldots, N)$ indicates any node, and N is the total number of nodes of both MLPG and FE. The concept of nodes with local domains is implicitly introduced, which is at the basis of the MLPG formulation; the FE local domain is then nothing but a particular choice of Ω^I_{test}. The sub-domain Ω^I_{test} is thus called the *local domain* of node I. In the present Thesis, the sub-domain Ω^I_{test} is taken to be a circle in the MLPG formulation and a polygon[1] surrounding node I in the FE, but, in its full generality, it can be a rectangle, a polygonal shape or an ellipse in two dimensions, and it can be extended to any kind of geometry **??**

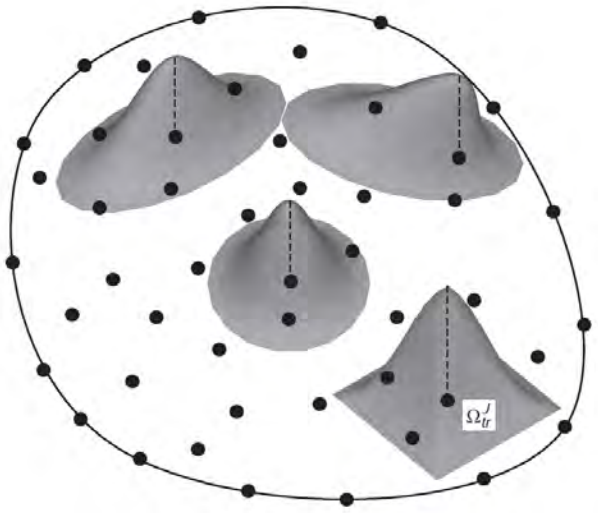

FIGURE 2.1: Some possible domains for the trial function along with some shape functions.

2.2 The Differential Problem of Elastostatics

The aim of this Thesis is to solve the well known *differential problem* (D) of elastostatics, in two dimensions:

$$\begin{cases} \vec{\nabla} \cdot \boldsymbol{\sigma} + \vec{b} = \vec{0}, & \vec{x} \in \Omega \\ \vec{u} = \underline{\vec{u}} & \vec{x} \in \partial\Omega \end{cases}$$

[1] which is in turn partitioned in each of the (non degenerate) triangles that share node I. This arises naturally in the creation of the mesh

where $\boldsymbol{\sigma}$ is the *stress* tensor, $\vec{\underline{u}}$ the prescribed boundary conditions, and $\vec{b}$ the distributed load, namely:

$$\boldsymbol{\sigma} = \begin{bmatrix} \sigma_{xx} & \sigma_{xy} \\ \sigma_{yx} & \sigma_{yy} \end{bmatrix}, \quad \vec{b} = \begin{bmatrix} b_x \\ b_y \end{bmatrix}$$

and $\vec{\nabla}$ the usual differential operator. Note that $\sigma_{xy} = \sigma_{yx}$ will be requested in the formulation; this follows theoretically by imposing angular momentum equilibrium, at the differential level. The solution $\vec{u}$, in terms of displacement, belongs to a generic (functional) space $\mathcal{V}$, that will be specified later. In repeated index notation, the differential problem above reads[2]:

$$\sigma_{ij} + b_i \quad i = 1, 2$$

where the summation is carried out over j.

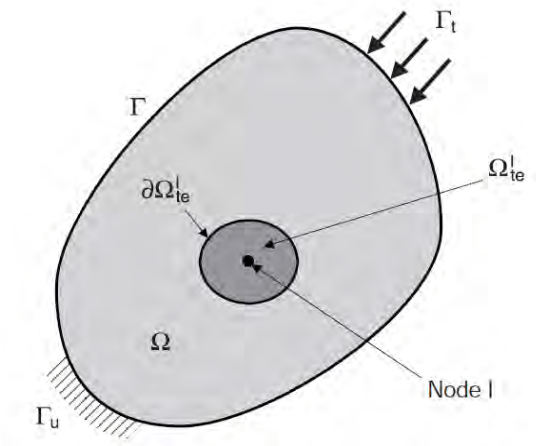

FIGURE 2.2: The Global and the Local Domain.

2.3 The Variational Formulation

It is possible to write a *variational formulation* (V) of the differential problem (D) written above, for the *local subdomain*, which, in matrix form reads:

[2]Note that i and j here do not represent the nodes I and J

$$\int_{\Omega_{test}} (\vec{\nabla} \cdot \boldsymbol{\sigma} + \vec{b})\, V d\Omega - \alpha \int_{\Gamma_{Dir}} (\vec{u} - \underline{\vec{u}})\, V d\Gamma = 0$$

where Γ^I_{Dir} is the intersection of the physical boundary Γ_{Dir} and the boundary $\partial\Omega^I_{test}$; $\underline{\vec{u}}$ is the prescribed displacement, if any[3], α is a penalty parameter to impose the essential boundary conditions discussed later, and V is the *test function* matrix that reads $V = \begin{bmatrix} V_1 & V_2 \\ V_3 & V_4 \end{bmatrix}$.

Note that the equation written above is in vector form, i.e., it comprises two scalar equations. Thus, two sets of independent test functions have to be chosen. Since the test functions can be chosen arbitrarily, the simplest selection would be $V = \begin{bmatrix} v & 0 \\ 0 & v \end{bmatrix}$. This choice simplifies the final form of the equations.

If the sub-domain Ω^I_{test} is located entirely within the global domain Ω, and there is no intersection between the local boundary $\partial\Omega^I_{test}$ and the global boundary Γ, the boundary integral over Γ vanishes.

Applying the following vector calculus identity $(v_i\sigma_{ij})_{,j} = v_{i,j}\sigma_{ij} + v_i\sigma_{ij,j}$ to each of the two scalar equations yields:

$$\int_{\Omega^I_{test}} (\sigma_{ij}v_i)_{,j}\, d\Omega - \int_{\Omega^I_{test}} (\sigma_{ij}v_{i,j} - b_i v_i) d\Omega - \alpha \int_{\Gamma^I_{Dir}} (u_i - \underline{u_i}) v_i d\Gamma = 0$$

Using the divergence theorem, the following *weak form* of the variational problem is obtained:

$$\int_{\partial\Omega^I_{test}} (\sigma_{ij}n_j v_i) d\Omega - \int_{\Omega^I_{test}} (\sigma_{ij}v_{i,j} - b_i v_i) d\Omega - \alpha \int_{\Gamma^I_{Dir}} (u_i - \underline{u_i}) v_i d\Gamma = 0 \qquad (2.1)$$

where $[n_1, n_2]^T$ is the outward unit normal to the boundary $\partial\Omega^I_{test}$. This will be referred to as *the* variational problem in any part of this Thesis. Note, indeed, that any solution of the differential problem (D), from which (V) originates, is also a solution of the last variational formulation (V); the converse, in general, is not true, as some more *regularity* requirements must be carried out in order to

[3] generally speaking, I can be an interior node so no boundary conditions are specified on its domain

satisfy (D).
It is noted that the use of the foregoing expression for one node (and hence for one local domain) will yield two linear equations of u, i.e., for u_x and u_y separately.

2.3.1 The Petrov-Galerkin Method

In the following development, the Petrov-Galerkin method is used. The Petrov-Galerkin Method is used whenever a selection of similar functional space for test function and solution function is not possible. In the original MLPG as proposed by Atluri [16], [8], the test function and the solution function approximations cannot be identical, hence they must be approximated separately. Since the problem loses symmetry, the final coefficient matrix is also not symmetric. This somehow complicates the underlying mathematical theory [9] to show existence and uniqueness of the solution, and from a numerical viewpoint, the solver selection must be made carefully, as the computational cost for solving the final system of equations increases due to the missing symmetry. In view of this consideration, the FEM approximation can be considered as a particular selection of the two functional spaces, which are in fact the same. This has many advantages, but since the proposed methodology involves a combination of *both* FEM and MLPG variational formulations, only the more general Petrov-Galerkin method will be considered in the present elastostatics problem.

2.3.2 A theoretical constraint on the set of subdomains $\{\Omega^I_{trial}\}$

It is worth noting that the test functions need not vanish on the boundary of the domain Ω where the essential boundary conditions are specified. In particular, all the points of the boundaries need to be covered by at least one local subdomain Ω^I_{test}, in order to prescribe the essential or natural boundary conditions. Again, this stems from the more general demand that *any* point in the whole domain should be covered by at least one local subdomain Ω^I_{test}. Theoretically, as long as the union of all local domains covers the global domain, the equilibrium equation and the boundary conditions will be satisfied in the global domain Ω and over its boundary Γ, respectively. This somewhat natural request is automatically satisfied in finite elements, as the domain is *partitioned* during the creation of the mesh.

The meshless local domains, conversely, do not form any domain partition. In case that the local subdomains are not big enough as to leave no points uncovered, error in the solution process are to be expected. It is not difficult to envision some of the situations where an ordinary selection of the local subdomain dimensions (e.g., a circle with a radius equal to the closest node) does not create a patch Ω^I_{test} such that $\Omega \supseteq \bigcup_I \Omega^I_{test} \subseteq \Omega$. This is a drawback of the MLPG scheme, which leaves to the user the crucial task of ensuring that Ω^I_{test} is such that $\Omega \supseteq \bigcup_I \Omega^I_{test} \subseteq \Omega$ which is rather difficult to check during runtime, and can easily go unnoticed by the user.

2.3.3 Simplification of the above equations and Functional Space $\mathcal{V}$

The functional space $\mathcal{V}$ from which the test and trial functions can be chosen, before discretization, has not been specified yet.
In order to simplify equation 2.1, a selection is operated on the test functions v such that they vanish over $\partial\Omega^I_{test}$, except when they intersect with the global boundary Γ, that is, $\partial\Omega^I_{test} \cap \Omega \neq \{\varnothing\}$. This can be easily accomplished in both the MLPG and FE methods by using the test function whose value at the local boundary is zero, as long as $\partial\Omega^I_{test}$ does not intersect with Γ. Outside Ω^I_{test} their value is zero, to preserve the locality of the method. Separating each contribution at the boundary yields to:

$$\int_{\partial\Gamma^I_{Dir}} (\sigma_{ij} n_j v_i) d\Omega + \int_{\partial\Gamma^I_{Neu}} (\sigma_{ij} n_j v_i) d\Omega - \int_{\Omega^I_{test}} (\sigma_{ij} v_{i,j} - b_i v_i) d\Omega - \alpha \int_{\Gamma^I_{Dir}} (u_i - \underline{u_i}) v_i d\Gamma = 0$$

since now

$$\int_{\partial\Omega^I} (\sigma_{ij} n_j v_i) d\Omega = 0$$

was requested.

Rearranging:

$$\int_{\Omega^I_{test}} \sigma_{ij} v_{i,j} d\Omega \; + \; \alpha \int_{\Gamma^I_{Dir}} u_i v_i d\Gamma \; + \int_{\partial\Gamma^I_{Dir}} (\sigma_{ij} n_j v_i) d\Omega \;\; =$$

$$= \alpha \int_{\Gamma^I_{Dir}} \underline{u_i} v_i d\Gamma + \int_{\partial\Gamma^I_{Neu}} (\sigma_{ij} n_j v_i) d\Omega + \int_{\Omega^I_{test}} b_i v_i d\Omega$$

What is left unsaid from before is the space[4] $\mathcal{V}$, where the test and trial functions originate. This is beyond the scope of this Thesis. However, it is mentioned that the space must allow at the very least to "write down" these equations. Therefore, one should require that the derivatives of functions in this space are *square integrable*. Now, there is actually a Hilbert space $H^1_0(\Omega)$ of functions with weak derivatives in $L^2(\Omega)$, with appropriate boundary conditions, which fulfills this purpose. Hence, it is possible to routinely verify the hypothesis presented in the more theoretical introduction of this Thesis, to show existence and uniqueness of the solution [14].

The vector notation in now exploited with the application of the two independent test functions $v_x = v_y = v$ for each node I, to obtain:

$$\int_{\Omega_s} \boldsymbol{\epsilon}_{\mathbf{v}} \boldsymbol{\sigma} \, d\Omega + \alpha \int_{\Gamma_{Dir}} \mathbf{Vu} \, d\Gamma - \int_{\Gamma_{Dir}} \mathbf{Vt} \, d\Gamma = \alpha \int_{\Gamma_{Dir}} \mathbf{Vu} \, d\Gamma + \int_{\Gamma_{Neu}} \mathbf{Vt} \, d\Gamma + \int_{\Omega_s} \mathbf{Vb} \, d\Omega \tag{2.2}$$

where

$$\boldsymbol{\sigma} = [\sigma_{xx}, \sigma_{yy}, \sigma_{xy}]^T,$$

$$\boldsymbol{\epsilon}_{\mathbf{v}} = \begin{bmatrix} v_{x,x} & 0 & v_{y,x} \\ 0 & v_{y,y} & v_{x,y} \end{bmatrix} = \begin{bmatrix} v_{,x} & 0 & v_{,x} \\ 0 & v_{,y} & v_{,y} \end{bmatrix}$$

$$\mathbf{V} = \begin{bmatrix} v_x & 0 \\ 0 & v_y \end{bmatrix} = \begin{bmatrix} v & 0 \\ 0 & v \end{bmatrix}$$

which can be verified to be nothing but the previous expression, written conveniently for a generic node I in matrix form.

2.4 Discretization and Constitutive Law

Now consider the final form of the equation 2.2 and *restrict* the functional space of the solution $\mathcal{V}$ to it subset $\mathcal{V}^h$. The space of the test function is restricted, too.

[4] before discretization

The forms the trial and test functions, respectively, can be written as, for both FEM and MLPG:

$$\mathbf{u}^h(\mathbf{x}) = \sum_J \phi_J(\mathbf{x})\widehat{\mathbf{u}}_J$$

$$\mathbf{v}^h(\mathbf{x}) = \sum_I \psi_I(\mathbf{x})\widehat{\mathbf{v}}_I$$

where

$$\psi_I(\mathbf{x}) \in \mathcal{V}^{test}$$

$$\phi_J(\mathbf{x}) \in \mathcal{V}^{trial}$$

Further consider that ϕ_J, ψ_I are zero everywhere but in their domain of definition and this "allows" one to call ϕ_J, ψ_I the *nodal shape functions* for trial and test functions centered at nodes J and I. In general, $\widehat{\mathbf{u}}_J$, $\widehat{\mathbf{v}}_I \in \mathbb{R}^2$ consist of two fictitious nodal values, in 2D, that is, one for each dimension. Substitution of this equation into the last form of the variational principle leads to the following discretized system of linear equation:

$$\sum_J^N \int_{\Omega_s} \boldsymbol{\epsilon}_I(\mathbf{x})\,\mathbf{D}\mathbf{B}_J\widehat{\mathbf{u}}_J\,d\Omega + \alpha \sum_J^N \int_{\Gamma_{Dir}} \mathbf{V}_I(\mathbf{x})\,\mathbf{S}\Phi_J\widehat{\mathbf{u}}_J\,d\Gamma - \sum_J^N \int_{\Gamma_{Dir}} \mathbf{V}_I(\mathbf{x})\,\mathbf{NDSB}_J\widehat{\mathbf{u}}_J\,d\Gamma$$
$$= \int_{\Gamma_{Neu}} \mathbf{V}_I(\mathbf{x})\,\mathbf{t}\,d\Gamma + \alpha \int_{\Gamma_{Dir}} \mathbf{V}_I(\mathbf{x})\,\mathbf{S}\overline{\mathbf{u}}\,d\Gamma + \int_{\Omega_s} \mathbf{V}_I(\mathbf{x})\,\mathbf{b}\,d\Omega \qquad (2.3)$$

where

$$\mathbf{N} = \begin{bmatrix} n_1 & 0 & n_2 \\ 0 & n_2 & n_1 \end{bmatrix}$$

$$\mathbf{B}_J = \begin{bmatrix} \phi_{J,1} & 0 \\ 0 & \phi_{J,2} \\ \phi_{j,2} & \phi_{J,1} \end{bmatrix}$$

$$\mathbf{D} = \frac{\overline{E}}{1-\overline{\nu}^2} \begin{bmatrix} 1 & \overline{\nu} & 0 \\ \overline{\nu} & 1 & 0 \\ 0 & 0 & \frac{(1-\overline{\nu})}{2} \end{bmatrix}$$

$$\mathbf{V} = \begin{bmatrix} v_1 & 0 \\ 0 & v_2 \end{bmatrix} = \begin{bmatrix} v & 0 \\ 0 & v \end{bmatrix}$$

$$\overline{E} = \begin{cases} E & \text{for plane stress} \\ \frac{E}{1-\nu^2} & \text{for plane strain} \end{cases}$$

$$\overline{\nu} = \begin{cases} \nu & \text{for plane stress} \\ \frac{\nu}{1-\nu} & \text{for plane strain} \end{cases}$$

$$\mathbf{S} = \begin{bmatrix} S_1 & 0 \\ 0 & S_2 \end{bmatrix}$$

$$S_i = \begin{cases} 1 & \text{if } u_i \text{ is prescribed on } \Gamma \\ 0 & \text{if } u_i \text{ is not prescribed on } \Gamma \end{cases}$$

In the above equations, $[n_1, n_2]^T$ is the normal vector at the boundary, and E and ν are the Young modulus and Poisson's ratio, respectively. The local symmetric weak form makes the "stiffness" entries $\mathbf{K}^{IJ}$, which is the local stiffness 2x2 matrix, in the entry corresponding to the node I, and to the nodes J, in the multidimensional matrix $\mathcal{K}$; the global stiffness matrix $\mathcal{K}$ is such that $\mathcal{K}_{IJ} = [\mathbf{K}^{IJ}]$, that is, each entry in the global stiffness matrix is a 2 x 2 local stiffness matrix. The pattern of the non zero entries in $\mathcal{K}$ depends on the non-zero values of the integrands in the weak form, where $\partial\Omega^I_{test} \cap \partial\Omega^J_{trial} \supsetneq \{\emptyset\}$.
The locality of the methods ensure that $\mathcal{K}$ is sparse, and in general its sparsity will be largely affected by the radii of the shape and trial functions in MLPG, and on the respective sizes of triangles and meshless local subdomains and domains of definition, in the coupling blocks described later, which form the global stiffness matrix. Conversely, FEM does not come with such "user selectable" parameters that affect the sparsity of the global stiffness matrix.
Now, the global equation can be written as:

$$\sum_I \mathbf{K}_{IJ} \cdot \widehat{\mathbf{u}} = \mathbf{f}_I, \quad I = 1, \ldots, N$$

which is a multidimensional matrix that comprises $2 \cdot I$ number of equations, where

$$\mathbf{K}_{IJ} = \int_{\Omega_s} \boldsymbol{\epsilon}_I(\mathbf{x})\,\mathbf{DB}_J\,d\Omega \;+\; \alpha \int_{\Gamma_{Dir}} \mathbf{V}_I(\mathbf{x})\,\mathbf{S}\Phi_J\,d\Gamma \;-\; \int_{\Gamma_{Dir}} \mathbf{V}_I(\mathbf{x})\,\mathbf{NDSB}_J\,d\Gamma$$

$$\mathbf{f}_I = \int_{\Gamma_{Neu}} \mathbf{V}_I(\mathbf{x})\,\mathbf{t}\,d\Gamma \;+\; \alpha \int_{\Gamma_{Dir}} \mathbf{V}_I(\mathbf{x})\,\mathbf{S}\overline{\mathbf{u}}\,d\Gamma \;+\; \int_{\Omega_s} \mathbf{V}_I(\mathbf{x})\,\mathbf{b}\,d\Omega$$

Finally

$$\boldsymbol{\mathcal{K}}\cdot\widehat{\boldsymbol{u}} \;=\; \boldsymbol{f}$$

can be rewritten as a conventional $2N$ x $2N$ linear system to solve.

2.4.1 The choice of the sizes of the domain Ω^I_{test} and Ω^I_{trial}

Before making the final selection of the finite functional spaces $\mathcal{V}^h_{FE}$, $\mathcal{V}^h_{ML}$, a consideration about the local domains for the respective bases, and their nature, should be beneficial. The generation of the global stiffness matrix shares some similarities with the well known Galerkin FEM, and also some differences. The Petrov-Galerkin formulation enables us to use different interpolations for trial and test functions. Hence, the sizes and shapes of the sub-domains, i.e., the supports Ω^I_{test} and Ω^I_{trial} where the test and trial functions, respectively, are nonzero, need not be the same, both in size or in shape. Indeed this is the most frequent case in MLPG, where $\Omega^I_{test} \subset \Omega^I_{trial}$ to achieve proper results. Therefore, this approach encompasses the standard FEM as a particular case, where $\Omega^I_{test} = \Omega^I_{trial}$.
Now a selection of the actual domain shape must be performed. Following the approach done by Atluri [16], [8], the domains of definition for both the test and trial function will be chosen as circles for MLPG; Finite Element Method shall adopt the set of all the elements which share the node in question, which form a polygon in 2D. Note that the value of the trial function $u(x)$ at each point x inside Ω^I_{test} is influenced by a set of fictitious values (Figure **??**), since, in both methods, $u(x) = \sum_i \phi_i(x) u_i$. This is determined, in FE, by the nodes of the triangle where x lies. Indeed $u(x)$ is obtained by a *linear interpolation*, if the bases are linear, which considerably simplifies the reconstruction of the solution. Indeed the displacements of the nodal points are already contained in the solution vector that

stems from the solver, when Finite Elements are considered separately, as the previous equations simplifies to $u(x_I) = 1 \cdot u_I$. However in a meshless approach even the reconstruction of the solution at the nodal points involves some calculations, as $u(x) = \sum_i \phi_i(x) u_i$ does not simplify altogether. Indeed, the shape function of a node, which is not vanishing at a point x, is determined, for instance, by the radius of the weight functions in the MLS approximation, i.e., Ω^I_{trial} of the nodes in the immediate vicinity (Figure 2.3)

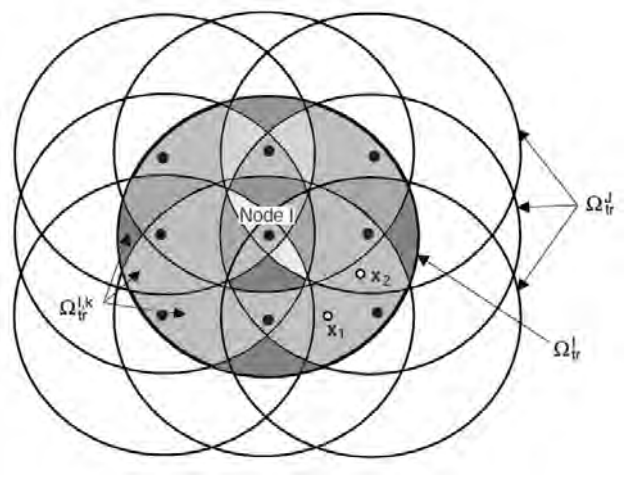

FIGURE 2.3: MLPG shape functions "covering" a node in a local subdomain.

In its full generality, when both bases are considered together, the local symmetric weak form leads, for each Ω^I_{test} to the I-th system of equations in the final stiffness matrix, involving all the J nodes, whose sub-domains Ω^J_{trial} intersect with Ω^I_{test} such that the integrand in the equation is non-zero, irrespective of their nature[5]. It is seen that if the sizes[6] of Ω^I_{test} and Ω^J_{trial} are the same (Figure **??**) for each I and J, the resulting stiffness matrix shall be *structurally symmetric*, in other words, the topology of the possible non-zero entries is symmetric.

Indeed, the (I, J) entry, in the final stiffness matrix, can be non zero as soon as $\Omega^I_{test} \cap \Omega^J_{trial} \neq \{\emptyset\}$, which in turn implies $\Omega^J_{trial} \cap \Omega^I_{test} = \Omega^J_{test} \cap \Omega^I_{trial} \neq \{\emptyset\}$, that is a necessary conditions for the (J, I) entry to be non-zero. Note that this selection of subdomain is natural in the Finite Element Method framework, but unfortunately will lead to poor solution accuracy if employed in the MLPG scheme.
Further, if the trial and test functions centered at node I and J are the *same* for each I and J, the global stiffness matrix will be *symmetric* according to the

[5] here no distinction is operated between FEM and MLPG
[6] the shape being the very same

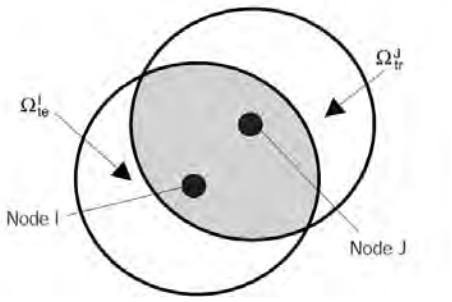

FIGURE 2.4: A selection of the domain for the trial and test function that leads to a structurally symmetric matrix

usual definition $\mathcal{K}^T = \mathcal{K}$; otherwise not. Note again, this is somewhat natural with Finite Elements (Figure **??**), and gives rise to the well known *Ritz - Galerkin* approach.

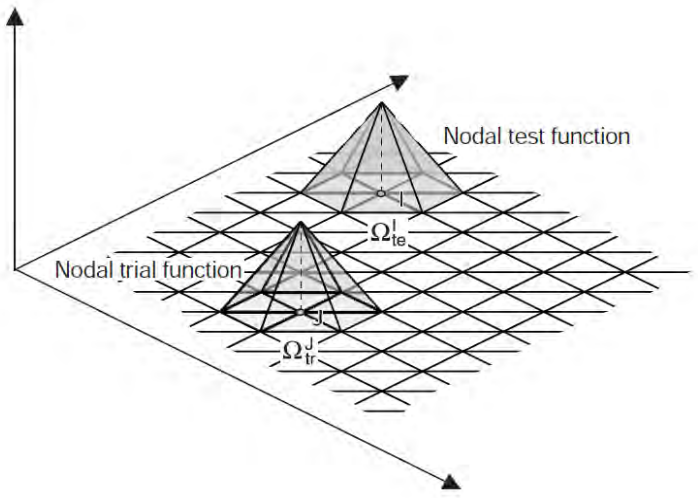

FIGURE 2.5: A selection of the domain for the trial and test function, that leads to a symmetric matrix, as commonly done in FEM

This choice, that has many interesting properties, also greatly simplifies the solution of the linear system of equation, but may never be used by MLPG as proposed by Atluri in its original form [16], as the test and trial function are always chosen to be *different*. Hence the coupling blocks $\mathbf{K}_{FM}$ and $\mathbf{K}_{MF}$ will also be *not mutually symmetric*, and not even (mutually) structurally symmetric. Having the full system of equations, with both FE and MLPG, with a non symmetry due to the use of MLPG, will demand for a unsymmetric algorithm for the solution of the linear system; should a partially coupled approach be employed as discussed later,

a multistep algorithm may be used, and the FEM and MLPG problems can be solved sequentially, hence, in independent phases.

2.4.2 Final selection of the Functional Spaces $\mathcal{V}^h_{FE}$, $\mathcal{V}^h_{ML}$

Now the final selection of the finite functional space $\mathcal{V}^h_{FE}$, $\mathcal{V}^h_{ML}$ is operated. By taking full advantage of the topology, the choice that leads to the well known Finite Element Method is operated, i.e., choosing

$$\mathbf{u}^h_{FE}(\mathbf{x}) \;=\; \sum_{J=1}^{n_{FE}} \phi^{FE}_J(\mathbf{x})\widehat{\mathbf{u}}^{FE}_J$$

such that ϕ^{FE} is *piecewise linear*, i.e., linear over each element, with the additional constraint that, for each of the n_{FE} nodes:

$$\begin{cases} \phi^{FE}_J(\mathbf{x}_J) & = 1 \\ \phi^{FE}_J(\mathbf{x}_M) & = 0, \quad \forall M \neq J \end{cases}$$

Further, for the FEM test function

$$\psi^{FE}_I = \phi^{FE}_I$$

and hence $\mathcal{V}^{test}_{FE} \;=\; \mathcal{V}^{trial}_{ML}$. This approach is well renowned in literature and further considerations are not deemed necessary.

Conversely, for MLPG, as done by Atluri in [16], [8],

$$\mathbf{u}^h_{ML}(\mathbf{x}) \;=\; \sum_{J} \phi^{ML}_J(\mathbf{x})\widehat{\mathbf{u}}^{ML}_J$$

where $\phi^{ML}_J(\mathbf{x})$ stems from the minimization of the functional

$$\mathcal{J}_{MLS} \;=\; \sum_i w\left(||\overline{\mathbf{x}} - \mathbf{x}_i||\right) \cdot \left(\mathbf{u}^h_{\overline{\mathbf{x}}}(\mathbf{x}) - \mathbf{u}_i\right)^2$$

already discussed in detail, and for the test functions:

$$v_1 = v_2 = w_i(\mathbf{x}) \;=\; \begin{cases} \frac{e^{(\frac{d}{c})^2} - e^{-(\frac{r}{c})^2}}{1 - e^{-(\frac{r}{c})^2}} & d < r \\ 0 & d > r \end{cases}$$

by imposing $r/c = 1$ as already discussed, resulting in $\mathcal{V}_{ML}^{test} \neq \mathcal{V}_{ML}^{trial}$.

Here it is noted that the shape functions, for FE and MLPG, when considered separately, form a basis of $\mathcal{V}_{ML}^{trial}$ and $\mathcal{V}_{FE}^{trial}$, respectively. When considered together,

$$\mathcal{V}_{FE}^{trial} + \mathcal{V}_{ML}^{trial} = \mathcal{V}^h$$

but in general

$$\mathcal{V}_{FE}^{trial} \oplus \mathcal{V}_{ML}^{trial} = \mathcal{V}^h$$

is *not* true. That the global space $\mathcal{V}^h$ cannot be a *direct sum* [12] of $\mathcal{V}_{FE}^{trial}$ and $\mathcal{V}_{ML}^{trial}$ is equivalent to saying

$$\{\phi_1^{FE}, \ldots, \phi_{n_{FE}}^{FE}, \phi_1^{ML}, \ldots, \phi_{n_{ML}}^{ML}\}$$

does not form a basis for $\mathcal{V}^h$, in the most general case. Indeed it may be shown that a linear field may not be represented uniquely by the use of the above set of shape functions, which however span $\mathcal{V}^h$. Hence the consideration done in the more theoretical introduction regarding the uniqueness of the solution of the system of equations here no longer applies, and the final linear system may admit infinitely many solutions; while in fact the solution in $\mathcal{V}^h$ is unique. In general, it may be necessary to suppress as many shape functions as required to recover the uniqueness of the representability of a generic element in the vector space, in order to have a non singular final matrix. However, other methods are also possible and are addressed in the relevant section of this Thesis.

2.5 Discretized Block Matrices

In view of the distinction made between the test and trial basis functions, it is possible to re-write the final discretized form of the equations as done in the

theoretical introduction:

$$\begin{bmatrix} \mathbf{K}_{FE} & \mathbf{K}_{MF} \\ \mathbf{K}_{FM} & \mathbf{K}_{ML} \end{bmatrix} \cdot \begin{bmatrix} \mathbf{u}_{FE} \\ \mathbf{u}_{ML} \end{bmatrix} = \begin{bmatrix} \mathbf{f}_{FE} \\ \mathbf{f}_{ML} \end{bmatrix}$$

where the global stiffness matrix is

$$\mathcal{K} = \begin{bmatrix} \mathbf{K}_{FE} & \mathbf{K}_{MF} \\ \mathbf{K}_{FM} & \mathbf{K}_{ML} \end{bmatrix}$$

and the forcing vector:

$$\boldsymbol{f} = \begin{bmatrix} \mathbf{f}_{FE} \\ \mathbf{f}_{ML} \end{bmatrix}$$

where now, the local stiffness matrix reads:

$$\mathbf{K}_{IJ}^{FE} = \sum_{J}^{N} \int_{\Omega_I^{FE}} \boldsymbol{\epsilon}_I^{FE}(\mathbf{x})\, \mathbf{DB}_J^{FE}\, d\Omega \;+\; \alpha \sum_{J}^{N} \int_{\Gamma_{Dir}} \mathbf{V}_I^{FE}(\mathbf{x})\, \mathbf{S}\Phi_J^{FE}\, d\Gamma + - \sum_{J}^{N} \int_{\Gamma_{Dir}} \mathbf{V}_I^{FE}(\mathbf{x})\, \mathbf{NDSB}_J^{FE}\, d\Gamma$$

$$\mathbf{K}_{IJ}^{MF} = \sum_{J}^{N} \int_{\Omega_I^{FE}} \boldsymbol{\epsilon}_I^{FE}(\mathbf{x})\, \mathbf{DB}_J^{ML}\, d\Omega \;+\; \alpha \sum_{J}^{N} \int_{\Gamma_{Dir}} \mathbf{V}_I^{FE}(\mathbf{x})\, \mathbf{S}\Phi_J^{ML}\, d\Gamma + - \sum_{J}^{N} \int_{\Gamma_{Dir}} \mathbf{V}_I^{FE}(\mathbf{x})\, \mathbf{NDSB}_J^{ML}\, d\Gamma$$

$$\mathbf{K}_{IJ}^{FM} = \sum_{J}^{N} \int_{\Omega_I^{ML}} \boldsymbol{\epsilon}_I^{ML}(\mathbf{x})\, \mathbf{DB}_J^{FE}\, d\Omega \;+\; \alpha \sum_{J}^{N} \int_{\Gamma_{Dir}} \mathbf{V}_I^{ML}(\mathbf{x})\, \mathbf{S}\Phi_J^{FE}\, d\Gamma + - \sum_{J}^{N} \int_{\Gamma_{Dir}} \mathbf{V}_I^{ML}(\mathbf{x})\, \mathbf{NDSB}_J^{FE}\, d\Gamma$$

$$\mathbf{K}_{IJ}^{ML} = \sum_{J}^{N} \int_{\Omega_I^{ML}} \boldsymbol{\epsilon}_I^{ML}(\mathbf{x})\, \mathbf{DB}_J^{ML}\, d\Omega \;+\; \alpha \sum_{J}^{N} \int_{\Gamma_{Dir}} \mathbf{V}_I^{ML}(\mathbf{x})\, \mathbf{S}\Phi_J^{ML}\, d\Gamma +$$

$$- \quad \sum_{J}^{N} \int_{\Gamma_{Dir}} \mathbf{V}_I^{ML}(\mathbf{x})\, \mathbf{NDSB}_J^{ML}\, d\Gamma$$

$$\mathbf{f}_I^{FE} = \int_{\Gamma_{Neu}} \mathbf{V}_I^{FE}(\mathbf{x})\, \mathbf{t}\, d\Gamma \; + \; \alpha \int_{\Gamma_{Dir}} \mathbf{V}_I^{FE}(\mathbf{x})\, \mathbf{S}\overline{\mathbf{u}}^{FE}\, d\Gamma \; + \; \int_{\Omega_I^{FE}} \mathbf{V}_I^{FE}(\mathbf{x})\, \mathbf{b}\, d\Omega$$

$$\mathbf{f}_I^{ML} = \int_{\Gamma_{Neu}} \mathbf{V}_I^{ML}(\mathbf{x})\, \mathbf{t}\, d\Gamma \; + \; \alpha \int_{\Gamma_{Dir}} \mathbf{V}_I^{ML}(\mathbf{x})\, \mathbf{S}\overline{\mathbf{u}}^{ML}\, d\Gamma \; + \; \int_{\Omega_I^{ML}} \mathbf{V}_I^{FE}(\mathbf{x})\, \mathbf{b}\, d\Omega$$

If no distinction is operated between the functional bases, the local stiffness matrix for the generic node I can be written as:

$$\mathbf{K}_{IJ} = \underbrace{\sum_{J}^{N} \int_{\Omega_s} \boldsymbol{\epsilon}_I(\mathbf{x})\, \mathbf{DB}_J\, d\Omega}_{\mathbf{K}_{IJ}^{\Omega}} \; + \; \underbrace{\alpha \sum_{J}^{N} \int_{\Gamma_{Dir}} \mathbf{V}_I(\mathbf{x})\, \mathbf{S}\Phi_J\, d\Gamma}_{\mathbf{K}_{IJ}^{Dir}} \; +$$

$$\underbrace{- \sum_{J}^{N} \int_{\Gamma_{Dir}} \mathbf{V}_I(\mathbf{x})\, \mathbf{NDSB}_J\, d\Gamma}_{\mathbf{K}_{IJ}^{\mathbf{t}Dir}}$$

and the left hand side as:

$$\mathbf{f}_I = \underbrace{\int_{\Gamma_{Neu}} \mathbf{V}_I(\mathbf{x})\, \mathbf{t}\, d\Gamma}_{\mathbf{f}_I^{Neu}} \; + \; \underbrace{\alpha \int_{\Gamma_{Dir}} \mathbf{V}_I(\mathbf{x})\, \mathbf{S}\overline{\mathbf{u}}\, d\Gamma}_{\mathbf{f}_I^{Dir}} \; + \; \underbrace{\int_{\Omega_s} \mathbf{V}_I(\mathbf{x})\, \mathbf{b}\, d\Omega}_{\mathbf{f}_I^{dist}}$$

It is seen that each local matrix $\mathbf{K}_{IJ}^{FE}, \mathbf{K}_{IJ}^{FM}, \mathbf{K}_{IJ}^{MF}, \mathbf{K}_{IJ}^{ML}$ in its full generality consists of three terms:

- $\mathbf{K}_{IJ}^{\Omega} = \sum_J^N \int_{\Omega_s} \boldsymbol{\epsilon}_I(\mathbf{x})\, \mathbf{DB}_J\, d\Omega$, that accounts for the stiffness inside Ω and should require no longer explanation; it is the usual stiffness matrix that also arise in FEM, before the imposition of the essential boundary conditions
- $\mathbf{K}_{IJ}^{Dir} = \alpha \; \sum_J^N \int_{\Gamma_{Dir}} \mathbf{V}_I(\mathbf{x})\, \mathbf{S}\Phi_J\, d\Gamma$, that stems from the imposition of the boundary conditions in Γ_{Dir} in a weak way, with the penalty formulation.

The entries of this matrix are generally $\sim \alpha$ times a regular entry in $\mathbf{K}^{\Omega}$. If the prescribed value for the displacement of node I $\overline{\mathbf{u}}$ is constant, then the vector equations, to enforce the essential BC, reduces to

$$\sum_{J}^{N} \int_{\Gamma_{Dir}} \mathbf{V}_I(\mathbf{x})\, \Phi_J \widehat{\mathbf{u}}_J \, d\Gamma \;=\; \int_{\Gamma_{Dir}} \mathbf{V}_I(\mathbf{x})\, \overline{\mathbf{u}} \, d\Gamma$$

which can be thought of as starting from

$$\sum_{I} \Phi_I \mathbf{u}_I = \overline{\mathbf{u}}$$

for a generic point, and then integrating by the use of the weight $\mathbf{V}_I$, since without the kronecker delta property the foregoing expression cannot be further simplified.

- $\mathbf{K}_{IJ}^{t_{Dir}} = -\sum_{J}^{N} \int_{\Gamma_{Dir}} \mathbf{V}_I(\mathbf{x})\, \mathbf{NDSB}_J \, d\Gamma$, that is the stress on the outer boundary where the essential boundary conditions are specified; indeed it is possible to write

$$-\sum_{J}^{N} \int_{\Gamma_{Dir}} \mathbf{V}_I(\mathbf{x})\, \mathbf{NDSB}_J \widehat{\mathbf{u}}_J \, d\Gamma \;= -\sum_{J}^{N} \int_{\Gamma_{Dir}} \mathbf{V}_I(\mathbf{x})\, \mathbf{t}$$

where $\mathbf{t}$ is the (still unknown) stress due to the presence of the essential boundary conditions. It is noted that this term is equivalent to $\int_{\Gamma_{Neu}} \mathbf{V}_I(\mathbf{x})\, \mathbf{t} \, d\Gamma = \mathbf{f}_I^{Neu}$, only that in this case $\mathbf{t}$ is expressed as a function of the unknown fictitious values.

At the same time, the forcing vector allows for a straightforward interpretation:

- $\mathbf{f}_I^{Neu} = \int_{\Gamma_{Neu}} \mathbf{V}_I^{FE}(\mathbf{x})\, \mathbf{t} \, d\Gamma$, which is the prescribed stress at the boundary. It is noted that the natural boundary conditions will, in general, not be satisfied after the discretized system have been solved. This is a limitation of the variational formulation used.
- $\mathbf{f}_I^{Dir} = \alpha \int_{\Gamma_{Dir}} \mathbf{V}_I(\mathbf{x})\, \mathbf{S}\overline{\mathbf{u}} \, d\Gamma$ that represents the prescribed essential boundary conditions, and complements the corresponding integral seen before.
- $\mathbf{f}_I^{dist} = \int_{\Omega_s} \mathbf{V}_I(\mathbf{x})\, \mathbf{b} \, d\Omega$, that represent the distributed load, if any.

The local contribution to the local stiffness matrix and the local forcing vector allow to write, for the global stiffness matrix:

$$\begin{cases} \left(\mathbf{K}_{FE}^{\Omega} + \mathbf{K}_{FE}^{Dir} + \mathbf{K}_{FE}^{t_{Dir}}\right)\mathbf{u}_{FE} + \left(\mathbf{K}_{MF}^{\Omega} + \mathbf{K}_{MF}^{Dir} + \mathbf{K}_{MF}^{t_{Dir}}\right)\mathbf{u}_{ML} &= \mathbf{f}_{FE}^{dist} + \mathbf{f}_{FE}^{Dir} + \mathbf{f}_{FE}^{Neu} \\ \left(\mathbf{K}_{FM}^{\Omega} + \mathbf{K}_{FM}^{Dir} + \mathbf{K}_{FM}^{t_{Dir}}\right)\mathbf{u}_{FE} + \left(\mathbf{K}_{ML}^{\Omega} + \mathbf{K}_{ML}^{Dir} + \mathbf{K}_{ML}^{t_{Dir}}\right)\mathbf{u}_{ML} &= \mathbf{f}_{ML}^{dist} + \mathbf{f}_{ML}^{Dir} + \mathbf{f}_{ML}^{Neu} \end{cases} \tag{2.4}$$

The foregoing expression contains, in its full generality, all the terms for the so called fully coupled enrichment.

It is seen that regions of complex shape arise when evaluating the integrals in the coupling blocks, because the integrand is, in general, not smooth enough.

It is also possible to neglect, as outlined in the introduction, the coupling block $\mathbf{K}_{MF}$ or $\mathbf{K}_{FM}$ to give rise to the so called uncoupled enrichment. Finally, it is noted that at least one between FEM domain and MLPG domain must extend untill the boundary where the boundary conditions are prescribed.

Chapter 3

A Critical Assessment of the Method

This chapter provides an *insight* to the proposed methodology, leaving the *numerical results* to the next chapter.

3.1 Boundary Conditions

In non-interpolating schemes, such as MLS, it is not easy to impose the essential boundary conditions, as the interpolation scheme does not have the property that $\phi^I(x_I)u^I = u_I(x_I)$, where ϕ^I is the shape function of node I of coordinates x_I. This considerably complicates the imposition of the essential boundary conditions. A methodology that could be used is, for instance, a Lagrange multiplier technique, as recently proposed by Atluri [17]. Here however a penalty method as originally proposed by Atluri in MLPG [16], [8] is extended to the general case, hence, encompassing the traditional FEM approach; the final enriched solution calculated on FE nodes, indeed, does not have the Kronecker property any longer. The penalty coefficient α, used to enforce the prescribed essential boundary conditions, must be commensurate to the order of magnitude of the integrands that form the entries in the final stiffness matrix. Thus, α is best chosen as *some* order of magnitude higher than the elastic modulus E, rather than as a fixed parameter. The value of α can be thought as an equivalent stiffness of the constraints; hence, its value should be high enough to properly approximate the boundary conditions, but low enough as to avoid ill-conditioning of the matrix. In the present Thesis,

a value of $\alpha = 10^8$ has been found[1] to be the minimum value for the which there is no sensitive variation of the solution.

Here it is noted that the boundary conditions are satisfied with an accuracy that depends on α, if the trial function $\mathbf{u}^h(\mathbf{x})$ is able to represent them exactly. The form of the unknown approximant of $\mathbf{u}^h(\mathbf{x})$ can otherwise be the ultimate limiting factor for the satisfaction of the essential boundary conditions, all along Γ_{Dir}. It is worth noting that, as commonly done by practitioners, in FEM the essential boundary conditions are imposed in a strong way, i.e, by imposing the correct value of the displacement at the so called "Dirichlet Nodes". However, this way of imposing boundary conditions in FEM (by prescribing the exact solution on the nodes) is by no means any more correct than imposing the boundary conditions by the use of the present penalty approach. Indeed, in FEM, the displacement is imposed correctly on these Dirichlet Nodes and the essential boundary conditions are satisfied, a posteriori, exactly on these nodes. Note, however, that the essential boundary condition are generally violated along Γ_{Dir}, that is made up of element edges, apart from the already discussed Dirichlet Nodes, which satisfy them exactly. Imposing the boundary conditions in a weak form, as done in this Thesis, requires that the boundary conditions be satisfied *on average* all along Γ_{Dir}. Thus one might expect that the displacement field, when evaluated on the nodes on $\in \Gamma_{Dir}$, slightly violates the essential boundary conditions. This is not a flaw of the weak form or either related to the choice of the penalty coefficient α; conversely, it is a feature of the different aim of the two methods to impose the essential boundary conditions. It is also possible to expect a slightly superior performance of FEM, in general, when the essential boundary conditions are imposed in a weak way, as the boundary conditions are, on average, better prescribed. However, the greater effort for the prescription of the boundary conditions does not justify the small gain in accuracy obtained, and it is therefore best avoided if at all possible[2].

Finally, it is noted that the concept of a "Dirichlet Node" or that of "Neumann Node" lose their meaning in a Meshless context, as it is not possible to establish, a priori, which nodes have some boundary conditions prescribed. In FEM there is a mesh, and the boundaries of the discretized domain coincides with the physical boundary $\partial\Omega$. In fact, the mesh provides the boundary nodes with a test function

[1] with $E = 1$

[2] and whenever this is possible, it will be highlighted in this Thesis

that reflects that $v \neq 0$ when $\partial\Omega_I$ intersect with Γ_{Dir}. Conversely, a Meshless approach retains its higher flexibility regarding the geometry; particles can be added freely in the domain, and in particular, they need not be placed on the boundary of the physical domain. In particular, as already mentioned, their test functions need not vanish where the essential boundary conditions are prescribed. This is a necessary condition for imposing the essential boundary condition[3]; in MLPG this operation is done during runtime, and depends upon the selection of the radii of the test functions. This, in turn, does not require that the nodes be located on the boundary Γ_{Dir} where the boundary conditions are prescribed, as long as their test function[4] intersects with the boundary. Hence, a so called "Dirichlet Node" need not be placed on Γ_{Dir}, and, conversely, not every node that has boundary conditions prescribed is a node on the boundary. Further, a "Dirichlet Node" can also be a "Neumann Node", if its test function intersects with two edges with different physical representation, which is also quite common. Finally, a meshless node on the interior of the computational domain can by no restriction intersect with several edges, where different analytical law are prescribed as Neumann and Dirichlet boundary conditions. In short, as the Meshless nodes are not bound to any topological or geometrical constrains, they can be freely placed inside the domain, as long as their test functions cover the whole domain; the price, however, is the added programming effort which is, in general, much higher for the prescription of the boundary conditions than for the rest of the computation of the local stiffness matrix; in fact, for each node, the multiple intersections, which may also be disjoint, have to be identified and the outer normal calculated, before seeking for all of the non vanishing shape functions, of each of the two bases; only at that point can the quadrature be performed on each segment. Moreover, the geometry of the domain has to be supplied separately.

Doing a MLPG enrichment only in the interior of the computational domain clearly saves a lot of programming effort, as it avoids the prescription of the boundary conditions in a weak way.

[3] and quite obvioulsy, also for imposing the Neumann boundary conditions

[4] they can, for any reason, even be outside the computational domain

3.2 Numerical Quadrature

Numerical integration plays a crucial role in the convergence of the numerical solution of FE - MLPG coupled approach. In classical Finite Element Method, numerical integration generally isn't a problem, as the integrals may be accurately evaluated. If the element, say in two dimension, is a triangle, the element-nodal shape functions for trial as well as test functions are linear (Figure: 3.1); hence their derivatives arising in the weak form, are constant over each element.

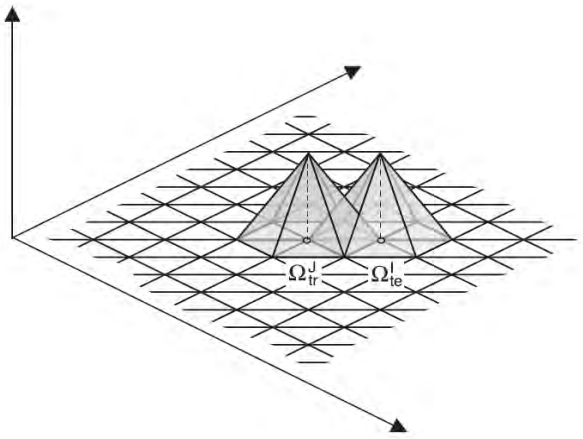

FIGURE 3.1: Intersection between a Finite Element Shape Function and Finite Element Test Function, with resulting non zero entries in the local stiffness matrix.

Conversely, it is more difficult to evaluate the energy for the stiffness matrix of MLPG and that of the coupling blocks between FE and MLPG, due to the complexities of:

- the integrand
- the domain of integrations where the integrand is sufficiently regular

Throughout this section the difficulties of the numerical integrations will be briefly outlined, along with their effect and a suggestion for a solution.

3.2.1 The Shape of the Trial Functions

This subsection outlines how the shape of the trial function can affect negatively the numerical accuracy in the integral calculations. The shape functions with

meshless techniques have a different form in each small region Ω_I^{trial}; the gaussian weight function, used in both the test and trial function, produces irregular forms of the shape function 3.2, 2.1.

FIGURE 3.2: An MLPG shape functions.

Further, the use of the weak form worsen the situation, as the derivatives have, in general, an oscillatory behavior, with indentations and peaks **??**. Also note

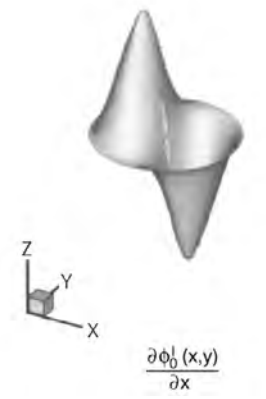

FIGURE 3.3: An MLPG shape function derivative along one direction.

that shape functions have a much wider domain of definition, in general, than the test function. As a result, when the integration is performed for evaluating the entries in the $\mathbf{K}_{ML}$ matrix, Ω_I^{test} is advised (see also Atluri [16], [8] [17]) as a domain of integration instead[5] of Ω_I^{trial}. Also, multiplication by FEM test functions will make discontinuities arise across element edges; conversely, inside the elements the integrand is not overly complicated, as FEM have a constant representation of their derivatives. There is not much to do to fix such an issue but to use an appropriate quadrature rule, and wherever possible, address the integrand

[5]integration over Ω_I^{trial}, unless other methods are used to enhance the accuracy, will lead to very poor results, due to its higher size. Thus, the practice is discouraged

discontinuity problem by a convenient domain subdivision. This transforms the integration problem to a proper domain decomposition. In this case, coupling FE and MLPG does not lead to any newer difficulty for the integration of the energy, once that the domain for quadrature has been carefully selected.

3.2.2 The Loss of Consistency due to non Smooth Integrand

Consider a simple numerical quadrature problem in one dimension,

$$\int_a^b f(x)dx \simeq \sum_i w_i f(x_i)$$

It is possible, in principle, to freely choose the points where to compute the function values, and then to make the formula exact for polynomials up to some degree. The next step is to use the positions of the sample points x_i as *additional* parameters to make the formula exact for higher polynomial degrees.The refined Gauss quadrature rule has been obtained, with an order of consistency $2n-1$, where $2n-1$ is the order of the polynomial the formula is able to integrate exactly with n sample points. Intuitively, the closer in shape to a polynomial up to this degree, the more accurate the quadrature should be.

However the situation is different when dealing with functions that are substantially different from polynomials. Suppose, for example, that one needs to integrate a discontinuous function. The evaluation of the entries in the stiffness matrix relies on discontinuous functions, if, for instance, $\Omega^{trial}_{I_{FE}} \cap \Omega^{test}_{I_{ML}} \neq \{\emptyset\}$ is not further restricted.
In order to fully understand what happens with a discontinuous function, let, at first, f be a continuous function such that:

$$\begin{aligned} f: \quad [a,b] &\longmapsto \mathbb{R}^n \\ x &\longmapsto f(x) \end{aligned} \tag{3.1}$$

with $a < x_1 < \cdots < x_n < b$ a set of n sampling points, and I^h the approximate value of the integral,

$$I = \int_a^b f(x)dx \simeq \sum_i w_i f(x_i) = I^h$$

Consider any extension of f outside its domain of definition, such that

$$\begin{aligned} \widetilde{f}: \quad [\widetilde{a}, b] &\longmapsto \mathbb{R}^n \\ x &\longmapsto \widetilde{f}(x) \end{aligned} \tag{3.2}$$

where $\widetilde{a} < a$ and $f(x) = \widetilde{f}(x),\ \forall x \in [a, b]$,

and consider the numerical integration problem *on the same domain* $[a, b]$

$$\widetilde{I}^h = \sum_i w_i \widetilde{f}(x_i) = \sum_i w_i f(x_i) = I^h$$

however clearly the integration performed on $[\widetilde{a}, b]$

$$\widetilde{I} = \int_{\widetilde{a}}^b f(x)dx = \int_{\widetilde{a}}^a f(x)dx + \int_a^b f(x)dx = \int_{\widetilde{a}}^a f(x)dx + I \neq I$$

In other worlds, since the domain for the numerical quadrature is unchanged, the additional part has not been accounted for.

Now think to restrict the domain $[a, b]$ *slightly*, such that

$$\begin{aligned} \widehat{f}: \quad [\widehat{a}, b] &\longmapsto \mathbb{R}^n \\ x &\longmapsto \widehat{f}(x) = f(x) \end{aligned} \tag{3.3}$$

where $a < \widehat{a} < x_1$, and x_1 is the first sample point for quadrature in $[a, b]$, and $f(x) = \widehat{f}(x),\ \forall x \in [\widehat{a}, b]$.

If one considers the numerical integration problem *on the same domain* $[a, b]$,

$$\widehat{I}^h = \sum_i w_i \widehat{f}(x_i) = \sum_i w_i f(x_i) = I^h$$

because in this example still $\forall x_i \in [\widehat{a}, b]$ and in particular $x_1 \in [\widehat{a}, b]$ hence $\widehat{f}(x_1)$ is well defined; but now again the integration performed on $[\widehat{a}, b]$

$$\widehat{I} = \int_{\widehat{a}}^{b} \widehat{f}(x)dx = \int_{\widehat{a}}^{b} f(x)dx \neq \int_{a}^{b} f(x)dx = I$$

In other words, if the small reduction in the domain is such that none of the quadrature points has to be "disregarded", simply there will be no difference in the numbers to put into the formula, and the result will still be the same. Now, however, there is a portion *less* of domain, namely $[a, \widehat{a}]$ to account for.
Now let $f(x) = 1$ everywhere in its domain of definition; clearly

$$I = I^h$$

because the formula is able to reproduce exactly the constant solution but, when $\widehat{f}(x) = 1$

$$\widehat{I} \neq \widehat{I}^h$$

which means that not accounting for the (even slight) reduction in the domain shall make the formula lose any consistency. In other words, the extremely elaborated and sophisticated quadrature rule, usually referred to as Gauss quadrature rule, has failed even to represent the constant solution, if the actual quadrature domain has not been changed accordingly: *the order of consistency is not even zero* in this case. It should be now clear that there is something wrong with this approach.
Now further, consider the more general:

$$\begin{aligned} \overline{f}: \quad & [a, b] \longmapsto \mathbb{R}^n \\ & x \longmapsto \overline{f}(x) \end{aligned} \tag{3.4}$$

and let $\overline{a}$ be anywhere in $[a, b]$ such that:

$$\overline{f}(x) = \begin{cases} f(x) & x > \overline{a} \\ 0 & x < \overline{a} \end{cases}$$

Eventually f is *discontinuous* at $x = \overline{a}$.

It should now be not difficult to realize that

$$\overline{I}^h = \sum_i w_i \overline{f}(x_i)$$

is still not consistent with

$$\overline{I} = \int_{\overline{a}}^{b} f(x)dx$$

when $f(x)$ is a polynomial. Note that the foregoing approach is, in practice, very easily implementable; indeed it requires only disregarding those quadrature points outside the domain where $\overline{f}(x) \neq 0$, i.e. by setting $w_i = 0,\ \forall i \leq m$ where $x_m = \max\{x_i < \overline{a}\}$.
Note again, $\forall \overline{a}$ such that $x_m < \overline{a} < x_m + 1$ will produce identical outputs on

$$\overline{I}^h = \sum_{i>m} w_i \overline{f}(x_i)$$

because one is putting the very same numbers into the formula, that is $\forall \overline{a} \in [x_m, x_m + 1]$ delivers identical numerical outputs in the numerical approximation of the integral, while in fact

$$\overline{I} = \int_{\overline{a}}^{b} f(x)dx$$

does change as $\overline{a}$ is moved between the two sample points.

It should be now clear that this approach is totally different from starting from the "true" problem

$$\begin{aligned} \overline{f}: \quad & [a,b] \longmapsto \mathbb{R} \\ & x \longmapsto \overline{f}(x) \end{aligned} \tag{3.5}$$

and defining $\overline{f}_1, \overline{f}_2$ such that, in our case,

$$\begin{aligned} \overline{f}_1: \quad & [a,\overline{a}] \longmapsto \mathbb{R} \\ & x \longmapsto \overline{f}_1(x) = 0 \end{aligned} \tag{3.6}$$

$$\begin{aligned} \overline{f}_2: \quad & [\overline{a},b] \longmapsto \mathbb{R} \\ & x \longmapsto \overline{f}_2(x) = f(x) \end{aligned} \tag{3.7}$$

which are continuos in their respective domain and calculate individually

$$\begin{aligned}\int_a^b \overline{f}(x)dx &= \int_a^{\overline{a}} \overline{f}_1(x)dx + \int_{\overline{a}}^b \overline{f}_2(x)dx \\ &= \sum_i w_i \overline{f}_1(x_i) + \sum_i w_i \overline{f}_2(x_i)\end{aligned} \tag{3.8}$$

that is, mapping the position of the $n_1+n_2 = n$ sample points such that $[-1,1] \longmapsto [\overline{a}, b]$ and $[-1,1] \longmapsto [a, \overline{a}]$, which retains consistency up to some order (say $2\cdot\overline{n}_i - 1$, if $\overline{n}_i$ is the number of gauss point at an interval).

Hence neglecting or disregarding the integrand regularity can be dangerous as far as the accuracy of integration is concerned. There is no doubt that increasing the number of quadrature points ultimately will achieve convergence, but normally consistency is a desired feature that assess the method's quality. As a matter of fact, adding more quadrature points will simply increase the computational cost with no tangible improvement. Further, it is the number of quadrature points that dictates the running time almost entirely, as shape function needs to be calculated at each sample point.

3.2.3 The Use of Background Cells

Background cells[6] have already been used in other Meshless methods, and proposed before MLPG [10]. They required a background mesh for the integration of the energy. However, MLPG as proposed by Atluri [16], [8], [17] avoids such background meshes, as MLPG aims at being a *truly* meshless method.
However, this appears not to be a problem in the proposed coupling between FEM and MLPG, because here an enrichment of FEM is done with MLPG. Finite Elements do provide a background mesh; however the mesh used for integration cannot be chosen arbitrarily, but should be carefully designed as to provide a truly working method, with sufficient accuracy. In fact, the mesh bound to the Finite Element may not provide the best solution. For example, when the number of particles is increased, that is, MLPG alone is refined, the background FE mesh stays unchanged, and does not reflect the need for the higher density of quadrature points. Moreover, there is no "embedded" information into the mesh about

[6] of any shape

where should a higher quadrature point density be placed, as FEM mesh is totally independent from the MLPG refinement. As a matter of fact, the FEM mesh do not lead to an effective partition of Ω for the integration of the energy.

3.2.4 The Use of the Meshless Local Subdomain

As far as MLPG alone is concerned, a local subdomain Ω_I^{trial} or Ω_I^{test} might be the natural choice for integration. As a consequence, the choice of either Ω_I^{trial} or Ω_I^{test} for the integration as done by Atluri [16], [8], seems quite reasonable.

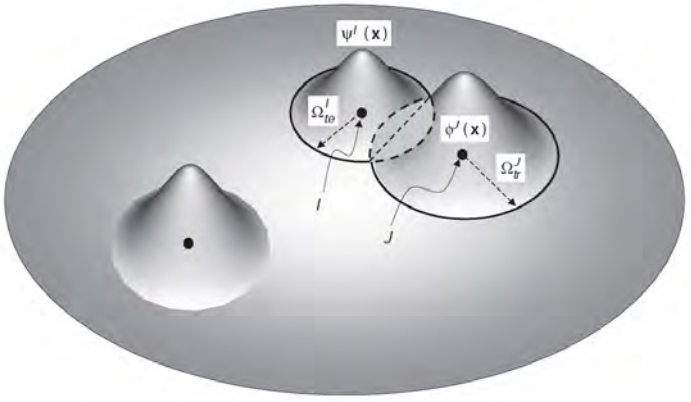

FIGURE 3.4: Intersection between ML test and shape functions.

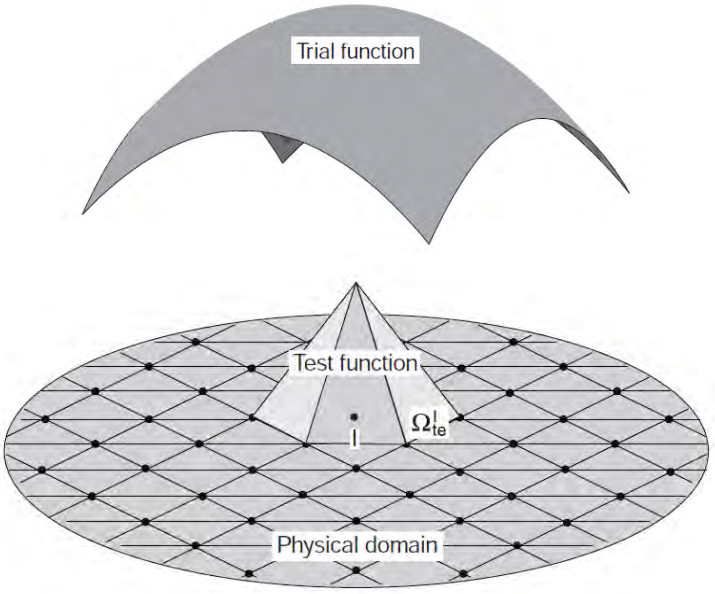

FIGURE 3.5: Integration for the $\mathbf{K}_{FM}$ entries

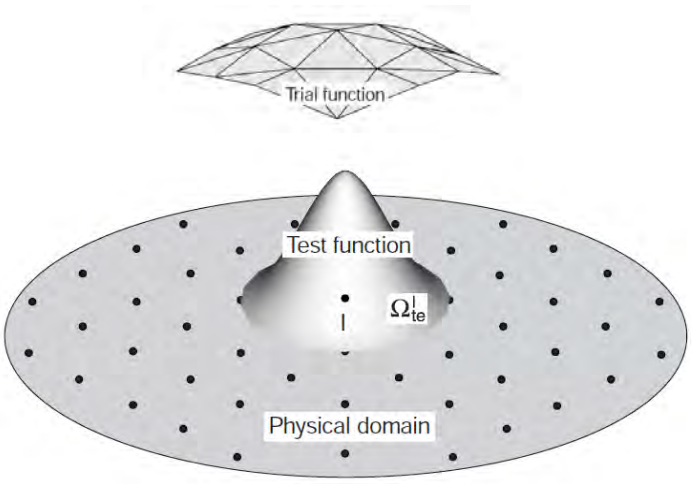

FIGURE 3.6: Integration for the $\mathbf{K}_{FM}$ entries

The value of the integrand is non zero as soon as $\Omega^{trial}_{I_{FE}} \cap \Omega^{test}_{I_{ML}} \neq \{\emptyset\}$, but ϕ^{FE}_{J} is not differentiable over its local subdomain $\Omega^{trial}_{I_{FE}}$ Numerical integration scheme with discontinuous functions should be used with caution, as explained before. In region of mutual intersection between ϕ^{J}_{FE}, v^{I}_{ML} and ψ^{I}_{FE}, ϕ^{J}_{ML} the natural choice for the domain for the integration of the energy is not so straightforward. However, the theoretical rate of convergence of the proposed methodology can be obtained only if the integrals are computed exactly. When dealing with meshless, and, consequently, when coupling MLPG with FEM, it is important to gain an insight on the numerical integration errors, because MLPG shape and test functions have a complex shape, exacerbated by the discontinuities of FEM basis functions. An inaccurate integration can lead to a deterioration of the solution or even to catastrophic results. This is somewhat worsened if the domain for the integration of the energy is "hardwired" to one method alone in the coupling matrices. For instance, an integration over a triangle, when ϕ^{I}_{ML} intersects ψ^{J}_{FE}, may deliver almost exact results as soon as the nodal density and pattern is fairly the same for both FE and MLPG [7]. Conversely, the integration over Ω^{I}_{ML} will not yield to satisfactory results, because the integrand is not smooth enough in this domain. But, as MLPG is refined, an integration over a (now single) element will not reflect the higher density of particles. The shape function can indeed be so small that not even a gauss point is located inside its domain of definitions. Clearly, the integration of the energy over $\Omega^{trial}_{I_{ML}}$ is now a much more natural choice, and will

[7] Recall that the radius of ML shape function is, in general, at least four time the distance to the closest node, and any directional derivative that far is nearly zero, hence its derivative is continuous

now lead to very satisfactory results. As a result, a transition from the integration over triangles to the integration over Ω_I^{trial} must occur *smoothly* when MLPG is refined; and this has to be carefully designed.

3.2.5 A Proposed Domain for Quadrature

In view of the previous considerations, the actual shape of the domain will be accounted for. One might reasonably consider that, in a proper domain, the integrand shall at least be continuos[8], and this will be the criteria for the integration in the present Thesis. Obviously, this approach will necessarily create a patch $\{\Omega_{int}\}$ such that the entries of $\mathbf{K}_{FM}, \mathbf{K}_{MF}$ are evaluated as integrals in the intersections of Finite Elements and $\Omega_{I_{ML}}^{trial}$ or $\Omega_{I_{ML}}^{test}$:

$$\bigcup \Omega_{int}^{IJ} \begin{cases} \Omega_{int}^{J} = (\cup \Omega_{test}^{I_{FE}^{elem}}) \cap \Omega_{trial}^{J_{ML}} & \text{for } \mathbf{K}_{MF} \text{ entries} \\ \Omega_{int}^{I} = \Omega_{test}^{I_{ML}} \cap (\cup \Omega_{trial}^{J_{FE}^{elem}}) & \text{for } \mathbf{K}_{FM} \text{ entries} \end{cases}$$

Furthermore, it requires the definition of a bijection between the standard integration domain $[-1;1]^2$ and the domain for integration $\mathcal{D}$. The map will vary at *each* integration, so a common methodology must be employed[9]. *All* of the possible intersections $\Omega_{triangle} \cap \Omega_{ML}^{I} = \Omega_{int}$ between a circle and a triangle give rise to a lot of different possibilities. However, a closer look will soon reveal they can mostly be thought as a quadrilateral figure with curved edges.

More specifically, the quadrilateral can be obtained by connecting two non necessarily not degenerate simple[10] curves with two non necessarily non degenerate segments.
Consider two curves that have, no point of intersections[11]. Now consider they are connected by two segments, each of which can degenerate to a single point (in this case the curves are in fact connected, but it is useful to think of them as if they were connected by a degenerate segment). Those four entities are placed such that they form a figure that is *topologically* equivalent to a quadrilateral. Moreover, if an edge is a curve the opposite edge shall be a curve and likewise with the segments. A curve can also be a segment, or even degenerate to a point. With this

[8] always recall that the weak form is being used

[9] This is has to be done mathematically first, but the implementation has to follow that level of abstraction, or it'll be of no use

[10] in a mathematical sense

[11] with one another as well as with themselves

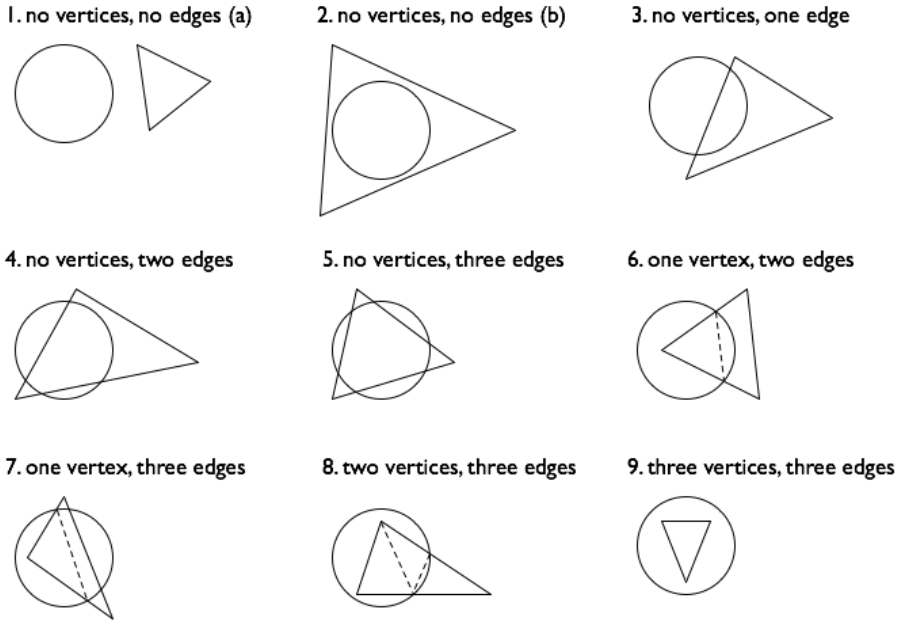

FIGURE 3.7: Some possible intersection between a triangle and a local subdomain, or, equivalently, a domain of definitions. Note that the integration with three edges soon disappears as MLPG nodal density is increased, for the Meshless test function. The Meshless shape function derivative, conversely, is continuos on the boundary of its domain of definition and leads to less problem for the integration of the energy

abstraction, any boundary of the intersection $+\partial\big(\ \Omega_{triangle} \cap \Omega_{ML}\ \big) = +\partial\ \Omega_{int}$ can be represented. Additionally, the definition of a proper orientation for these curves must be carried out.

Now, the following map is defined. Consider a curve

$$\begin{aligned} \mathcal{C}_1 : \quad [-1,1] &\longrightarrow \mathcal{D}_1 \subset \mathbb{R}^2 \\ t &\longmapsto \vec{x}_1(t) \end{aligned} \tag{3.9}$$

and equivalently,

$$\begin{aligned} \mathcal{C}_2 : [-1,1] &\longrightarrow \mathcal{D}_2 \subset \mathbb{R}^2 \\ t &\longmapsto \vec{x}_2(t) \end{aligned} \tag{3.10}$$

Since they are connected by straight lines, it is somewhat natural to define

$$\begin{aligned} \mathcal{T} : [-1,1]^2 &\longrightarrow \mathcal{D} \subset \mathbb{R}^2 \\ (\alpha, t) &\longmapsto \vec{x}(t) \end{aligned} \tag{3.11}$$

and more explicitly

$$(\alpha, t) \longmapsto \vec{x}(t) = (1-\alpha)\vec{x}_1(t) + (1-\alpha)\vec{x}_2(t)$$

Note that the straight segments and the curves $\mathcal{C}_1$, $\mathcal{C}_2$ themselves are α-curves and t-curves, respectively. The quadrature points will be placed all along the α-curve and t-curve, where α and t are the (linear) coordinates of sample points in $[-1, 1]$ for quadrature. In short, this is a *linear combinations* of the two curves.

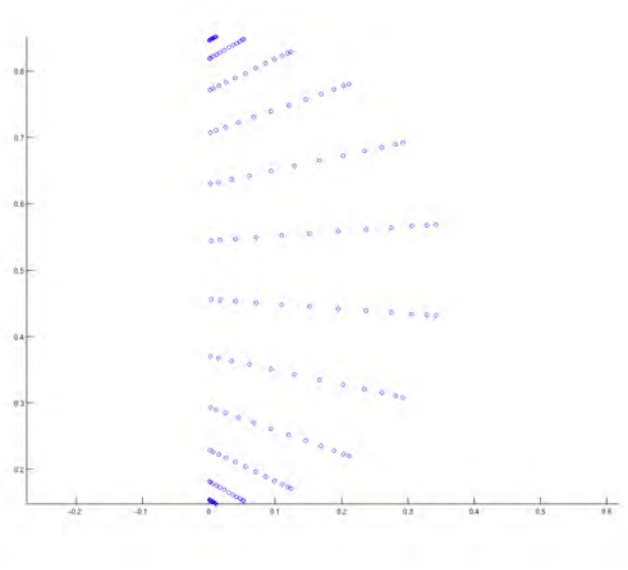

FIGURE 3.8: Quadrature points placed all along α-curves and t-curves in the actual quadrature domain, the boundary of the which is a straight line and an arch

It's necessary that, once the closed path is considered, the two curve be oriented in *opposite* directions, for instance, one counterclockwise and the other clockwise, or the map won't be *onto*[12] the closed path, therefore not *bijective*. In addition, it can be seen that the map is non degenerate *almost everywhere*[13]. Also note that, when a curve degenerates to a point, the Jacobian of the map is singular at

[12] in a mathematical sense (also *surjective*)
[13] in a mathematical sense

that point, but still it is not singular almost everywhere. Clearly the curves are arches, but the approach was kept in its most generality. The presentation of the algorithmic implementation, which is rather sophisticated in nature, is here not deemed necessary, as it does not add anything to the reader's comprehension.

3.3 Fully Coupled Enrichment

The fully coupled enrichment involves all of the final equations obtained before, namely:

$$\begin{bmatrix} \mathbf{K}^{\Omega}_{FE} + \mathbf{K}^{Dir}_{FE} + \mathbf{K}^{t_{Dir}}_{FE} & \mathbf{K}^{\Omega}_{MF} + \mathbf{K}^{Dir}_{MF} + \mathbf{K}^{t_{Dir}}_{MF} \\ \mathbf{K}^{\Omega}_{FM} + \mathbf{K}^{Dir}_{FM} + \mathbf{K}^{t_{Dir}}_{FM} & \mathbf{K}^{\Omega}_{ML} + \mathbf{K}^{Dir}_{ML} + \mathbf{K}^{t_{Dir}}_{ML} \end{bmatrix} . \begin{bmatrix} \mathbf{u}_{FE} \\ \mathbf{u}_{ML} \end{bmatrix} = \begin{bmatrix} \mathbf{f}^{dist}_{FE} + \mathbf{f}^{Dir}_{FE} + \mathbf{f}^{Neu}_{FE} \\ \mathbf{f}^{dist}_{ML} + \mathbf{f}^{Dir}_{ML} + \mathbf{f}^{Neu}_{ML} \end{bmatrix}$$

However, if none of the meshless local subdomain Ω^I_s intersect with $\partial\Omega$, the terms over $\partial\Omega$, involving $\mathbf{V}$, namely:

$$\mathbf{K}^{Dir}_{MF} + \mathbf{K}^{t_{Dir}}_{MF} = \alpha \sum_J^N \int_{\Gamma_{Dir}} \mathbf{V}^{ML}_I(\mathbf{x})\, \mathbf{S}\Phi^{FE}_J \, d\Gamma - \sum_J^N \int_{\Gamma_{Dir}} \mathbf{V}^{ML}_I(\mathbf{x})\, \mathbf{NDSB}^{FE}_J \, d\Gamma$$

$$\mathbf{K}^{Dir}_{ML} + \mathbf{K}^{t_{Dir}}_{ML} = \alpha \sum_J^N \int_{\Gamma_{Dir}} \mathbf{V}^{ML}_I(\mathbf{x})\, \mathbf{S}\Phi^{ML}_J \, d\Gamma - \sum_J^N \int_{\Gamma_{Dir}} \mathbf{V}^{ML}_I(\mathbf{x})\, \mathbf{NDSB}^{ML}_J \, d\Gamma$$

and

$$\mathbf{f}^{Dir}_{ML} + \mathbf{f}^{Neu}_{ML} = \int_{\Gamma_{Neu}} \mathbf{V}^{ML}_I(\mathbf{x})\, \mathbf{t}\, d\Gamma + \alpha \int_{\Gamma_{Dir}} \mathbf{V}^{ML}_I(\mathbf{x})\, \mathbf{S}\overline{\mathbf{u}}\, d\Gamma$$

vanish. The final expression simplifies to:

$$\begin{bmatrix} \mathbf{K}^{\Omega}_{FE} + \mathbf{K}^{Dir}_{FE} + \mathbf{K}^{t_{Dir}}_{FE} & \mathbf{K}^{\Omega}_{MF} + \mathbf{K}^{Dir}_{MF} + \mathbf{K}^{t_{Dir}}_{MF} \\ \mathbf{K}^{\Omega}_{FM} & \mathbf{K}^{\Omega}_{ML} \end{bmatrix} . \begin{bmatrix} \mathbf{u}_{FE} \\ \mathbf{u}_{ML} \end{bmatrix} = \begin{bmatrix} \mathbf{f}^{dist}_{FE} + \mathbf{f}^{Dir}_{FE} + \mathbf{f}^{Neu}_{FE} \\ \mathbf{f}^{dist}_{ML} \end{bmatrix}$$

If, additionally, the domain of definition of each node Ω_{trial} does not intersect with $\partial\Omega$ either, that is, none of the meshless shape function is non vanishing on $\partial\Omega$, the final stiffness matrix simplifies even further to:

$$\begin{bmatrix} \mathbf{K}^{\Omega}_{FE} + \mathbf{K}^{Dir}_{FE} + \mathbf{K}^{t_{Dir}}_{FE} & \mathbf{K}^{\Omega}_{MF} \\ \\ \mathbf{K}^{\Omega}_{FM} & \mathbf{K}^{\Omega}_{ML} \end{bmatrix} \cdot \begin{bmatrix} \mathbf{u}_{FE} \\ \\ \mathbf{u}_{ML} \end{bmatrix} = \begin{bmatrix} \mathbf{f}^{dist}_{FE} + \mathbf{f}^{Dir}_{FE} + \mathbf{f}^{Neu}_{FE} \\ \\ \mathbf{f}^{dist}_{ML} \end{bmatrix}$$

It is noted that only the FEM contribution represents the entire solution on $\partial\Omega$, hence, on $\Gamma_{Dir} \subset \partial\Omega$:

$$\mathbf{u}^h(\mathbf{x}) = \sum_I \phi^{FE}_I(\mathbf{x})\mathbf{u}^{FE}_I$$

that implies, as just explained, that only FEM now have the essential or natural boundary conditions enforced; thus the kronecker delta property now holds again and

$$\sum_I \Phi_I(\mathbf{x})\mathbf{u}_I = \overline{\mathbf{u}}_I$$

can be further simplified, when evaluated at $\mathbf{x}_I$, as

$$\mathbf{u}_I = \overline{\mathbf{u}}_I$$

which allows for a straightforward implementation of the boundary conditions in a strong way; hence, it is possible to neglect $\mathbf{K}^{Dir}_{FE} + \mathbf{K}^{t_{Dir}}_{FE}$ and calculate directly:

$$\begin{bmatrix} \mathbf{K}^{\Omega}_{FE} & \mathbf{K}^{\Omega}_{MF} \\ \\ \mathbf{K}^{\Omega}_{FM} & \mathbf{K}^{\Omega}_{ML} \end{bmatrix} \cdot \begin{bmatrix} \mathbf{u}_{FE} \\ \\ \mathbf{u}_{ML} \end{bmatrix} = \begin{bmatrix} \mathbf{f}^{dist}_{FE} + \mathbf{f}^{Neu}_{FE} \\ \\ \mathbf{f}^{dist}_{ML} \end{bmatrix}$$

which is singular and deserves a strong imposition of the essential boundary conditions, in the usual way. This ultimately greatly simplifies a meshless enrichment, especially if thought as an "add on" to an existing FEM solver for PDEs.
However, in this last case, one has to exercise extreme caution to ensure that the enriched region, made of all the domains of definition of the meshless shape functions never intersects with the boundary[14] $\partial\Omega$, at runtime.

[14] this in turn implies that even the test function, that are centered at the same points, never intersects with the boundary, as their radius is generally much smaller than that of the shape functions.

3.3.1 Representability of a Linear Solution

The following section discusses the uniqueness of the solution of the final linear system of equations of a fully coupled, global enrichment with boundary conditions applied on both FE and MLPG contribution blocks and coupling blocks. Some preliminary considerations are mandatory.

Finite Element and Linear Solution Finite Elements made up of triangles with linear basis functions [15] are able to represent a linear solution exactly. That is to say, the displacement complies with the linear map:

$$\mathcal{T}_\Omega : \begin{bmatrix} x \\ y \end{bmatrix} \mapsto \begin{bmatrix} a_{11} & a_{12} \\ a_{21} & a_{22} \end{bmatrix} \cdot \begin{bmatrix} x \\ y \end{bmatrix} + \begin{bmatrix} b_1 \\ b_2 \end{bmatrix}$$

for any value of the coefficients. Note that there are *six* coefficients that define the linear map written above. Thus the linear displacement request that all six degrees of freedom of a triangle be used for the satisfaction of the displacement law. This can be repeated for any element and, eventually, for any element both d.o.f of exactly three nodes have to be specified to comply with the specified displacement $\mathcal{T}_\Omega$. Hence, $\mathbf{v}_{FE}(\mathbf{x})$ is such that $\mathbf{v}_{FE}(\mathbf{x}) = \mathcal{T}_\Omega(\mathbf{x}),\ \forall \mathbf{x} \in \Omega$ that implies $\mathcal{T}_\Omega \in \mathcal{V}^h_{FE} \subset \mathcal{V}_{FE}$, that is, the linear map is exactly represented by the finite element space.

MLPG and Linear Solution As opposed to FEM, MLPG does not allow for a "node-wise" approach, but re-examining the functional, which originated the shape functions, will reveal that also MLPG is able to reproduce a linear displacement, when a linear basis is employed. Indeed, from basic geometry it is known that a plane, that is, a linear map in the form $z = a_o + a_x x + a_y y$ is well defined[16] as soon as three *non aligned*[17] different points are specified. Since independent basis functions are used for x and y displacement, a linear displacement field of the form:

[15] independently in each direction

[16] the solution exists and is unique

[17] in the FE framework not aligned is equivalent to non degenerate element, which, of course, may never happen for many other reasons

$$\mathcal{T}_\Omega : \begin{bmatrix} x \\ y \end{bmatrix} \mapsto \begin{bmatrix} a_{11}\ a_{12} \\ a_{21}\ a_{22} \end{bmatrix} \cdot \begin{bmatrix} x \\ y \end{bmatrix} + \begin{bmatrix} b_1 \\ b_2 \end{bmatrix}$$

can be specified and will be represented exactly by MLPG. With the same argument as before, $\mathbf{v}_{ML}(\mathbf{x})$ is such that $\mathbf{v}_{ML}(\mathbf{x}) = \mathcal{T}_\Omega(\mathbf{x}),\ \forall \mathbf{x} \in \Omega$, which implies $\mathcal{T}_\Omega \in \mathcal{V}^h_{ML} \subset \mathcal{V}_{ML}$, that is, the linear map is exactly representable by MLPG.

Finally, here it is noted that the order of consistency, that is one in this case for both discrete functional spaces, is a feature that should reflect the maximum order of derivative of the (weak) form of the equations, i.e., exactly one in the case of elastostatics, to achieve convergence.

3.3.2 Theoretical Estimate of the Number of Zero Eigenvalues

The final stiffness matrix, obtained with a fully coupled enrichment is singular. In view of the foregoing considerations it is now possible to understand why.
The variational problem (V) has a solution $\mathbf{u}^{true}(x)$ that cannot be exactly represented by any of the two discrete functional spaces, nor their union. However a unique solution to the variational problem (V) in the functional space $\mathcal{V}^h_{FE} \cup \mathcal{V}^h_{ML}$ exits. Let $\mathbf{u}^h(\mathbf{x}) = \mathbf{u}^h_{FE}(\mathbf{x}) + \mathbf{u}^h_{ML}(\mathbf{x})$ be that solution, where $\mathbf{u}^h_{ML}(\mathbf{x})$, $\mathbf{u}^h_{FE}(\mathbf{x})$ are the contributions to the final solution from ML and FE, respectively. It is easy to realize that:

$$\begin{cases} \overline{\mathbf{u}^h}_{FE} = \mathbf{u}^h_{FE} + \mathbf{u}_L \\ \overline{\mathbf{u}^h}_{ML} = \mathbf{u}^h_{ML} - \mathbf{u}_L \end{cases} \tag{3.12}$$

are also contributions to the unique solution of the variational problem (V) in $\mathcal{V}^h_{FE} \cup \mathcal{V}^h_{ML}$. Here $\mathbf{u}_L$ is *any* linear map of the form:

$$\mathcal{T}_\Omega : \begin{bmatrix} x \\ y \end{bmatrix} \mapsto \begin{bmatrix} a_{11}\ a_{12} \\ a_{21}\ a_{22} \end{bmatrix} \cdot \begin{bmatrix} x \\ y \end{bmatrix} + \begin{bmatrix} b_1 \\ b_2 \end{bmatrix} \tag{3.13}$$

defined by six parameters. Note that expression 3.12 is equivalent to saying that both FE and MLPG are able to represent one of the elements of their own functional space *plus* a linear superimposition of a *linear* function, since a linear function also belongs to the space. Indeed, for either MLPG or FE separately:

$$\begin{aligned}\overline{\mathbf{u}^h}(x) &= \mathbf{u}^h(x) + \mathbf{u}_L(x) \\ &= \Sigma_i \Phi_i(\mathbf{x}) \cdot \mathbf{u}_i + \Sigma_i \Phi_i(\mathbf{x}) \cdot \mathbf{u}_i^L \\ &= \Sigma_i \Phi_i(\mathbf{x}) \cdot \left(\mathbf{u}_i + \mathbf{u}_i^L\right) \\ &= \Sigma_i \Phi_i(\mathbf{x}) \cdot \overline{\mathbf{u}}_i\end{aligned} \tag{3.14}$$

Alternatively, one could just think that $\mathbf{u}^h(\mathbf{x}) \in \mathcal{V}^h$, $\mathbf{u}_L(\mathbf{x}) \in \mathcal{V}^h$, and hence $(\mathbf{u}^h(\mathbf{x}) + \mathbf{u}_L(\mathbf{x})) \in \mathcal{V}^h$, that is equivalent to saying $\overline{\mathbf{u}^h}(\mathbf{x}) \in \mathcal{V}^h$.
These considerations apply to both x and y directions, and to both FE and MLPG.

Now:

$$\overline{\mathbf{u}^h} = \overline{\mathbf{u}^h}_{FE} + \overline{\mathbf{u}^h}_{ML} = \mathbf{u}^h$$

is still *the*[18] solution in $\mathcal{V}^h_{FE} \cup \mathcal{V}^h_{ML}$ to the discretized variational problem, because

$$\begin{aligned}\overline{\mathbf{u}^h}(\mathbf{x}) &= \overline{\mathbf{u}^h}_{FE}(\mathbf{x}) + \overline{\mathbf{u}^h}_{ML}(\mathbf{x}) \\ &= \left(\mathbf{u}^h_{FE}(\mathbf{x}) + \mathbf{u}_L(\mathbf{x})\right) + \left(\mathbf{u}^h_{ML}(\mathbf{x}) - \mathbf{u}_L(\mathbf{x})\right) \\ &= \mathbf{u}^h_{FE}(\mathbf{x}) + \mathbf{u}^h_{ML}(\mathbf{x}) \\ &= \mathbf{u}^h(\mathbf{x}) \in \left(\mathcal{V}^h_{FE} \cup \mathcal{V}^h_{ML}\right)\end{aligned} \tag{3.15}$$

Hence, the determination of $\mathbf{u}^h$ can be done after specifying six parameters that define the linear map.

Here it is remarked again that the solution in the discrete variational space

$$\mathcal{V}^h = \mathcal{V}^h_{FE} + \mathcal{V}^h_{ML}$$

is unique. However, since the discretization is not done by expressing the trial function $\mathbf{u}^h$ as a function of the vectors of a basis of $\mathcal{V}^h$,

$$\mathbf{u}^h(\mathbf{x}) = \sum_I \phi_I^{FE}(\mathbf{x})\, \widehat{\mathbf{u}}_I^{FE} + \sum_I \phi_I^{ML}(\mathbf{x})\, \widehat{\mathbf{u}}_I^{ML}$$

[18] the solution to the discretized variational problem can be proven to be unique

does not admit unique representation of $\widehat{\mathbf{u}}_I^{FE}, \widehat{\mathbf{u}}_I^{ML} \in \mathbb{R}^2$, because

$$< \phi_1^{FE}, \ldots, \phi_{n_{FE}}^{FE}, \phi_1^{ML}, \ldots, \phi_{n_{ML}}^{ML} > = \mathcal{V}^h$$

without, however, being a basis of $\mathcal{V}^h$.

If N is the total number of nodes (FE and MLPG), one obtains

$$2N \;=\; \dim(\mathcal{V}^h) \;+\; 6$$

because

$$\mathcal{V}_{FE}^h \;\cap\; \mathcal{V}_{ML}^h = \{\; \mathcal{T}_\Omega^\lambda \mid \lambda \in \mathcal{R}^6\} \;\Rightarrow\; \dim(\mathcal{V}_{FE}^h \;\cap\; \mathcal{V}_{ML}^h) = 6$$

Finally, it is noted that the present arguments hold if the enrichment is fully coupled, that is, comprising all of the terms presented in the theory, and "fully global", that is, extending over all the computational domain Ω.

3.3.3 Numerical Verification of the number of zero Eigenvalues

It is highly difficult to numerically detect the zero eigenvalues, as predicted by the theory, which should reflect those number of degrees of freedom left floating. This is due to numerical (in)accuracy, more specifically:

- when evaluating the entries of the stiffness matrix for interior nodes
- when evaluating the entries of the stiffness matrix that stems from the imposition of the essential boundary conditions
- when imposing such boundary conditions with a penalty formulations
- when accounting for $\int_{\Omega_s} \boldsymbol{\epsilon}^{ML} \boldsymbol{\sigma}^{FE} d\Omega$, and $\int_{\Omega_s} \boldsymbol{\epsilon}^{FE} \boldsymbol{\sigma}^{ML} d\Omega$

This poses a major concern when it comes to distinguishing the zero eigenvalues from the actual small eigenvalues. Indeed they can be just two or three order of magnitude apart. A complete knowledge of the performance of integration and of

all the aforementioned points is required in this context to verify they are in the right number[19]. Moreover, accounting for the terms:

$$\int_{\Gamma_{Dir}} \boldsymbol{\epsilon}^{FE}\boldsymbol{\sigma}^{FE} d\Omega$$

$$\int_{\Gamma_{Dir}} \boldsymbol{\epsilon}^{FE}\boldsymbol{\sigma}^{ML} d\Omega$$

$$\int_{\Gamma_{Dir}} \boldsymbol{\epsilon}^{ML}\boldsymbol{\sigma}^{FE} d\Omega$$

$$\int_{\Gamma_{Dir}} \boldsymbol{\epsilon}^{ML}\boldsymbol{\sigma}^{ML} d\Omega$$

makes the final stiffness matrix no more than close to being singular. However, one has to be careful and realize that increasing the penalty coefficient would increase the order of magnitude of:

$$\alpha \sum_{J}^{N} \int_{\Gamma_{Dir}} \mathbf{V}_I^{FE}(\mathbf{x})\, \mathbf{S}\Phi_J^{FE}\widehat{\mathbf{u}}_J \, d\Gamma$$

$$\alpha \sum_{J}^{N} \int_{\Gamma_{Dir}} \mathbf{V}_I^{FE}(\mathbf{x})\, \mathbf{S}\Phi_J^{ML}\widehat{\mathbf{u}}_J \, d\Gamma$$

$$\alpha \sum_{J}^{N} \int_{\Gamma_{Dir}} \mathbf{V}_I^{ML}(\mathbf{x})\, \mathbf{S}\Phi_J^{FE}\widehat{\mathbf{u}}_J \, d\Gamma$$

$$\alpha \sum_{J}^{N} \int_{\Gamma_{Dir}} \mathbf{V}_I^{ML}(\mathbf{x})\, \mathbf{S}\Phi_J^{ML}\widehat{\mathbf{u}}_J \, d\Gamma$$

while

$$\int_{\Gamma_{Dir}} \boldsymbol{\epsilon}^{FE}\boldsymbol{\sigma}^{FE} d\Omega, \quad \int_{\Gamma_{Dir}} \boldsymbol{\epsilon}^{FE}\boldsymbol{\sigma}^{ML} d\Omega, \quad \int_{\Gamma_{Dir}} \boldsymbol{\epsilon}^{ML}\boldsymbol{\sigma}^{FE} d\Omega, \quad \int_{\Gamma_{Dir}} \boldsymbol{\epsilon}^{ML}\boldsymbol{\sigma}^{ML} d\Omega$$

stays unchanged and soon will add nothing[20] to the relevant matrix entries. That is to say:

$$\mathbf{K}_{FE}^{Dir} + \mathbf{K}_{FE}^{t_{Dir}} \approx \mathbf{K}_{FE}^{Dir}$$

[19] It is mentioned that increasing the number of quadrature points to approach machine precision with the integration accuracy is more of an hindrance than of an help, as it will exceed any computational power with just few nodes and start to highlight the computer's finite representability of real numbers

[20] to machine precision

$$\mathbf{K}_{MF}^{Dir} + \mathbf{K}_{MF}^{t_{Dir}} \approx \mathbf{K}_{MF}^{Dir}$$

$$\mathbf{K}_{FM}^{Dir} + \mathbf{K}_{FM}^{t_{Dir}} \approx \mathbf{K}_{FM}^{Dir}$$

$$\mathbf{K}_{ML}^{Dir} + \mathbf{K}_{ML}^{t_{Dir}} \approx \mathbf{K}_{ML}^{Dir}$$

as α grows large.

Thus, either neglecting these terms or increasing the penalty coefficient, the numerical integration being accurate to machine precision, ultimately reveals that exactly as many eigenvalues as predicted by the theory are in fact zeros, for a fully coupled, global enrichment.

3.3.4 Compatibility Conditions in the Fully Coupled Global Enrichment

Mathematically speaking, one has to suppress as many shape functions as needed to obtain a basis for $\mathcal{V}^h$, thus, as many as six in a global fully coupled enrichment.

Practically, a different approach that could be used involves the imposition of compatibility conditions on some points, that one might reasonably call "compatibility points". By requesting $\mathbf{u}_{FE}^h(\mathbf{x}) = \beta \mathbf{u}_{ML}^h(\mathbf{x})$ for three non aligned points yields to:

$$\sum_{I}^{FE} \phi_I(\mathbf{x})\ \widehat{\mathbf{u}}^{FE} = \beta \sum_{I}^{ML} \phi_I^{ML}(\mathbf{x})\ \widehat{\mathbf{u}}^{ML}, \qquad \mathbf{x} = \mathbf{x}_1, \mathbf{x}_2, \mathbf{x}_3 \tag{3.16}$$

where $\beta \in \mathbb{R} - \{0\}$ is an arbitrary scalar value.

Conditions 3.16 can be regarded as the request that the planes encompassing $\big(\mathbf{x}_k, \mathbf{u}^{FE}(\mathbf{x}_k)\big)$ and $\big(\mathbf{x}_k, \mathbf{u}^{ML}(\mathbf{x}_k)\big)$ are the same plane. It will be possible to develop a variational formulation, prescribing

$$\mathbf{u}_{FE}^h(\mathbf{x}) = \mathbf{u}_{ML}^h(\mathbf{x}), \qquad \mathbf{x} = \mathbf{x}_1, \mathbf{x}_2, \mathbf{x}_3$$

using, Dirac distributions.

The approach above gives rise to one more idea of reducing the degrees of freedom in excess, by "hardwiring" a solution contribution, that is, either $\mathbf{u}_{FE}^h(\mathbf{x})$ or $\mathbf{u}_{ML}^h(\mathbf{x})$. In other words, instead of requesting:

$$\mathbf{u}^h_{FE}(\mathbf{x}_k) = \beta \mathbf{u}^h_{ML}(\mathbf{x}_k), \qquad k = 1, 2, 3$$

the following can be requested:

$$\mathbf{u}^h_{FE}(\mathbf{x}_k) = \mathbf{u}^{comp}_k, \qquad k = 1, 2, 3$$

for some $\mathbf{u}^{comp}_k \in \mathbb{R}^2 \quad k = 1, 2, 3.$

Instead of requesting coincidence between osculating planes, one of the two planes is fixed. This can be easily accomplished by prescribing a displacement[21], on exactly three non aligned nodes, for instance, over a whole finite element. Here it is noted that as many points as desired by the user can be hardwired, in a region where the enrichment is effective. This operation suppresses some shape function coefficients by fixing the values of the fictitious solution, hence leaving to the remaining basis the duty of "compensating" it.
However, the problem can be solved, by directly avoiding any possible "creation" of zero eigenvalues in the final matrix. Indeed, it is possible to neglect some terms in the final system of equations, to obtain:

$$\begin{bmatrix} \mathbf{K}^{\Omega}_{FE} + \mathbf{K}^{Dir}_{FE} + \mathbf{K}^{t_{Dir}}_{FE} & \mathbf{K}^{\Omega}_{MF} \\ \mathbf{K}^{\Omega}_{FM} & \mathbf{K}^{\Omega}_{ML} + \widehat{\mathbf{K}}^{Dir}_{ML} + \widehat{\mathbf{K}}^{t_{Dir}}_{ML} \end{bmatrix} \cdot \begin{bmatrix} \mathbf{u}_{FE} \\ \mathbf{u}_{ML} \end{bmatrix} = \begin{bmatrix} \mathbf{f}^{dist}_{FE} + \mathbf{f}^{Dir}_{FE} + \mathbf{f}^{Neu}_{FE} \\ \mathbf{f}^{dist}_{ML} \end{bmatrix}$$

where $\widehat{\mathbf{K}}^{Dir}_{ML} + \widehat{\mathbf{K}}^{t_{Dir}}_{ML}$ are obtained by prescribing zero displacement at the boundary of the enriched region $\partial\Omega_{enr} = \partial\Omega = \widehat{\Gamma}_{Dir}$, as can be seen in (Figure 3.9)

In this case, however, the meshless contribution is no longer effective for the satisfaction of the boundary conditions, and this can be, in the most general case, a limiting factor for convergence. In general, it is possible to opt for a partially coupled enrichment at the boundary of the computational domain, while retaining a fully coupled enrichment in the interior; this, however, depends upon the geometry and the position of the essential boundary conditions, and should be done with caution.

[21] similarly to imposing Dirichlet boundary conditions

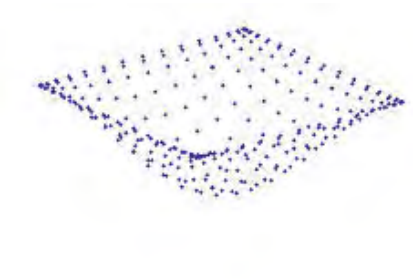

FIGURE 3.9: Displacement due to MLPG contribution, in one direction, where a zero displacement is enforced at the boundary of a plate

3.4 Uncoupled Enrichment

As seen in the introduction, the so called uncoupled enrichment aims at an even less costly and more versatile alternative to the fully coupled enrichment. The purpose here is to have the FEM problem solved first and independently, as if there were no enrichment; then, at a second step, the added particles provide a refinement to enhance the solution.
To this aim, it is possible to deliberately neglect the whole $\mathbf{K}_{MF}$ matrix, obtaining:

$$\begin{bmatrix} \mathbf{K}_{FE}^{\Omega} + \mathbf{K}_{FE}^{Dir} + \mathbf{K}_{FE}^{t_{Dir}} & \mathbf{0} \\ \mathbf{K}_{FM}^{\Omega} + \mathbf{K}_{FM}^{Dir} + \mathbf{K}_{FM}^{t_{Dir}} & \mathbf{K}_{ML}^{\Omega} + \mathbf{K}_{ML}^{Dir} + \mathbf{K}_{ML}^{t_{Dir}} \end{bmatrix} \cdot \begin{bmatrix} \mathbf{u}_{FE} \\ \mathbf{u}_{ML} \end{bmatrix} = \begin{bmatrix} \mathbf{f}_{FE}^{dist} + \mathbf{f}_{FE}^{Dir} + \mathbf{f}_{FE}^{Neu} \\ \mathbf{f}_{ML}^{dist} + \mathbf{f}_{ML}^{Dir} + \mathbf{f}_{ML}^{Neu} \end{bmatrix}$$

Hence $\mathbf{u}_{FE}$ can be obtained independently by solving first the FEM problem:

$$\left(\mathbf{K}_{FE}^{\Omega} + \mathbf{K}_{FE}^{Dir} + \mathbf{K}_{FE}^{t_{Dir}}\right) \cdot \mathbf{u}_{FE} = \mathbf{f}_{FE}^{dist} + \mathbf{f}_{FE}^{Dir} + \mathbf{f}_{FE}^{Neu}$$

which, as said before, can be further simplified to

$$\left(\mathbf{K}_{FE}^{\Omega}\right) \cdot \mathbf{u}_{FE} = \mathbf{f}_{FE}^{dist} + \mathbf{f}_{FE}^{Neu}$$

that admits infinitely many solutions before the imposition of the essential boundary conditions.
This first step involves the solution of the classical FEM problem.

Once the first solution has been obtained, it can routinely be refined by the use of the particles, that is, the problem

$$\left(\mathbf{K}_{FM}^{\Omega}+\mathbf{K}_{FM}^{Dir}+\mathbf{K}_{FM}^{t_{Dir}}\right)\cdot\mathbf{u}_{FE}+\left(\mathbf{K}_{ML}^{\Omega}+\mathbf{K}_{ML}^{Dir}+\mathbf{K}_{ML}^{t_{Dir}}\right)\cdot\mathbf{u}_{ML} \;=\; \mathbf{f}_{ML}^{dist}+\mathbf{f}_{ML}^{Dir}+\mathbf{f}_{ML}^{Neu}$$

is then solved at a second step. However, now $\mathbf{u}_{FE}$ is *known*, and thus the expression can be conveniently rewritten as:

$$\left(\mathbf{K}_{ML}^{\Omega}+\mathbf{K}_{ML}^{Dir}+\mathbf{K}_{ML}^{t_{Dir}}\right)\cdot\mathbf{u}_{ML} \;=\; \mathbf{f}_{ML}^{dist}+\mathbf{f}_{ML}^{Dir}+\mathbf{f}_{ML}^{Neu}-\left(\mathbf{K}_{FM}^{\Omega}+\mathbf{K}_{FM}^{Dir}+\mathbf{K}_{FM}^{t_{Dir}}\right)\cdot\mathbf{u}_{FE}$$

where the right hand side is straightforward.
It is noted that, in this second step, a *different* problem is solved, as it can be seen by looking at the forcing vector. Indeed the solution $\mathbf{u}^{ML}$ to the variational problem of this second step[22], will be the one that, superimposed to $\mathbf{u}^{FE}$, delivers the correct displacement field that satisfies, a posteriori, the equilibrium equation. This is different from the fully coupled enrichment, which tries to solve the elastostatics problem directly.
Further, $\mathbf{u}^{FE}$ can describe *any* continuous function.
Deliberately neglecting a whole coupling block and still obtaining the correct solution seems a bit magic, so now it will be shown how the foregoing expression can be obtained starting from the variational formulation (V), for the generic node I:

$$\int_{\Omega_s}\boldsymbol{\epsilon}_{\mathbf{v}}\boldsymbol{\sigma}\;d\Omega+\alpha\int_{\Gamma_{Dir}}\mathbf{V}\mathbf{u}\;d\Gamma-\int_{\Gamma_{Dir}}\mathbf{V}\mathbf{t}\;d\Gamma=\;\alpha\int_{\Gamma_{Dir}}\mathbf{V}\mathbf{u}\;d\Gamma+\int_{\Gamma_{Ne\mathbf{u}}}\mathbf{V}\mathbf{t}\;d\Gamma+\int_{\Omega_s}\mathbf{V}\mathbf{b}\;d\Omega$$

by writing the solution as

$$\mathbf{u}=\mathbf{u}_{ML}+\widetilde{\mathbf{u}}_{FE}$$

only that now $\widetilde{\mathbf{u}}_{FE}=\widetilde{\mathbf{u}}_{FE}^{h}$ is known, and *coincides* with the discrete solution obtained by FEM, at the first of the two steps algorithm.

Similarly, the discretization leads to:

[22] hence before discretization

$$\mathbf{u}^h = \sum_I \phi_I^{ML}(\mathbf{x})\widehat{\mathbf{u}}_I^{ML} + \widetilde{\mathbf{u}}^{FE}(\mathbf{x})$$

and since $\widetilde{\mathbf{u}}_{FE} = \widetilde{\mathbf{u}}_{FE}^h = \sum_I \phi_I^{FE}(\mathbf{x})\widetilde{\mathbf{u}}_I^{FE}$ it is possible to write

$$\mathbf{u}^h = \sum_I \phi_I^{ML}(\mathbf{x})\widehat{\mathbf{u}}_I^{ML} + \sum_I \phi_I^{FE}(\mathbf{x})\widetilde{\mathbf{u}}_I^{FE}$$

where $\widetilde{\mathbf{u}}_I^{FE}$ are the fictitious nodal values, that are also nodal values, already obtained by the solution of the FEM problem. Further substitution leads to:

$$\sum_J^{N_{ML}} \int_{\Omega_s} \boldsymbol{\epsilon}_I^{ML}(\mathbf{x})\,\mathbf{DB}_J\widehat{\mathbf{u}}_J^{ML}\,d\Omega \;+\; \alpha \sum_J^{N_{ML}} \int_{\Gamma_{Dir}} \mathbf{V}_I^{ML}(\mathbf{x})\,\mathbf{S}\Phi_J^{ML}\widehat{\mathbf{u}}_J^{ML}\,d\Gamma +$$

$$-\;\sum_J^{N_{ML}} \int_{\Gamma_{Dir}} \mathbf{V}_I^{ML}(\mathbf{x})\,\mathbf{NDSB}_J\widehat{\mathbf{u}}_J^{ML}\,d\Gamma \;= -\left(\sum_J^{N_{FE}} \int_{\Omega_s} \boldsymbol{\epsilon}_I^{ML}(\mathbf{x})\,\mathbf{DB}_J\widetilde{\mathbf{u}}_J^{FE}\,d\Omega\right.$$

$$\left.+\,\alpha \sum_J^{N_{FE}} \int_{\Gamma_{Dir}} \mathbf{V}_I^{ML}(\mathbf{x})\,\mathbf{S}\Phi_J^{FE}\widetilde{\mathbf{u}}_J^{FE}\,d\Gamma \;-\; \sum_J^{N_{FE}} \int_{\Gamma_{Dir}} \mathbf{V}_I^{ML}(\mathbf{x})\,\mathbf{NDSB}_J\widetilde{\mathbf{u}}_J^{FE}\,d\Gamma\right) +$$

$$+\int_{\Gamma_{Neu}} \mathbf{V}_I^{ML}(\mathbf{x})\,\mathbf{t}\,d\Gamma \;+\; \alpha \int_{\Gamma_{Dir}} \mathbf{V}_I^{ML}(\mathbf{x})\,\mathbf{S}\overline{\mathbf{u}}\,d\Gamma \;+\; \int_{\Omega_s} \mathbf{V}_I^{ML}(\mathbf{x})\,\mathbf{b}\,d\Omega$$

that is exactly, in matrix form,

$$\left(\mathbf{K}_{ML}^{\Omega} + \mathbf{K}_{ML}^{Dir} + \mathbf{K}_{ML}^{t_{Dir}}\right)\cdot\mathbf{u}_{ML} \;=\; \mathbf{f}_{ML}^{dist} + \mathbf{f}_{ML}^{Dir} + \mathbf{f}_{ML}^{Neu} - \left(\mathbf{K}_{FM}^{\Omega} + \mathbf{K}_{FM}^{Dir} + \mathbf{K}_{FM}^{t_{Dir}}\right)\cdot\widetilde{\mathbf{u}}_{FE}$$

as obtained before.

In practice, one is looking for $\mathbf{u}_{ML}^h$ such that, when added to $\widetilde{\mathbf{u}}_{FE}$, the displacement field $\mathbf{u} = \mathbf{u}_{ML} + \widetilde{\mathbf{u}}_{FE}$ "better" satisfies the elastostatics problem.

Note that this is a *one way* refinement, meaning that the first procedure, which is well consolidated in literature, is applied first and independently. At a second time, the meshless problem is solved, and this is also a procedure well detailed in literature. The idea of uncoupled enrichment, hence, transfer the displacement field, as calculated by FEM, to one equivalent forcing term that generated that displacement field. More specifically, the coupling term $\mathbf{K}^{\Omega}_{FM}$, evaluated in the interior of the computational domain Ω, can be rewritten as:

$$\mathbf{K}^{\Omega}_{FM}\widetilde{\mathbf{u}}^{FE} = \sum_{J}^{N_{FE}} \int_{\Omega_s} \boldsymbol{\epsilon}^{ML}_{I}(\mathbf{x})\,\mathbf{DB}_J\widetilde{\mathbf{u}}^{FE}_{J}\,d\Omega = \sum_{J}^{N_{FE}} \int_{\Omega_s} \boldsymbol{\epsilon}^{ML}_{I}\boldsymbol{\sigma}^{FE} d\Omega \qquad \forall I_{ML}$$

where $\boldsymbol{\sigma}^{FE}$ is *exactly* the stress field associated with $\mathbf{u}^{FE}$. In other words, the variational formulation of the coupling block $\boldsymbol{\sigma}^{FE}$ reads, *before* discretization:

$$\int_{\Omega_s} \boldsymbol{\epsilon}_{\mathbf{v}}\boldsymbol{\sigma}^{FE}\,d\Omega = \sum_{J}^{N_{FE}} \int_{\Omega_s} \boldsymbol{\epsilon}_{I}(\mathbf{x})\,\mathbf{DB}_J\widetilde{\mathbf{u}}^{FE}_{J}\,d\Omega$$

since

$$\boldsymbol{\sigma}^{FE} = \sum_{J}^{N_{FE}} \mathbf{DB}_J\widetilde{\mathbf{u}}^{FE}_{J}$$

is *exaclty* as calculated by FEM at the first step. This is important to understand, since discretization errors only occur in the solution of the Meshless problem, and repeatedly refining the meshless part does not have the previous discretization of the FEM solution, which is constant, as an ultimate limiting factor for convergence. Finally, it is noted that a prescription of a "worse" solution $\widetilde{\mathbf{u}}^{FE}$ only affects the current solution accuracy $\mathbf{u}^h$, but not the ability of the method to converge to the right solution, as the method aims at satisfying the elastostatics problem with the discrete solution $\mathbf{u}^h = \mathbf{u}^h_{FE} + \mathbf{u}^h_{ML}$. An analog reasoning can be done in the coupling blocks regarding the boundary conditions.

In the test case of Figures 3.10, 3.11, 3.12,3.13, a plate is constrained at its boundary with zero displacement. The exact solution is $\mathbf{u}(\mathbf{x}) = \mathbf{0}\forall x \in \Omega$. A very coarse FE mesh is adopted. A "wrong" displacement is prescribed, as fictitious value, to the FE node in the middle, resulting in a $\mathbf{u}^{FE}$ that has the stress field of Figure

3.10. This FE stress field is then computed, as an equivalent forcing vector, to MLPG (Figure 3.11), resulting in the MLPG stress field contribution of Figure 3.12. The final stress field is then shown in Figure 3.13.

Moreover, it is possible reduce the computational cost of the coupling block. It is possible to write the following term, of the variational formulation (V):

$$\int_{\Omega_s} \boldsymbol{\epsilon}_I \boldsymbol{\sigma}^{FE} d\Omega$$

by addictivity, element-wise, (i.e., over each FE element of domain Ω_{Elem}) as the elements are in equilibrium with the forces applied on their edges, and hence, doing one step back by the use of Green's Theorem:

$$\int_{\Omega_{Elem}} \boldsymbol{\epsilon}_I \boldsymbol{\sigma}^{FE} d\Omega = -\int_{\partial\Omega_{Elem}} \mathbf{V}_I \boldsymbol{\sigma}^{FE} \cdot \mathbf{n} \, d\Omega + \int_{\Omega_{Elem}} \mathbf{V}_I \left(\boldsymbol{\nabla} \cdot \boldsymbol{\sigma}^{FE} \right) d\Omega$$

and recalling that the stress is constant inside each finite element, if the basis is linear, further simplifies to

$$\int_{\Omega_{Elem}} \boldsymbol{\epsilon}_I \boldsymbol{\sigma}^{FE} d\Omega = -\int_{\partial\Omega_{Elem}} \mathbf{V}_I \boldsymbol{\sigma}^{FE} \cdot \mathbf{n} \, d\Omega$$

In short, before discretization, for the I-th meshless test function, the following holds true:

$$\sum_{J}^{N_{FE}} \int_{\Omega^J_{Elem}} \boldsymbol{\epsilon}^{ML}_I (\mathbf{x}) \, \mathbf{DB}_J \widetilde{\mathbf{u}}^{FE}_J \, d\Omega \; = - \sum_{J}^{N_{FE}} \int_{\partial\Omega^J_{Elem}} \mathbf{V}^{ML}_I (\mathbf{x}) \, \mathbf{NDB}_J \widetilde{\mathbf{u}}^{FE}_J \, d\Omega \tag{3.17}$$

where the right hand side is less costly. Indeed only mono-dimensional integrals have now to be evaluated, which can result in much less quadrature points used to obtain the same level of accuracy. In other words 3.17 provides a way to reduce the computational cost of the uncoupled enrichment even further. Moreover, if the particles density is high, most of their test functions do not intersect with the triangles, and therefore most of the computations can be directly avoided at runtime. It is noted that, in the last form, the calculation involves the computation

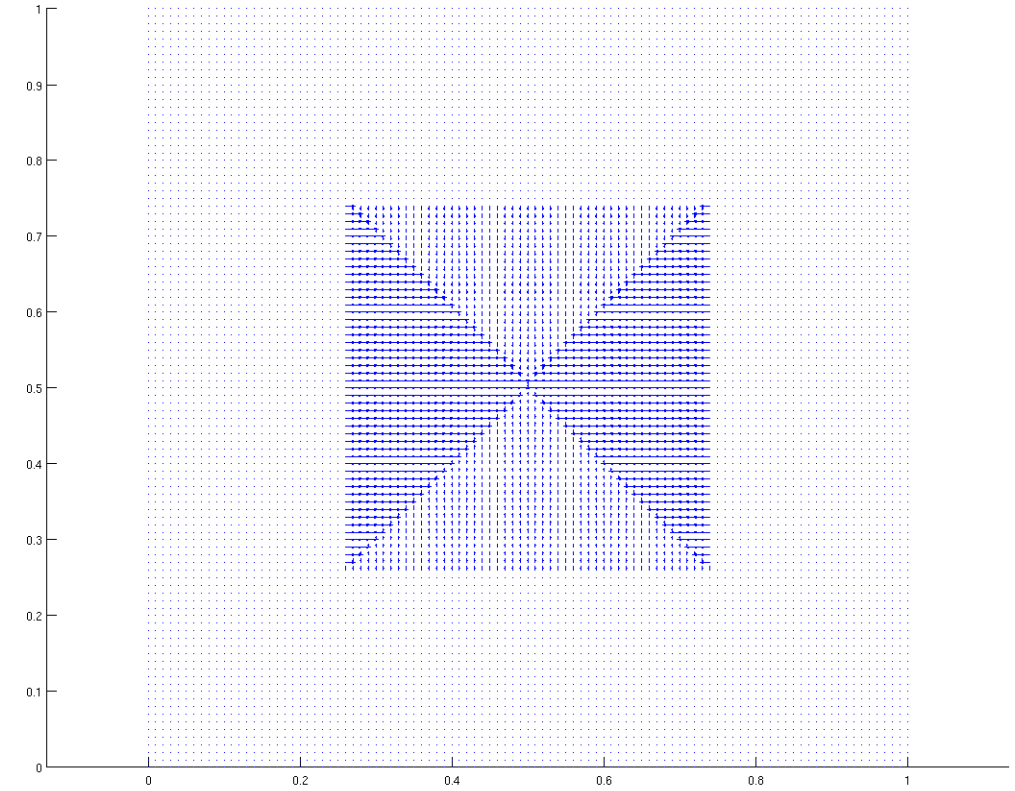

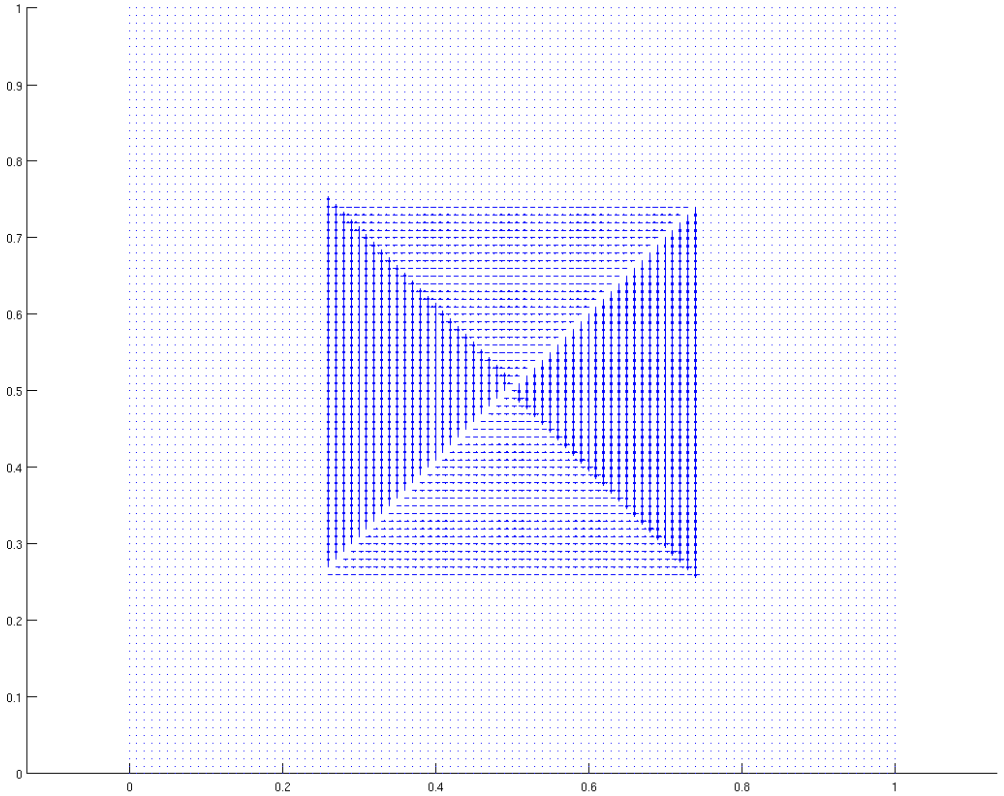

FIGURE 3.10: Stress $\boldsymbol{\sigma} \cdot [1;0]^T$ and $\boldsymbol{\sigma} \cdot [0;1]^T$ obtained by deliberately imposing an horizontal displacement on the node (of FEM) in the center of the computatinal domain (the solution field should be everywhere zero). The resulting stress field, affecting the neighbouring four elements, can be seen in the picture

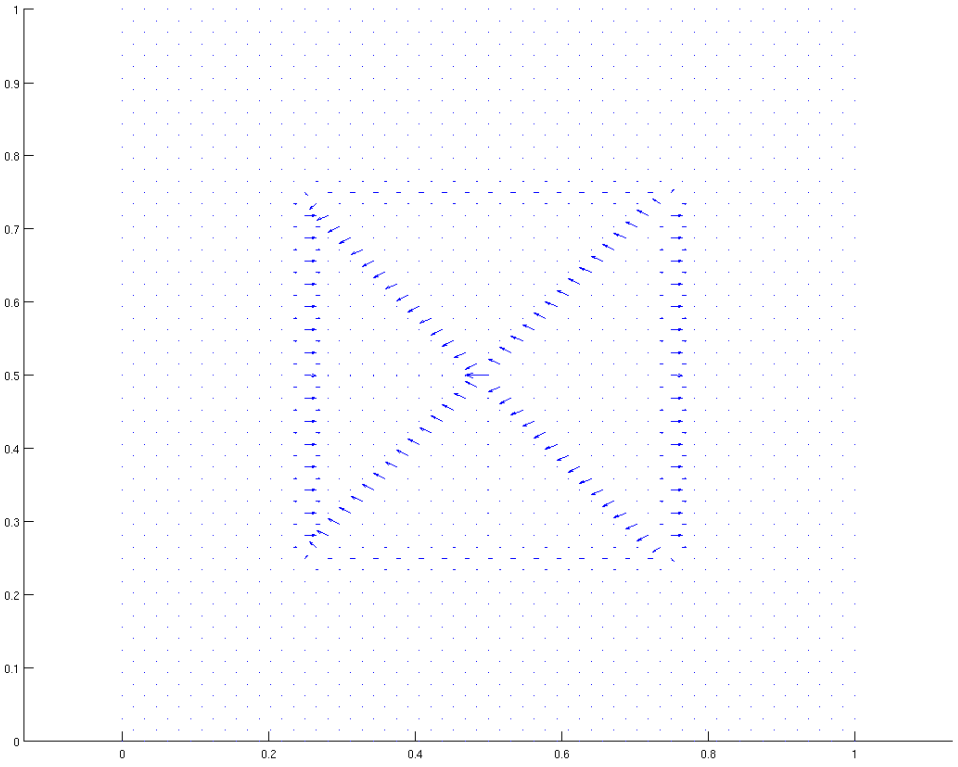

FIGURE 3.11: Equivalent forcing that stems form the coupling block. Note that the arrows plotted are not forces or stress, but $\int_{\Omega_{Elem}} \boldsymbol{\epsilon}_I \boldsymbol{\sigma}^{FE} d\Omega$ for any meshless node. Here the density of meshless node is much higher than that of FEM. Also note that only the variation of $\boldsymbol{\sigma}$ affects the forcing vector

of the normal $\mathbf{N}$ to each (intersected) edge of each triangle, which has however to be calculated also in the integration[23] in Ω_{Elem}, if the integration is done wisely.

Further, once the enriched solution has been computed, an additional refinement comes at a little cost. It is possible to routinely refine the solution by simply adding more particles, without solving again the full system of equations. Indeed the solution provided by Finite Elements has already been calculated; the computation of the meshless stiffness matrix $\mathbf{K}_{ML}$ is straightforward, and not too expensive, if few particles are added, and the coupling block $\mathbf{K}_{FM}$ is the less costly, however fine is the FE mesh. As the enrichment is local, $\mathbf{K}_{FM}$ is be sparse, and the computation of either the meshless shape functions or their derivatives is not involved. Even further, the computation of the integrals can be simplified by the use of line integrals, as detailed above, which can be easily calculated. Finally,

[23] along with much more; the idea will be briefly outlined in the relevant chapter, without, however, digging into too much detail

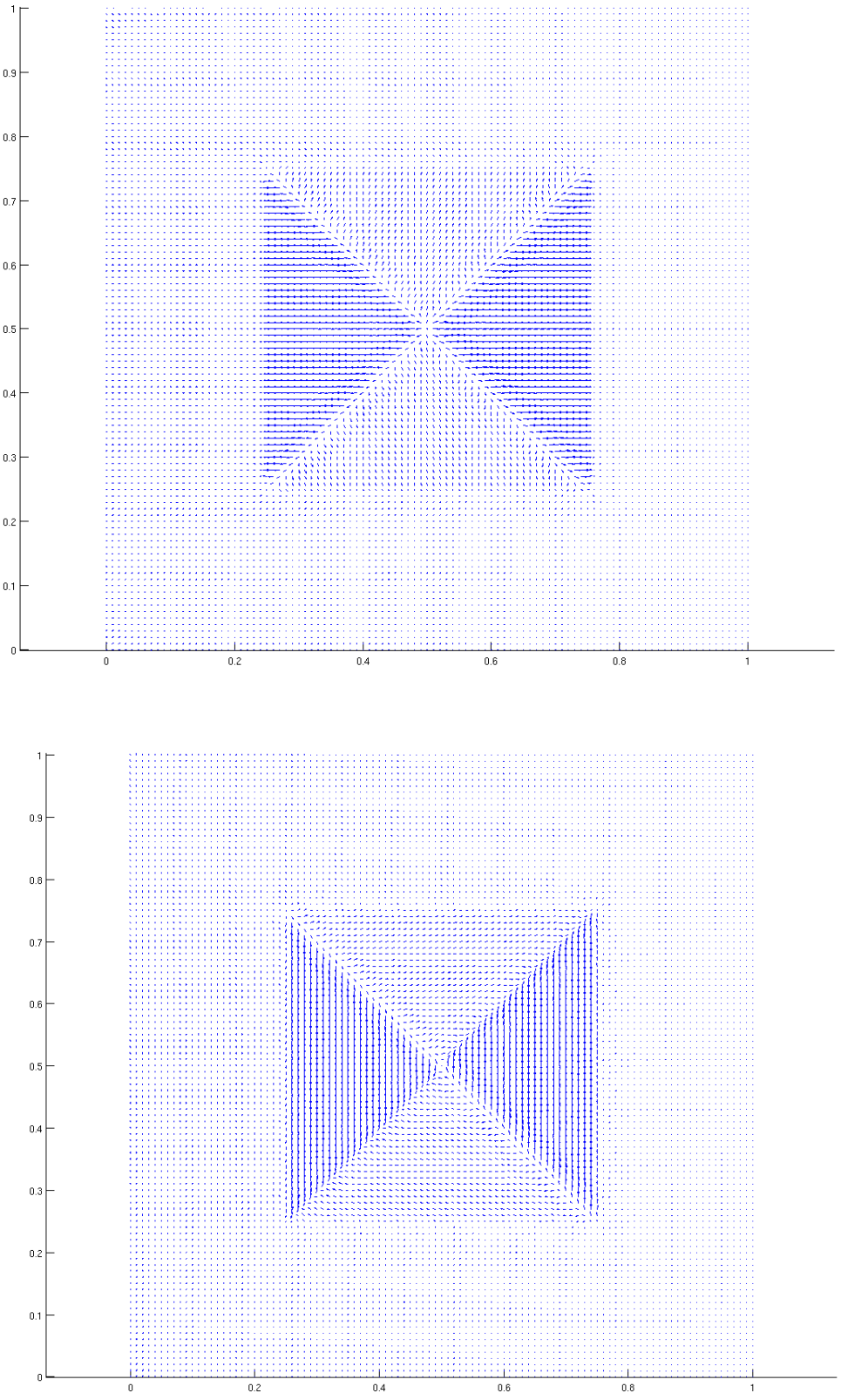

FIGURE 3.12: Stress $\boldsymbol{\sigma} \cdot [1;0]^T$ and $\boldsymbol{\sigma} \cdot [0;1]^T$ obtained by MLPG by solving the second of the two steps algorithm, due to the equivalent load seen before

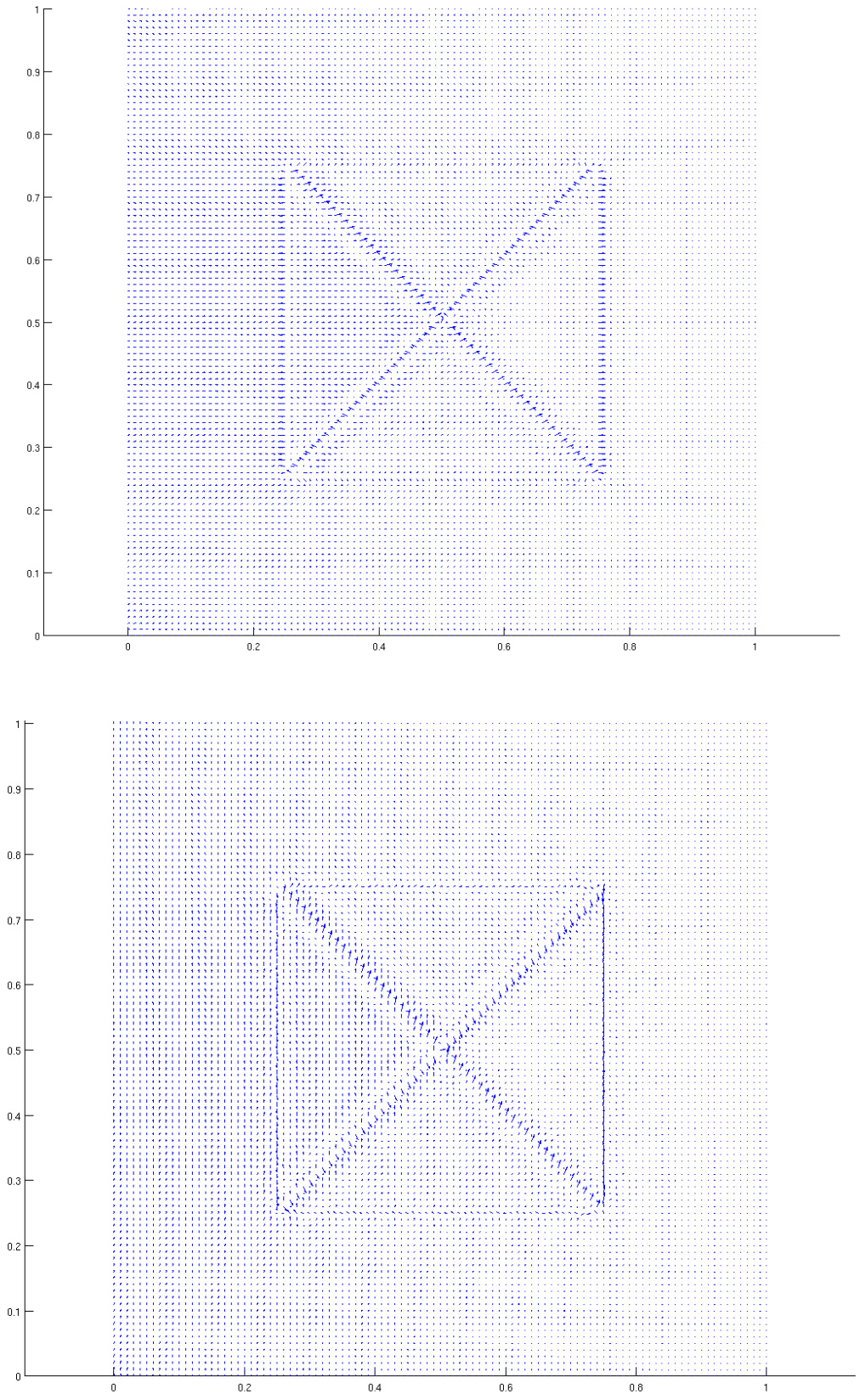

FIGURE 3.13: Final stress field $\boldsymbol{\sigma} \cdot [1;0]^T$ and $\boldsymbol{\sigma} \cdot [0;1]^T$ obtained by superimposing the MLPG and FE contributions. Note that the stress due to FEM cannot be fully compensated by finitely many MLPG nodes. Also note that, since a finite number of MLPG nodes cannot reproduce a discontinuous solution, the stress has an oscillatory behavior across element edges.

only a small linear system (as small as the number of particles added) needs to be solved at the final step.

3.5 Compatibility at the Boundary of the Enriched Region for a Local Enrichment

This section discusses, in the case of a local enrichment, the compatibility between the FE and MLPG solutions, such that they ensure the continuity of $\mathbf{u}^h$. The Meshless solution $\mathbf{u}^h_{ML} = \sum_I \Phi^{ML}_I(\mathbf{x})\mathbf{u}^{ML}_I$ to the discrete variational problem is continuous by construction. Moreover, at the boundary of the enriched region, considered as the union of all the domains of definition of the meshless shape functions, the shape functions, by construction, in general are different from zero. Hence, in order to recover the desired level of continuity, some compatibility conditions should be imposed. Indeed, when approaching a point $\mathbf{x}$ on $\partial\Omega_{Enr}$ from Ω_{Enr}:

$$\mathbf{u}^h = \sum_I \Phi^{FE}_I(\mathbf{x})\mathbf{u}^{FE}_I + \sum_I \Phi^{ML}_I(\mathbf{x})\mathbf{u}^{ML}_I$$

while approaching from $\Omega \setminus\Omega_{Enr}$, that is, from outside the enriched region, the solution has the form:

$$\mathbf{u}^h = \sum_I \Phi^{FE}_I(\mathbf{x})\mathbf{u}^{FE}_I$$

By continuity the value of $\mathbf{u}^h$ needs to be the same, thus:

$$\sum_I \Phi^{ML}_I(\mathbf{x})\mathbf{u}^{ML}_I = \mathbf{0}$$

which has $\mathbf{u}_I = \mathbf{0}$ as a solution $\forall I$-th nodes the which domain of definition covers the point $\mathbf{x} \in \partial\Omega_{Enr}$

Hence, it is necessary to impose *fictitious* boundary conditions, that is, boundary conditions on the fictitious values by enforcing:

$$\mathbf{u}_I = \mathbf{0}$$

for all the nodes that have a shape function such that

$$\Omega^{trial}_I \cap \partial\Omega_{enr} \neq \{\emptyset\}$$

Note that this can be easily enforced in a strong way, as done in FEM, if the enrichment is local.

3.6 Patch Test

The patch test is a criterion for verifying finite element convergence. Initially proposed by engineers, it consists of several elements equipped with proper boundary conditions, so that the exact solution is known. In this case, the prescribed exact solution is linear. The method passes the patch test if it is able to reproduce the exact solution [24]. Although originally conceived for Finite Element, it was proved numerically that MLPG satisfies the patch test[25]. The patch test is commonly referred to as *verification* process. This should not to be confused with checking that a model properly describes the observed phenomena, known as *validation*, which is a far more difficult task. It will be shown in the next subsection that passing the patch test is not sufficient for achieving convergence in this case. In FE-MLPG enrichment, indeed, passing the patch test is not even sufficient to assess that the model was implemented correctly.

3.6.1 A Patch Test for an Uncoupled Enrichment

Consider a rectangular plate where elements have no intersection with the boundaries. It is well known that triangular Finite Elements are able to represent a linear displacement to machine precision. The essential boundary conditions are enforced by the use of a penalty method, to retain the same approach used in MLPG. Finite Elements pass the patch test with an accuracy of the same order of magnitude as the inverse of the penalty coefficient [26]. Now consider again the final system of linear equations, after discretization:

$$\begin{cases} \mathbf{K}_{FE}\mathbf{u}_{FE} + \mathbf{K}_{MF}\mathbf{u}_{FE} & = \mathbf{b}_F \\ \mathbf{K}_{FM}\mathbf{u}_{FE} + \mathbf{K}_{ML}\mathbf{u}_{ML} & = \mathbf{b}_M \end{cases}$$

[24] to machine precision, in case of the finite element, or let me say that, to integration accuracy for MLPG

[25] Atluri

[26] with $E = 1$

The uncoupled enrichment, i.e. by setting $\mathbf{K}_{MF} = \mathbf{0}$ is *equivalent* to the two-step algorithm :

$$\begin{cases} \mathbf{K}_{FE}\mathbf{u}_{FE} & = \mathbf{b}_F \\ \mathbf{K}_{ML}\mathbf{u}_{ML} & = \mathbf{b}_M - \mathbf{K}_{FM}\mathbf{u}_{FE} \end{cases}$$

and the final solution is obtained, as usual, by:

$$\mathbf{u}^{linear}(\mathbf{x}) = \mathbf{u}^h_{FE}(\mathbf{x}) + \mathbf{u}^h_{ML}(\mathbf{x})$$

Since FE is able to reproduce it exactly, and it is also solved first and independently, i.e.

$$\mathbf{u}^{linear}(\mathbf{x}) = \mathbf{u}_{FE}(\mathbf{x})$$

one must obtain

$$\mathbf{u}_{ML}(\mathbf{x}) = \mathbf{0}, \quad \forall \mathbf{x} \in \Omega_{patch}$$

irrespective of the dimension of the enriched region.

Note that this equations holds $\forall x \in \Omega_{patch}$, hence it is possible to prove that

$$\widehat{\mathbf{u}}^I_{ML} = \mathbf{0}, \quad \forall I$$

that is, all the fictitious values must be zero, or equivalently, $\widehat{\mathbf{u}}_{ML} = \mathbf{0}$ in the final system of equations. Indeed, $\mathcal{J}_{MLS} = \sum_i w\big(||x - x_i||\big)||u(x_i) - u_i||^2$ is satisfied exactly with, in each direction, $u_i = u(x_i) = 0$, $\forall i$. Since the solution to the linear system is unique because $\mathbf{K}_{ML}$ is non singular, the trivial solution is obtained if and only if

$$\mathbf{K}_{ML}\mathbf{u}_{ML} = \mathbf{b}_M - \mathbf{K}_{FM}\mathbf{u}_{FE} = \mathbf{0}$$

Note that the patch test requires that both $\mathbf{b}_F, \mathbf{b}_M$ be the null vector (in their relative vector space), hence one can finally write

$$\mathbf{K}_{FM}\mathbf{u}_{FE} = \mathbf{0}$$

that means $\mathbf{u}_{FE} \in \text{Ker}(\mathbf{K}_{FM})$ However, $\exists\overline{\mathbf{K}}_{FM} \neq f$ such that $\mathbf{u}_{FE} \in \text{Ker}(\overline{\mathbf{K}}_{FM})$ [27], so the patch test may get a "passed" even if the implementation is wrong. The patch test has to check out even when the mesh is refined, which is not so obvious, given all the quadrature problems of the procedure, which, in general, arise even at the boundary of the physical domain, under a different nature. Generally, one might expect to see the patch test being satisfied with slightly less accuracy as the nodal density is refined, and this is indeed what happens.

Despite these arguments that make the patch test less useful, the uncoupled enrichment(s) and the fully coupled one, both in the form of a local or global enrichment, did satisfy the patch test correctly.

3.7 A Local versus a Global Enrichment

A local refinement is, in principle, very attractive, as it aims at improving the solution only where it's *needed*. However, the improvement cannot be effective if also the global solution field is well resolved.

Let Ω be, as usual, the domain of a Dirichlet problem:

$$\begin{cases} \boldsymbol{\nabla}\cdot\boldsymbol{\sigma} + \mathbf{b} &= \mathbf{0} \quad \text{in } \Omega \\ \mathbf{u} &= \overline{\mathbf{u}} \quad \text{at } +\partial\Omega \end{cases}$$

and let $\overline{\mathbf{u}}$ be the exact solution in Ω.

Now let $\Omega_{enr} \subsetneq \Omega$ be the enriched region where consider the following problem is considered:

$$\begin{cases} \boldsymbol{\nabla}\cdot\boldsymbol{\sigma} + \mathbf{b} &= \mathbf{0} \quad \text{in } \Omega_{enr} \\ \mathbf{u} &= \overline{\mathbf{u}} \quad \text{at } +\partial\Omega_{enr} \end{cases}$$

[27] Take, for instance, the null matrix between those vector spaces

with $\overline{\mathbf{u}}$ restricted to Ω_{enr} as a solution.

This problem shares some similarities with a local enrichment, in which the coupling block $\mathbf{K}_{MF}$ is neglected. In this case, the problem above in Ω_{enr} has the prescribed solution, at the boundary of the enriched region, $\overline{\mathbf{u}}_{FE}$, that is, the solution field given by the Finite Element. Indeed, the Finite Element Method has already solved the analog discrete problem, and the solution field is not modified outside Ω_{enr}, after the enhancement. Hence, $\overline{\mathbf{u}}_{FE}$, is the *known*[28] displacement from FE, at the boundary of Ω_{enr} where compatibility conditions are implicitly enforced, and in general $\overline{\mathbf{u}}_{FE} \neq \overline{\mathbf{u}}$. These are the prescribed essential boundary conditions of the second step of the problem, with a local uncoupled enrichment. In order to understand the effect of a different boundary conditions prescribed at the boundary of the enriched region, consider a slightly different problem, on the same domain:

$$\begin{cases} \boldsymbol{\nabla} \cdot \boldsymbol{\sigma} + \mathbf{b} &= \mathbf{0} \quad \text{in } \Omega_{enr} \\ \mathbf{u} &= \overline{\mathbf{u}} + \boldsymbol{\alpha} \quad \text{at } + \partial\Omega_{enr} \end{cases}$$

with $\boldsymbol{\alpha} \in \mathbb{R}^2$. Note that both the domain and the differential equations are the same; only the boundary conditions have changed.
Now, it is known that the boundary conditions the solution is completely determined by the prescription of the boundary conditions. The foregoing differential problem has $\widetilde{\mathbf{u}} = \underline{\mathbf{u}} + \boldsymbol{\alpha}$ as a solution. By using repeated index notation, the constitutive law reads:

$$\sigma_{ij}(\mathbf{u}) = \lambda \nabla \cdot \mathbf{u} + \mu \epsilon_{ij}(\mathbf{u})$$

where

$$\mu = \frac{E}{1+\nu}, \quad \lambda = \frac{\nu E}{(1+\nu)(1-2\nu)}, \quad \epsilon_{ij} = \frac{1}{2}(u_{i,j} + u_{j,i})$$

and it is straightforward to note that

$$\begin{aligned} \sigma_{ij}(\mathbf{u}+\boldsymbol{\alpha}) &= \lambda \nabla \cdot (\mathbf{u}+\boldsymbol{\alpha}) + \mu \epsilon_{ij}(\mathbf{u}+\boldsymbol{\alpha}) \\ &= \lambda \nabla \cdot (\mathbf{u}) + \mu \epsilon_{ij}(\mathbf{u}) \end{aligned} \tag{3.18}$$

since $\boldsymbol{\alpha}$ does not depend on $\mathbf{x}$, hence any partial derivative of $\boldsymbol{\alpha}$ with respect to $\mathbf{x}$ is zero. Now if one calls $\widetilde{\boldsymbol{\sigma}} = \widetilde{\boldsymbol{\sigma}}(\mathbf{u}+\boldsymbol{\alpha})$, $\overline{\boldsymbol{\sigma}} = \overline{\boldsymbol{\sigma}}(\mathbf{u})$, $\boldsymbol{\sigma}_\alpha = \boldsymbol{\sigma}_\alpha(\boldsymbol{\alpha})$; by linearity[29], $\widetilde{\boldsymbol{\sigma}} = \overline{\boldsymbol{\sigma}} + \boldsymbol{\sigma}_\alpha$ and at the same time $\boldsymbol{\sigma}_{\boldsymbol{\alpha}} = \mathbf{0}_{2\text{x}2}$ since only the *derivatives* of the displacement appears in the computation of $\boldsymbol{\sigma}_\alpha$. Now immediately $\boldsymbol{\nabla} \cdot \boldsymbol{\sigma}_\alpha =$

[28] to realize it is known, just think of the two steps algorithm to solve it
[29] also referred to as superposition principle in elastostatics

$\boldsymbol{\nabla} \cdot \mathbf{0}_{2x2} = \mathbf{0}$, hence

$$\boldsymbol{\nabla} \cdot \widetilde{\boldsymbol{\sigma}} + \mathbf{b} = \boldsymbol{\nabla} \cdot (\overline{\boldsymbol{\sigma}} + \boldsymbol{\sigma}_\alpha) + \mathbf{b} = \boldsymbol{\nabla} \cdot \overline{\boldsymbol{\sigma}} + \mathbf{b} = \mathbf{0}$$

and $\widetilde{\boldsymbol{u}} = \overline{\boldsymbol{u}} + \boldsymbol{\alpha}$ at the boundary of the enriched region almost by definition. Thus, the problem is exactly satisfied by $\widetilde{\mathbf{u}} = \overline{\mathbf{u}} + \boldsymbol{\alpha}$.

It should now be clear enough that repeatedly ing the enriched region will make the numerical solution converge towards $\widetilde{\mathbf{u}} = \overline{\mathbf{u}} + \boldsymbol{\alpha}$, which obviously isn't the correct solution. This happens because one is prescribing a solution, at the boundary of the enriched region, as calculated by FE, that is different from the actual one. Therefore, when a particular part of the domain is enriched, the error associated with an erroneous solution of the displacement field, as supplied from FE, would be transferred, as boundary conditions, to the enriched area. When only the enriched area is refined, its solution would converge to the problem which has that slightly wrong BCs prescribed. This is not an inherent limitation of the proposed methodology; rather it is a limitation of doing only a *local* "one way" refinement. In practice the situation is more complex as $\boldsymbol{\alpha}$ is not constant all along $\partial\Omega_{enr}$; but the basic idea is simple, it might be a little more difficulty to fully comprehend what happens in the more general case, but the underlying limitation should now be understood.

Conversely, one might expect a superior performance when the two method are fully coupled, i.e., when none of the four blocks are neglected. In this case, indeed, MLPG and FE trial solutions *interact* to give a better result. That means $\overline{\mathbf{u}}_{FE}$ at the boundary cannot be thought to be constant any longer. This resembles a refinement using only FEM, but locally: the solution field outside the enriched region would be "interactively" influenced by the rest of the solution field, as the final discretized system of equations is solved simultaneously. As a result, one might expect the behavior of a fully coupled FE-MLPG to be superior to that of an uncoupled enrichment. However, even in this case, convergence may not be achieved by simply adding particles locally, as generally it is necessary to reduce some mesh parameter h_{mesh} that measures the coarseness of the global mesh[30]. In other words, it is generally necessary to increase *uniformly* and simultaneously the nodal density[31] to achieve convergence.

[30] here the term mesh should be thought in a broader sense, comprising the particles as well

[31] computed over the union of FE nodes and MLPG nodes

It is mentioned that the foregoing considerations do not apply so strictly in a variety of other situations, such as the one with source term or with different types of PDEs.

Chapter 4

Numerical Results

The previous chapters introduced two approaches suited for enriching the FEM by the use of MLPG, in Elastostatics, and discussed some of their properties from a theoretical viewpoint. This chapter assesses *numerically* the effectiveness of the proposed methodologies, providing evidence of the features discussed in the "Critical Assessment" chapter.

4.1 The Benchmark Test Case

To numerically evaluate the potential improvement of the accuracy in the solution field[1], provided by the MLPG enrichment, a well known test case has been chosen as a benchmark. The benchmark consist of an infinite plate with a hole (Figure 4.1), subject to uniform stress σ, at the farfield, in the x direction. The analytical solution, of both the displacement field and of the stress field, respectively, is known analytically, for the plain strain case:

$$\begin{cases} u_x &= \frac{1+\nu}{\mathrm{E}}\sigma\left(\frac{1}{1+\nu}r\cos\theta \;+\; \frac{2}{1+\nu}\frac{a^2}{r}\cos\theta \;+\; \frac{1}{2}\frac{a^2}{r}\cos 3\theta \;-\; \frac{1}{2}\frac{a^4}{r^3}\cos 3\theta\right) \\ u_y &= \frac{1+\nu}{\mathrm{E}}\sigma\left(\frac{-\nu}{1+\nu}r\sin\theta \;-\; \frac{1-\nu}{1+\nu}\frac{a^2}{r}\sin\theta \;+\; \frac{1}{2}\frac{a^2}{r}\sin 3\theta \;-\; \frac{1}{2}\frac{a^4}{r^3}\sin 3\theta\right) \end{cases}$$

[1] broadly speaking: the stress field, displacement field, or the peak stress

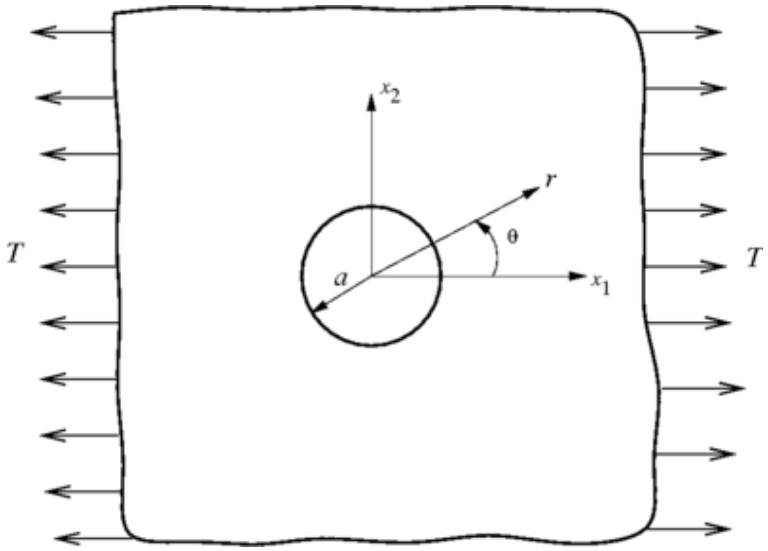

FIGURE 4.1: Computational domain for the test case and peak stress

and:

$$\begin{cases} \sigma_{xx} &= \sigma\left[1 - \frac{a^2}{r^2}\left(\frac{3}{2}\cos 2\theta + \cos 4\theta\right) + \frac{3a^4}{2r^4}\cos 4\theta\right] \\ \sigma_{yy} &= \sigma\left[-\frac{a^2}{r^2}\left(\frac{1}{2}\cos 2\theta - \cos 4\theta\right) - \frac{3a^4}{2r^4}\cos 4\theta\right] \\ \sigma_{xy} &= \sigma\left[-\frac{a^2}{r^2}\left(\frac{1}{2}\sin 2\theta + \sin 4\theta\right) + \frac{3a^4}{2r^4}\sin 4\theta\right] \end{cases}$$

where (r, θ) are the polar coordinates (Figure 4.2) of a point P, u_x, u_y the x and y displacement, respectively, and $\sigma_{xx}, \sigma_{yy}, \sigma_{xy}$ the components of the symmetric stress tensor $\boldsymbol{\sigma}$.

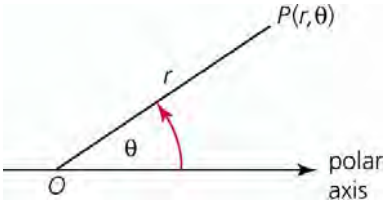

FIGURE 4.2: Polar coordinate system (the center O of the frame of reference is at the center of the hole)

The peak stress is at $\theta = \pm\pi/2$, $r = 1$ with $\sigma_{xx} = 3$.
For the sake of simplicity, the numerical experiments are performed with $E = 1$, $\sigma_{xx} = 1$ at the farfield, a radius $a = 1$ and an edge length (of the plate of the computational domain) of $l = 8$. In contrast to FEM, MLPG does not exhibit any volumetric locking [8]. However, a value of $\nu = 0.25$ has been chosen to avoid any locking phenomenon.

Since the above equations holds for an infinite plate, the discretized model takes it into account by either:

- extending the computational domain such that the boundary effect is negligible, i.e., the solution is nearly uniform at the boundary of the computational domain
- using a finite domain, and imposing the analytical displacement as boundary condition.

The first approach generally involves a large number of nodes. Hence, the second approach has been selected. In this case, it is possible to arbitrarily reduce the computational domain Ω with no accuracy loss. Then the solution field is prescribed on $\partial\Omega$, either as:

- displacement, or
- stress

that is, Dirichlet or Neumann boundary conditions, respectively. The two conditions are equivalent[2] from a theoretical viewpoint[3].

4.2 FEM and MLPG Performance

This section shows the convergence of linear Finite Elements and of the Meshless Local Petrov Galerkin method. Though the results are expected, this gives a "background acquaintance" with the two methodologies. The accuracy obtained with the proposed enrichments can then be compared with the two native approaches. By the way, it is to be emphasized that the purpose of the enrichment is improving, when needed, a FE solution, with no remeshing cost. In general, the accuracy of a numerical solution by the use of the Finite Element Method or the Meshless Local Petrov Galerkin Method ultimately depends on the number of

[2]except that, when imposing Neumann BC, also essential boundary conditions have to be imposed somewhere, to avoid infinitely many solutions resulting in a final singular stiffness matrix

[3]there may actually be a smaller, subtler difference regarding the ability of the discretized solution to represent the two different boundary conditions, but this is a secondary effect.

nodes in the discretization, when uniform mesh are used. Hence, a "fair" comparison[4] takes this into account. In the present numerical experiments, the triangular

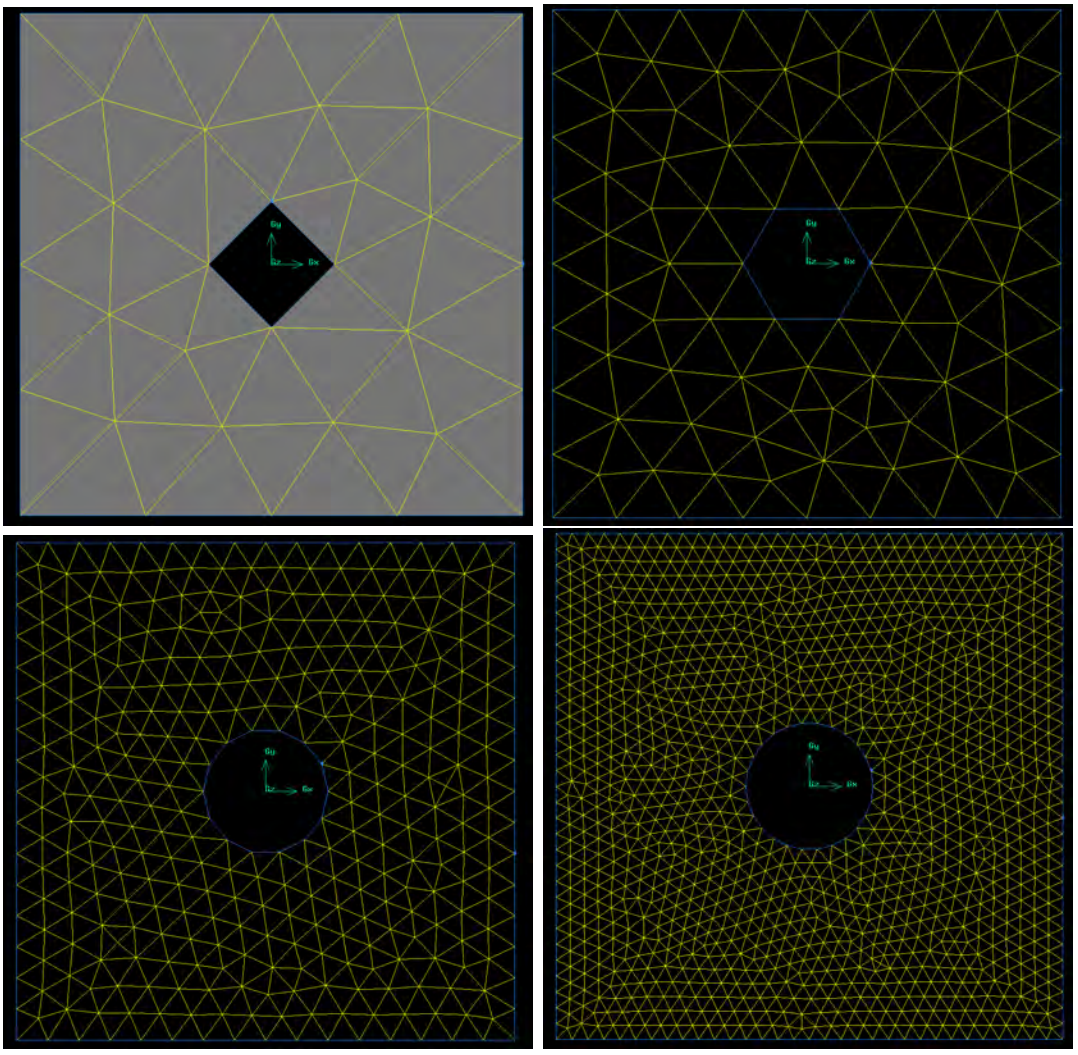

FIGURE 4.3: Nodal pattern for FEM and MLPG. Only the firs two meshes are used for the FEM. Note how the discretized geometry differs from the actual one, highlighted in the first image in grey

FE meshes consisting of 34, 96, 346, 1209 nodes, respectively, shown in Figure 4.3 were generated, with a mesh size of $h \backsim 2,\ 1,\ 0.5,\ 0.25$, respectively. The element vertices are then used for MLPG. The number of nodes of a pattern is used as an "independent variable", to assess the method's quality, since the nodal patterns are nearly uniform.

Throughout all the chapter, a radius $r_v = 1 \cdot c$ for the local subdomains and $r_u = 4 \cdot c$ for the domains of definition in the MLPG scheme are assumed, where

[4] how "fair" may be defined is an open question; the computational cost may, for instance, be the another term for comparison. However, this is not the object of the present Thesis.

c is taken to be the distance to the closest (MLPG) node. The relative error e_r^u, that measures the numerical accuracy of the approximation (Figure 4.4 and Table ??), is defined as:

$$e_r^u = \left(\frac{\sum_i^N ||\mathbf{u}^h(\mathbf{x}_i) - \mathbf{u}(\mathbf{x}_i)||_2^2}{\sum_i^N ||\mathbf{u}(\mathbf{x}_i)||_2^2} \right)^{1/2}$$

where $\mathbf{x}_i$ are the coordinates of the N nodes. $\mathbf{u}^h(\mathbf{x}_i)$ and $\mathbf{u}(\mathbf{x}_i)$ the computed and analytical displacement at $\mathbf{x}_i$, respectively.

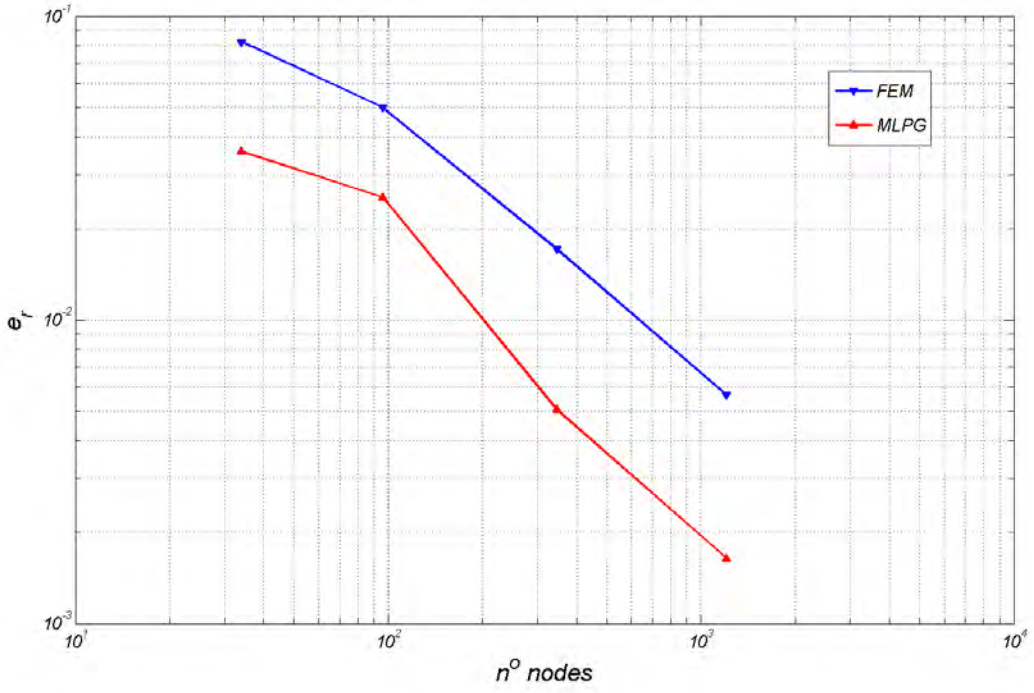

FIGURE 4.4: FEM and MLPG convergence for displacement $\mathbf{u}$

n nodes	e_r^u - FEM	e_r^u - MLPG
34	$8.02 \cdot 10^{-2}$	$3.57 \cdot 10^{-2}$
96	$5.01 \cdot 10^{-2}$	$2.53 \cdot 10^{-2}$
346	$1.70 \cdot 10^{-2}$	$5.06 \cdot 10^{-3}$
1209	$5.65 \cdot 10^{-3}$	$1.63 \cdot 10^{-3}$

TABLE 4.1: Relative error e_r^u for FEM and MLPG

Similarly, the relative error on the stress field has been defined, over the finest mesh of Figure 4.3 [5] as:

$$e_r^{\sigma} = \left(\frac{\sum_i^N ||\boldsymbol{\sigma}^h(\mathbf{x}_i) - \boldsymbol{\sigma}(\mathbf{x}_i)||_2^2}{\sum_i^N ||\boldsymbol{\sigma}(\mathbf{x}_i)||_2^2} \right)^{1/2}$$

where $\boldsymbol{\sigma} = [\sigma_{xx}, \sigma_{yy}, \sigma_{xy}]^T$. The results are reported in Figure 4.5 and Table ??

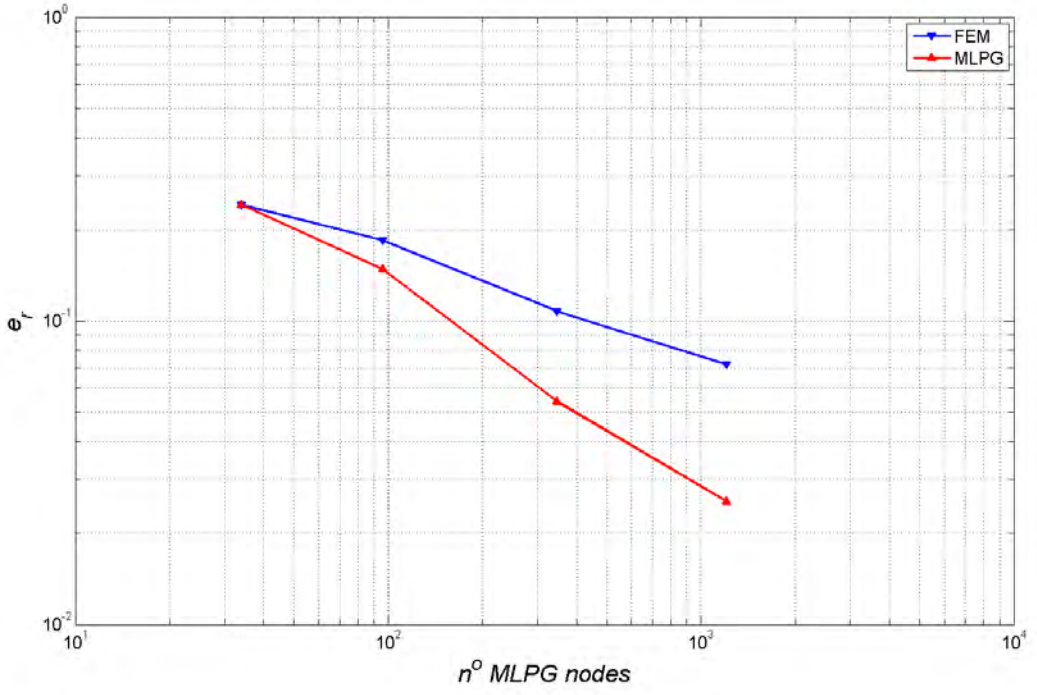

FIGURE 4.5: FEM and MLPG convergence for the stress $\boldsymbol{\sigma}$

n nodes	e_r^{σ} - FEM	e_r^{σ} - MLPG
34	$2.41 \cdot 10^{-1}$	$2.41 \cdot 10^{-1}$
96	$1.83 \cdot 10^{-1}$	$1.47 \cdot 10^{-1}$
346	$1.07 \cdot 10^{-1}$	$5.43 \cdot 10^{-2}$
1209	$7.19 \cdot 10^{-2}$	$2.53 \cdot 10^{-2}$

TABLE 4.2: Relative error e_r^{σ} for FEM and MLPG

It can be easily seen in Figure 4.4 that MLPG can be far more accurate than the Finite Element Method, when using the same number of nodes.
As compared to linear FE, the stress field is better represented as well. As we'll

[5] to avoid problems connected with discontinuities, as outlined later

see in detail later on, in Figure 4.11, the largest contribution to e_r^σ stems from the region close to the hole. Here the gradients of the stress are higher, and both FEM and MLPG do not satisfy exactly the natural boundary conditions implicitly enforced.

The peak stress σ_{xx} can be easily calculated, and approaches 3 as the mesh is refined. The MLPG scheme gives better prediction of the peak stress, then FE, as can be seen form Figure 4.6 and Table **??** . Note that, the local MLPG subdomains near the hole do account for the actual geometry of Ω. In the FEM, on the contrary, it is the discretized geometry that approximates[6] the "shape" of the hole for the integration of the energy. Note also that, there is a number of "user selectable" parameters in the MLPG scheme that can lead to different results, if changed. In general, the optimal choice of these parameters for the displacement field may be different from that for the stress prediction.

n nodes	e_r^σ - FEM	e_r^σ - MLPG
34	$1.48 \cdot 10^{-1}$	$2.21 \cdot 10^{-1}$
96	$2.24 \cdot 10^{-1}$	$2.59 \cdot 10^{-1}$
346	$2.81 \cdot 10^{-1}$	$2.97 \cdot 10^{-2}$
1209	$2.99 \cdot 10^{-2}$	$3.01 \cdot 10^{-2}$

TABLE 4.3: Comparison of FEM and MLPG computed peak stress $\boldsymbol{\sigma}$

[6] actually, curved edges may be adopted, but this has not been considered in the present Thesis

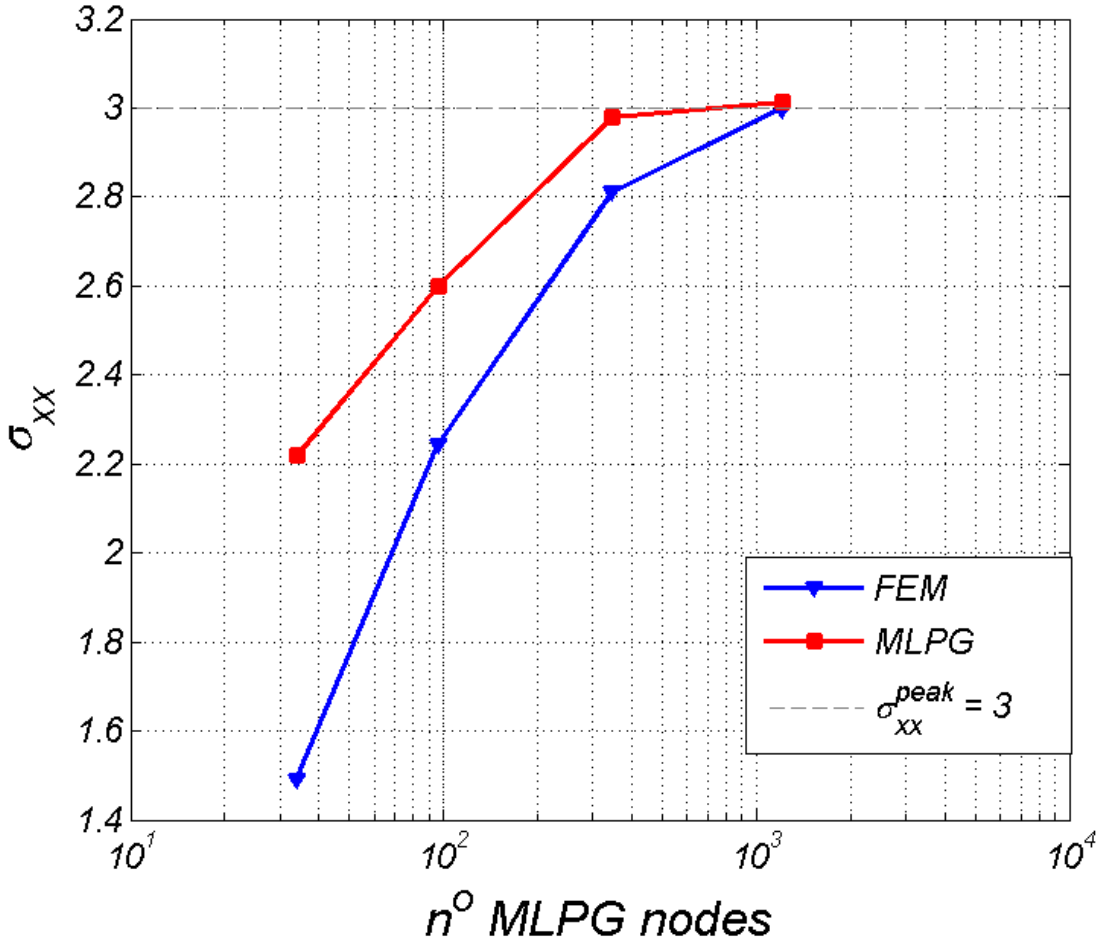

FIGURE 4.6: Comparison of FEM and MLPG computed peak stress $\boldsymbol{\sigma}$

4.3 Uncoupled Enrichment

The uncoupled global enrichment here is evaluated numerically.
As previously outlined, we recall that the FEM solves the problem first and independently, thus providing an initial solution field $\mathbf{u}^h_{FE}$, that should be improved by MLPG. Hence, the added particles try to account for the difference between the exact solution field $\mathbf{u}$, and the one supplied by the FEM $\mathbf{u}^h_{FE}$.
The effect of this type of uncoupled enrichment is an improvement in the solution field, as can be seen from the Figure 4.7 and Tables **??**, **??**, with just a few nodes added, using the pattern reported in Figure 4.3. Figure 4.7 shows the FEM relative error for two meshes in dashes lines, while the relative error e^u_r of the enrichment is plotted in solid lines.

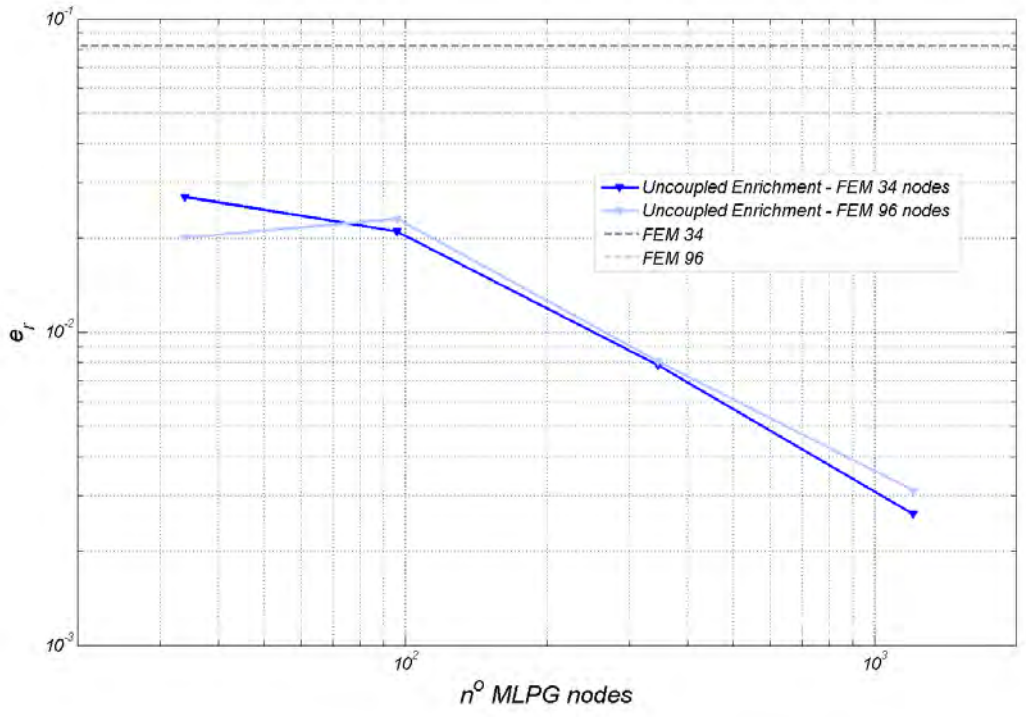

FIGURE 4.7: Convergence graph for displacement $\mathbf{u}$

Note that the position of the particles, in the coarser FEM mesh, has initially taken to be the node pattern as provided by the FE mesh. As a consequence, an initial refinement process, when operated by the user, is simplified. This pattern, which can however be far from the optimal (see table **??**, **??**, and Figure 4.7),

MLPG nodes	e_r^u - on FE-MLPG nodes	e_r^u - on FE nodes	e_r^u - on MLPG nodes
0	$8.02 \cdot 10^{-2}$	$8.02 \cdot 10^{-2}$	-
34	$2.69 \cdot 10^{-2}$	$2.69 \cdot 10^{-2}$	$2.69 \cdot 10^{-2}$
96	$2.09 \cdot 10^{-2}$	$1.68 \cdot 10^{-2}$	$2.22 \cdot 10^{-2}$
346	$7.81 \cdot 10^{-3}$	$5.04 \cdot 10^{-3}$	$8.06 \cdot 10^{-3}$
1209	$2.62 \cdot 10^{-3}$	$3.81 \cdot 10^{-3}$	$2.57 \cdot 10^{-3}$

TABLE 4.4: Relative error e_r in the uncoupeld enrichment, for the coarser FE mesh (34 FE nodes). Note that the 34 MLPG verteces coincides with the 34 vertices of the FE

MLPG nodes	e_r^u - on FE-MLPG nodes	e_r^u - on FE nodes	e_r^u - on MLPG nodes
0	$5.01 \cdot 10^{-2}$	$5.01 \cdot 10^{-2}$	-
34	$2.00 \cdot 10^{-2}$	$2.18 \cdot 10^{-2}$	$1.43 \cdot 10^{-2}$
96	$2.29 \cdot 10^{-2}$	$2.29 \cdot 10^{-2}$	$2.29 \cdot 10^{-2}$
346	$8.04 \cdot 10^{-3}$	$6.58 \cdot 10^{-3}$	$8.42 \cdot 10^{-3}$
1209	$3.11 \cdot 10^{-3}$	$2.98 \cdot 10^{-3}$	$3.12 \cdot 10^{-3}$

TABLE 4.5: Relative error e_r in the uncoupeld enrichment, for the finer FE mesh (96 FE nodes). Note that the 96 MLPG verteces coincides with the 96 vertices of the FE

may be used, for instance, to rapidly assess the accuracy of the initial solution field, as calculated by the FEM, without any further work from the user.

Additionally, even the stress is, on average, more accurate, *except across element edges*, as we'll see later in Figure 4.12, because of the discontinuities initially introduced by the FEM.

MLPG nodes	e_r^σ - FEM 34	e_r^σ - FEM 96
0	$2.41 \cdot 10^{-1}$	$1.15 \cdot 10^{-1}$
34	$2.23 \cdot 10^{-1}$	$1.83 \cdot 10^{-1}$
96	$1.59 \cdot 10^{-1}$	$1.64 \cdot 10^{-1}$
346	$7.69 \cdot 10^{-2}$	$8.90 \cdot 10^{-2}$
1209	$4.85 \cdot 10^{-2}$	$5.93 \cdot 10^{-2}$

TABLE 4.6: Relative error e_r^σ in the uncoupled enrichment

As a consequence, the peak stress, which is located on a FEM node in this example, carries some uncertainty regarding its value of $\boldsymbol{\sigma}$. The stress tensor $\boldsymbol{\sigma}$, as supplied by the FE, is constant over an element, but discontinuous across element edges. Hence, when computing the stress on a node, this node has to be associated

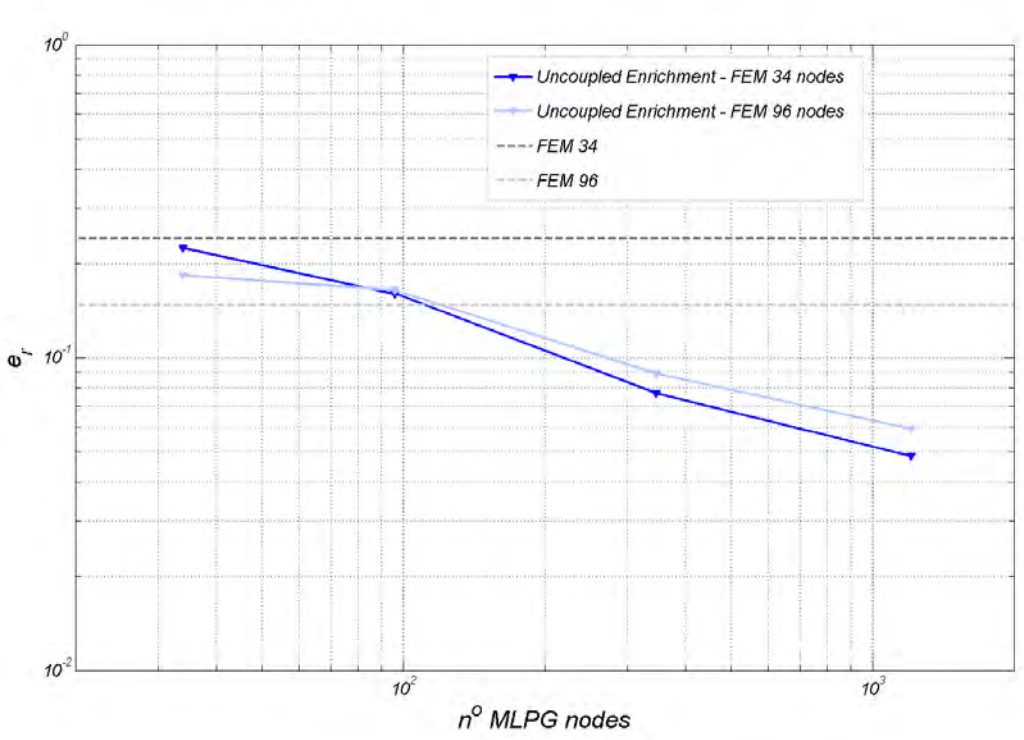

FIGURE 4.8: Convergence graph for stress $\boldsymbol{\sigma}$

with a triangle, and "inherits" its stress tensor. This arbitrary choice depends on the particular match in force during runtime. Since FEM is not backwardly influenced by the particles, the singularity is not reduced, as the density of particles is increased. The stress field may be better compensated elsewhere, but across the edges it cannot be improved. This is an inherent limitation of the uncoupled enrichment.

This is why the accuracy of the peak stress is somewhat less then expected, but still good, as seen in Figure 4.9 and Table

MLPG nodes	$\boldsymbol{\sigma}_{xx}^{peak}$ - FEM 34	$\boldsymbol{\sigma}_{xx}^{peak}$ - FEM 96
0	1.48	2.24
34	2.03	2.66
96	2.64	2.61
346	3.05	2.80
1209	3.16	3.15

TABLE 4.7: Peak stress $\boldsymbol{\sigma}_{xx}^{peak}$ in the uncoupled enrichment

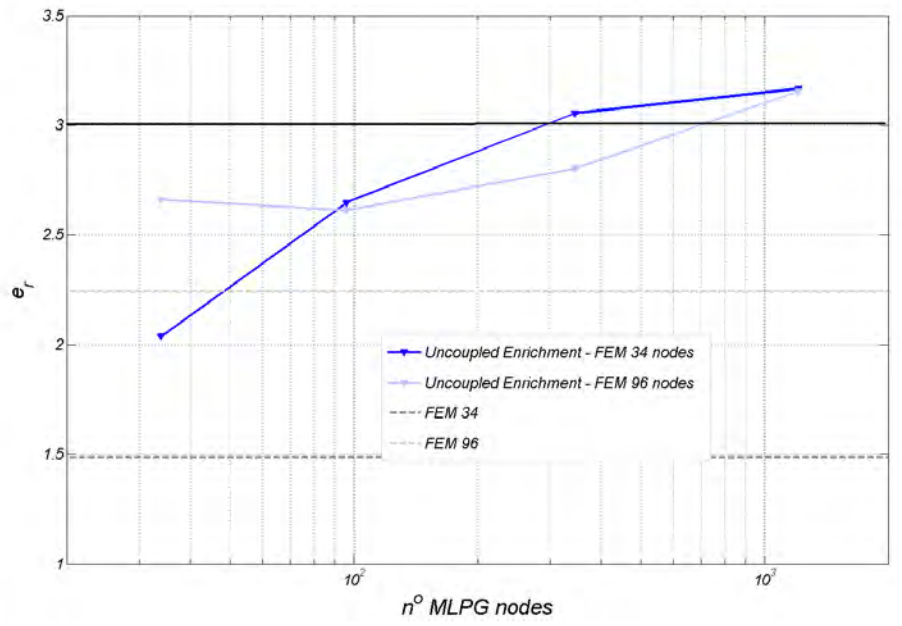

FIGURE 4.9: Peak stress $\boldsymbol{\sigma}_{xx}^{peak}$

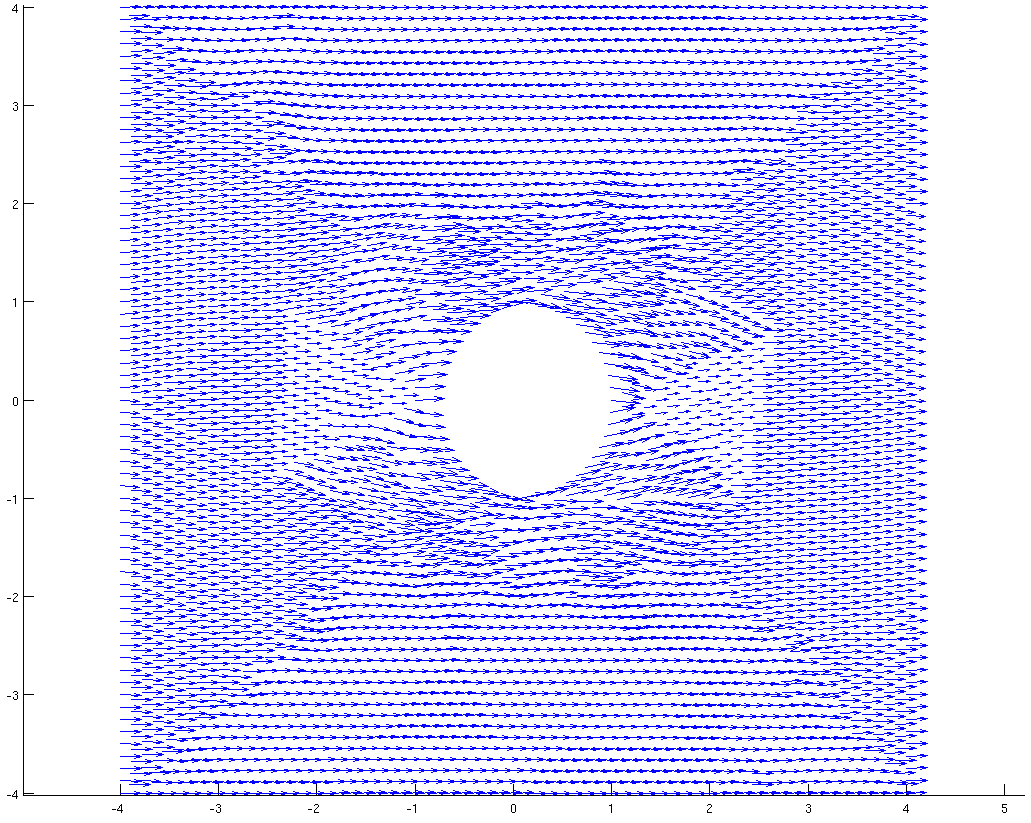

FIGURE 4.10: $\boldsymbol{\sigma} \cdot [1;0]^T$ as calculated by the FEM in the coarser mesh. The discontinuity across the triangles are clearly visible.

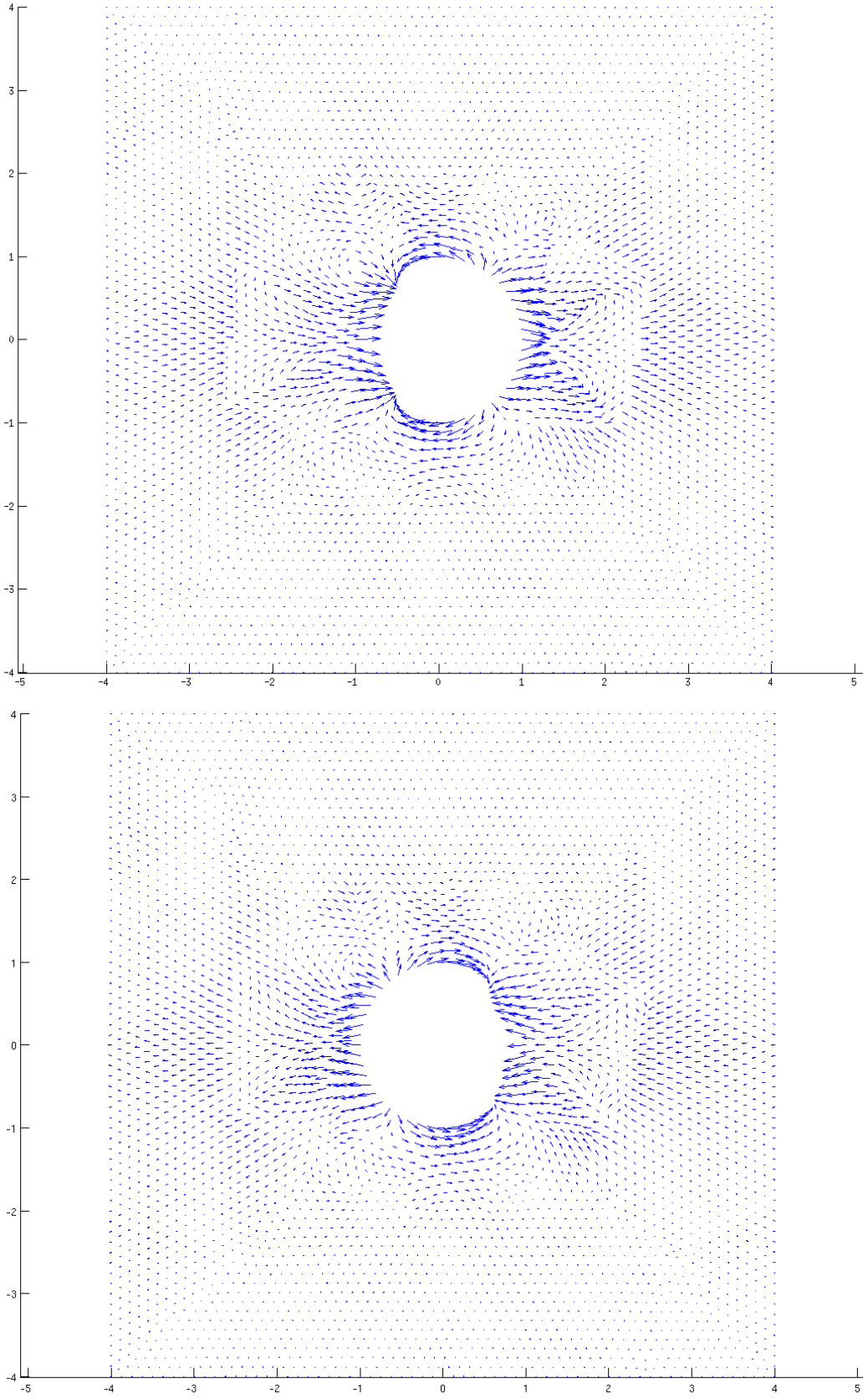

FIGURE 4.11: The error in the stress field $\boldsymbol{\sigma} \cdot [1;0]^T - \boldsymbol{\sigma}^{solution} \cdot [1;0]^T$, as calculated by the FEM, is shown above. Note that the largest contribution is close to the hole. The picture below shows the stress field resulting from MLPG contribution, which is expected to compensate the FEM error. Here the coarser FEM mesh and the finest nodal pattern for MLPG is used

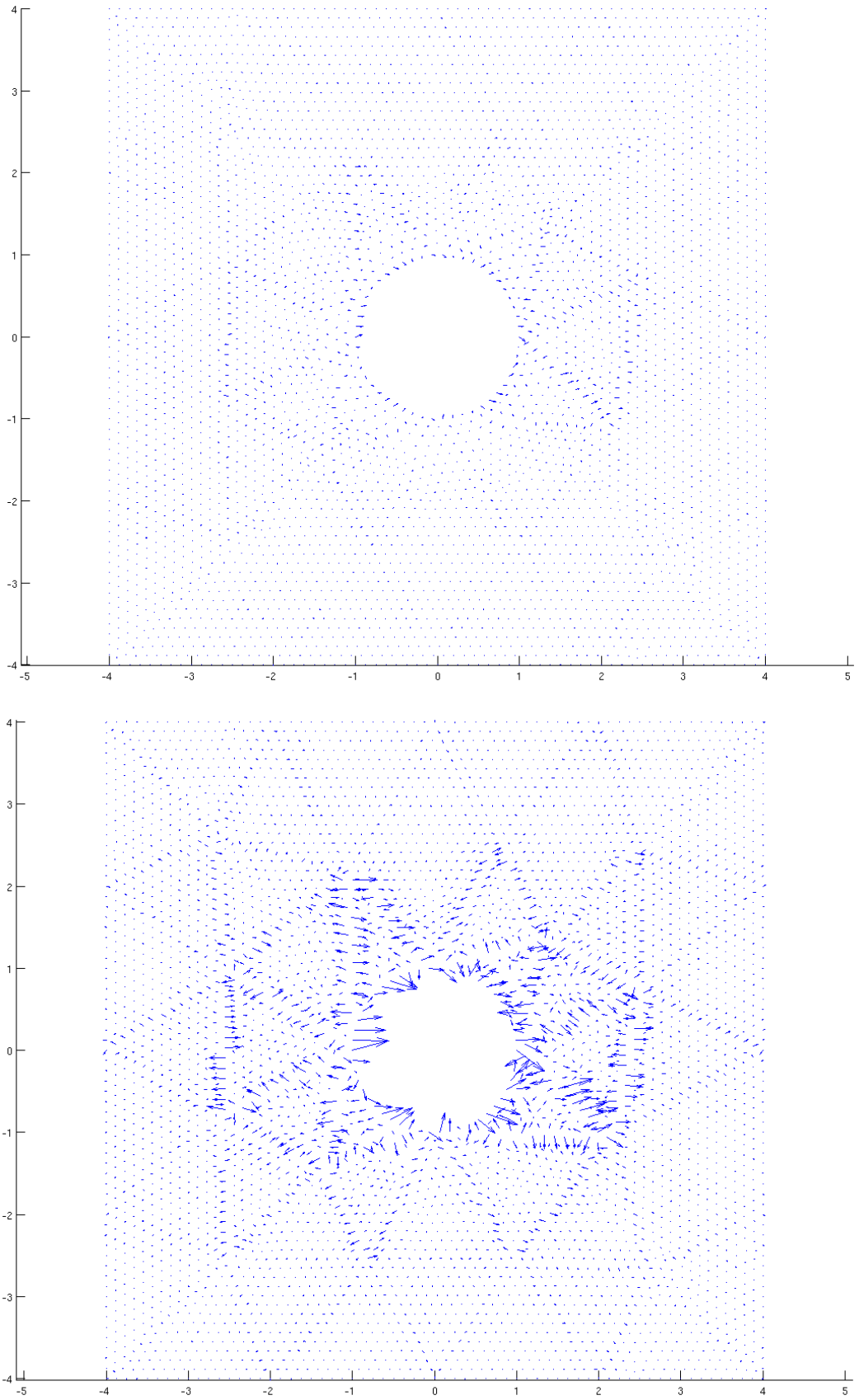

FIGURE 4.12: The final error in the stress field $\boldsymbol{\sigma} \cdot [1;0]^T - \boldsymbol{\sigma}^{solution} \cdot [1;0]^T$ as calculated by the uncoupled enrichment, is shown above. The error has greatly been compensated by the particles. The picture below still gives the error field, with the arrows are magnified 5 times. Here it is much clearer how the biggest error in the stress field stems from the element edges, where the stress field is discontinuous. Here the coarser FEM mesh and the finest nodal pattern for MLPG is used

4.4 Fully Coupled Enrichment

In this section, some numerical results are presented to illustrate the behavior of the global fully coupled enrichment, as introduced and discussed in the previous sections. It has been shown that the final system of equations is nearly singular, if no action is taken to eliminate the zero eigenvalues.

Different approaches may be used to eliminate the zero eigenvalues, as already explained. In particular, it is possible to impose two different types of boundary conditions, *separately* on FEM and on MLPG, that is:

- the actual boundary conditions at $\partial\Omega$ on FEM
- zero displacement at $\partial\Omega$ on MLPG

without any coupling[7] on the boundary conditions, as outlined before. In the interior of the computational domain, conversely, both contributions interact to form the solution field. The drawback of this approach is that the quality of the boundary conditions is limited by that of the basis being enriched, i.e., FE. Since the displacement field at the boundary may have a non linear feature, it cannot be represented by triangular FE, hence this type of enrichment ultimately may not converge to the analytical solution if only the number of particles is increased. However, in this example, the boundary conditions are prescribed at a distance of four times the dimension of the hole, and this effect is not initially[8] sensitive.
The actual shape of the computational domain allows for another approach, as implemented in the present numerical experiment, that is, the system:

$$\begin{bmatrix} \mathbf{K}^{\Omega}_{FE} + \mathbf{K}^{Dir}_{FE} + \mathbf{K}^{t_{Dir}}_{FE} & \mathbf{K}^{\Omega}_{MF} + \mathbf{K}^{Dir}_{MF} + \mathbf{K}^{t_{Dir}}_{MF} \\ \mathbf{K}^{\Omega}_{FM} & \mathbf{K}^{\Omega}_{ML} + \mathbf{K}^{Dir}_{ML} + \mathbf{K}^{t_{Dir}}_{ML} \end{bmatrix} \cdot \begin{bmatrix} \mathbf{u}_{FE} \\ \mathbf{u}_{ML} \end{bmatrix} = \begin{bmatrix} \mathbf{f}^{dist}_{FE} + \mathbf{f}^{Dir}_{FE} + \mathbf{f}^{Neu}_{FE} \\ \mathbf{f}^{dist}_{ML} + \mathbf{f}^{Dir}_{ML} + \mathbf{f}^{Neu}_{ML} \end{bmatrix}$$

is not singular, and admits unique solution. In this case, an uncoupled enrichment "on the boundary conditions" is implemented. That is, MLPG is required to satisfy the boundary conditions independently, all around the plate. As a result, the MLPG solution is fixed, at the boundary of the computational domain,

[7] K^{Dir} and $K^{t_{Dir}}$ are not computed in the coupling blocks.
[8] as long as the nodal density of the enriching basis is not too high

where FEM improves the satisfaction of the essential boundary conditions, hence obtaining a *quasi*-fully coupled enrichment. It is recommended that MLPG satisfy the essential boundary conditions independently. In this case, as we'll see later on in Figure 4.17 the contribution to the solution field $\mathbf{u}^h$ is mainly due to $\mathbf{u}^h_{ML}$. This effect is beneficial, because it keeps the FEM contribution $\mathbf{u}^h_{FE}$ low. This is important for a better stress prediction when MLPG alone is refined. A more theoretical proof of this fact will not be given in the present Thesis, but it is noted that the present numerical experiment seems to support this conjecture, which is also a necessary condition for a proper representability of the actual peak stress. The numerical results are reported in Figures 4.13, 4.14, 4.15, and Tables 4.8, 4.9, 4.10, 4.11, when the number of MLPG nodes is increased.

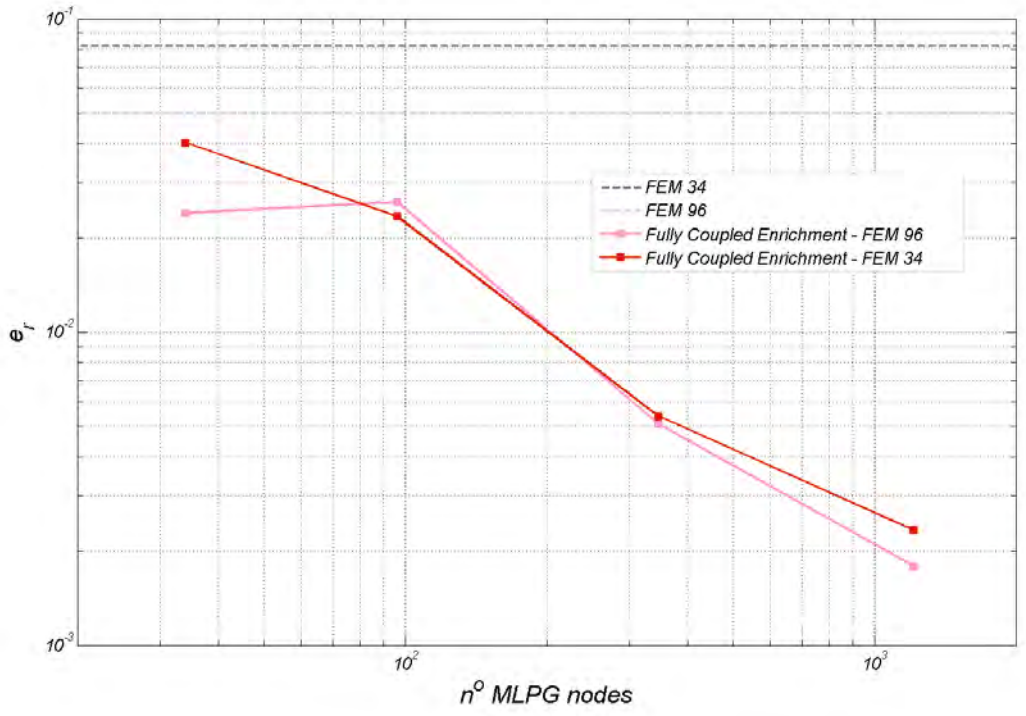

FIGURE 4.13: Convergence for the displacement $\mathbf{u}$ of the fully coupled enrichment

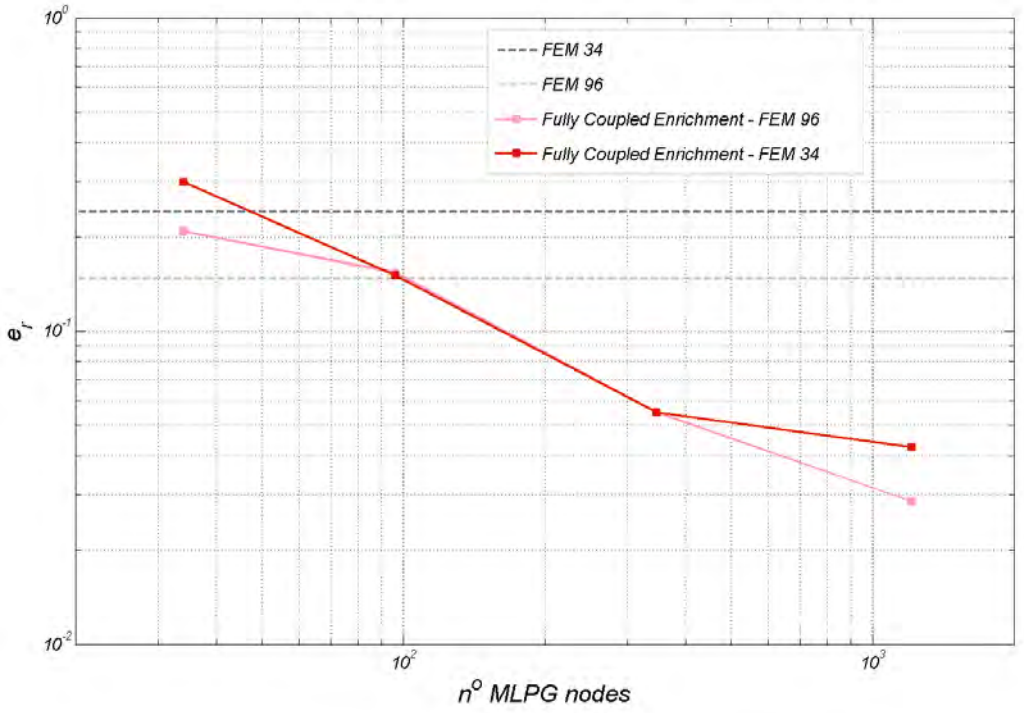

FIGURE 4.14: Convergence graph for stress $\boldsymbol{\sigma}$

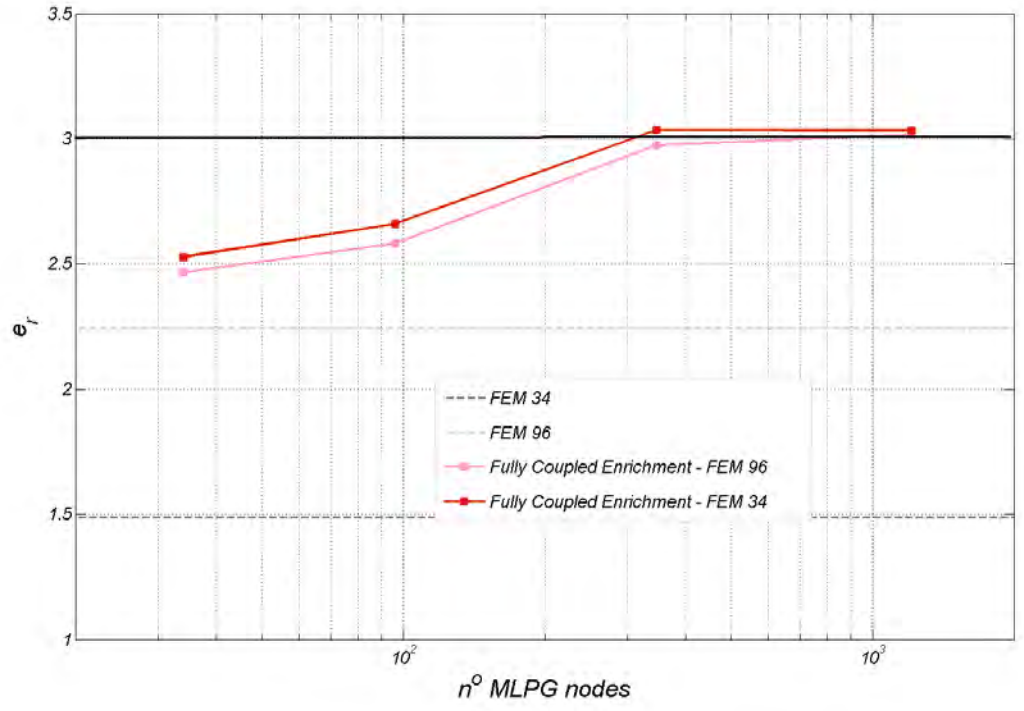

FIGURE 4.15: Peak stress $\boldsymbol{\sigma}_{xx}^{peak}$

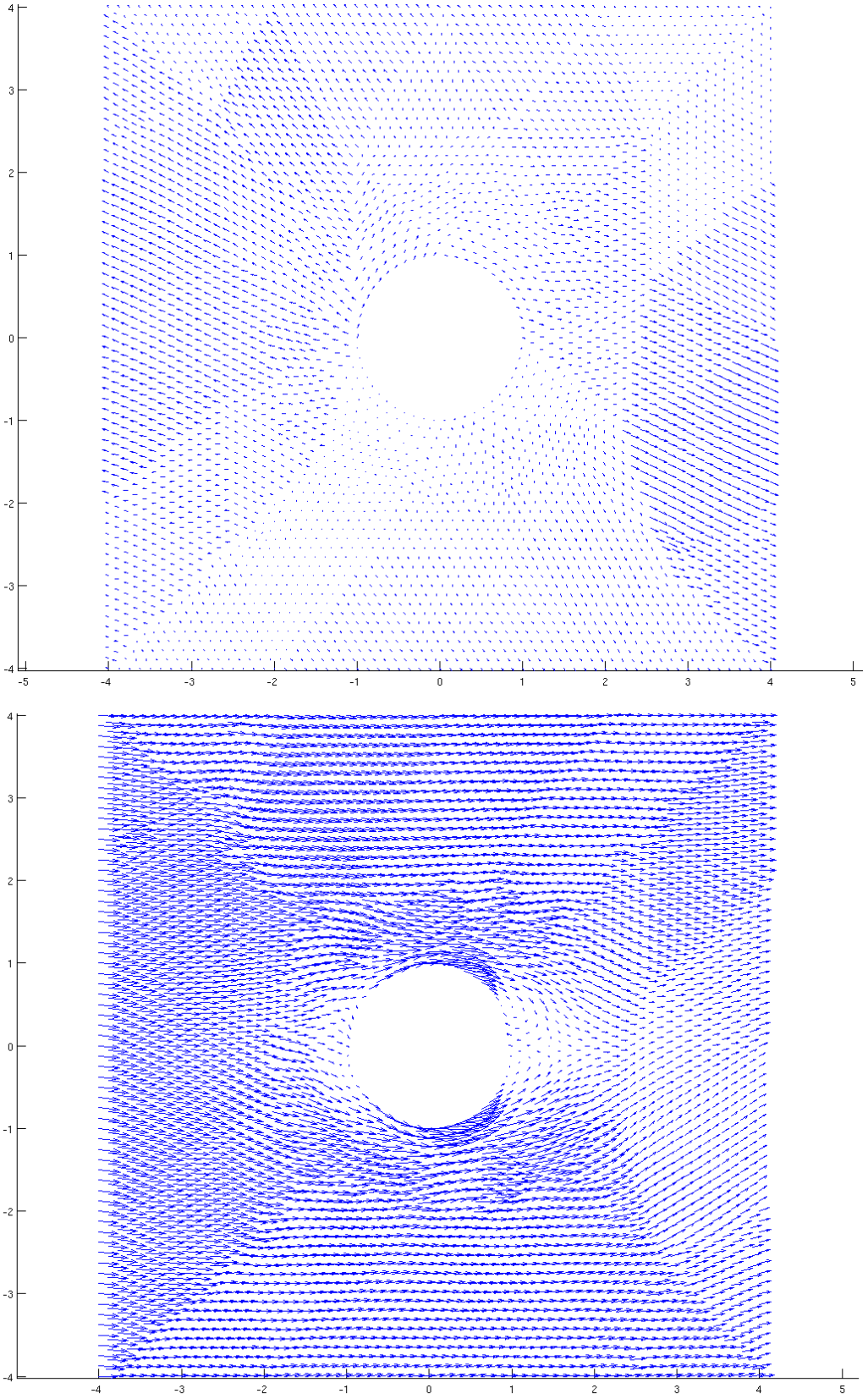

FIGURE 4.16: Stress field contribution $\boldsymbol{\sigma} \cdot [1;0]^T$ as calculated by the FEM (first image) and by MLPG (second image). The coarser FEM mesh and the finest MLPG pattern are used. It is seen that the FEM contribution to the final stress field is much lower, in value, then the unenriched one. The majority of the solution field, and that of the stress, is mainly due to MLPG. The resulting effect is that the discontinuities introduced by FEM are kept low, allowing for a much more uniform stress field.

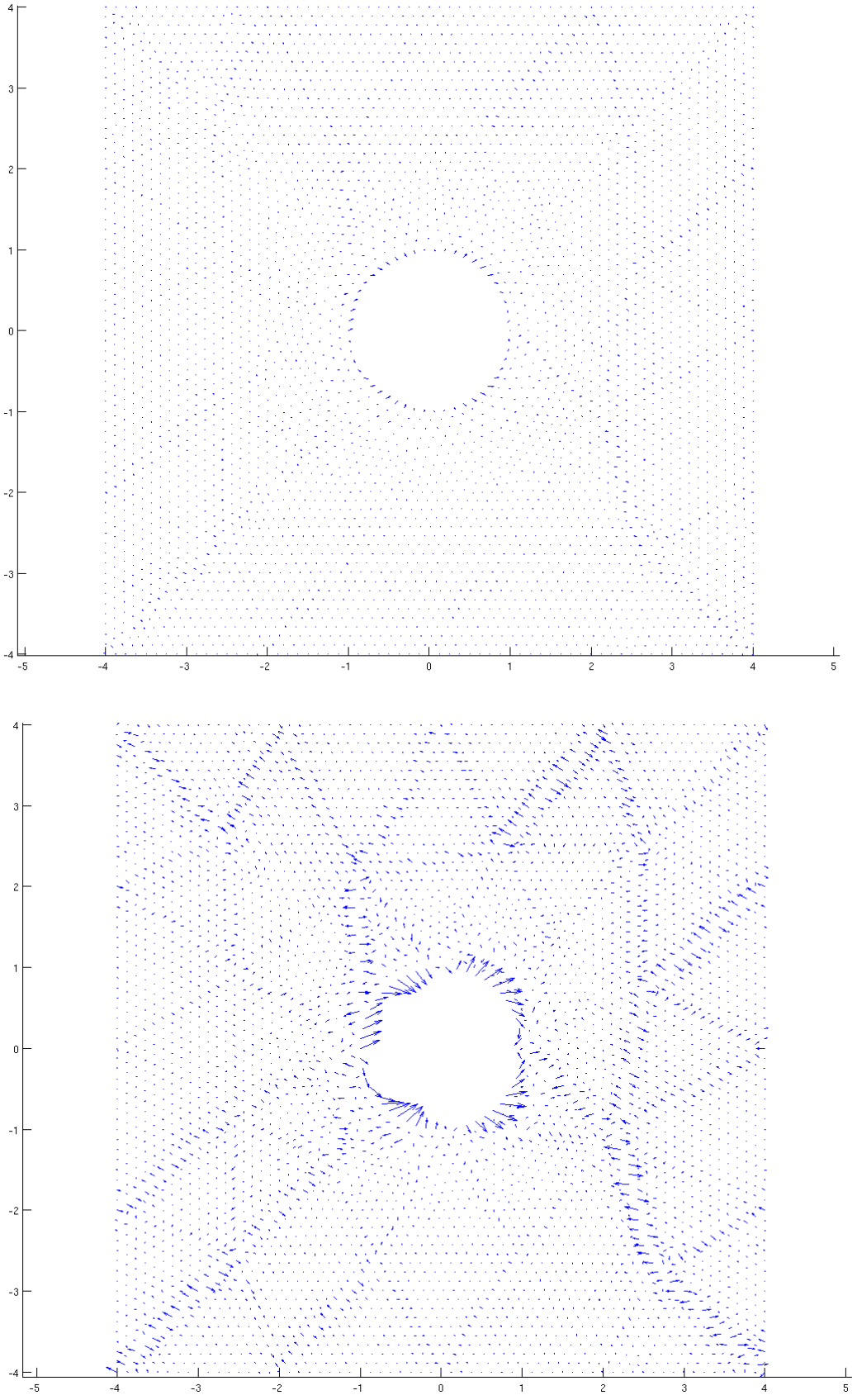

FIGURE 4.17: Stress field error $\boldsymbol{\sigma} \cdot [1;0]^T - \boldsymbol{\sigma}^{solution} \cdot [1;0]^T$ as calculated by the fully coupled enrichment. The coarser FEM mesh and the finest MLPG pattern are used. The discontinuities seen in the uncoupled enrichment have been partially reduced in the present approach. Note also, in the second picture, where the arrows are magnified 5 times, that the greatest error in the stress field happens to be near the hole, with a similar error field as if the MLPG solution was calculated separately.

MLPG nodes	e_r^u - on FE-MLPG nodes	e_r^u - on FE nodes	e_r^u - on MLPG nodes
0	$8.02 \cdot 10^{-2}$	$8.02 \cdot 10^{-2}$	-
34	$2.69 \cdot 10^{-2}$	$4.02 \cdot 10^{-2}$	$2.69 \cdot 10^{-2}$
96	$2.09 \cdot 10^{-2}$	$2.16 \cdot 10^{-2}$	$2.22 \cdot 10^{-2}$
346	$7.81 \cdot 10^{-3}$	$3.94 \cdot 10^{-3}$	$8.06 \cdot 10^{-3}$
1209	$2.62 \cdot 10^{-3}$	$1.91 \cdot 10^{-3}$	$2.57 \cdot 10^{-3}$

TABLE 4.8: Relative error e_r in the fully coupled enrichment, for the coarser FE mesh (34 FE nodes). Note that the 34 MLPG verteces coincides with the 34 vertices of the FE

MLPG nodes	e_r^u - on FE-MLPG nodes	e_r^u - on FE nodes	e_r^u - on MLPG nodes
0	$5.01 \cdot 10^{-2}$	$5.01 \cdot 10^{-2}$	-
34	$2.39 \cdot 10^{-2}$	$2.37 \cdot 10^{-2}$	$2.45 \cdot 10^{-2}$
96	$2.59 \cdot 10^{-2}$	$2.59 \cdot 10^{-2}$	$2.59 \cdot 10^{-2}$
346	$5.09 \cdot 10^{-3}$	$5.16 \cdot 10^{-3}$	$5.07 \cdot 10^{-3}$
1209	$1.79 \cdot 10^{-3}$	$1.61 \cdot 10^{-3}$	$1.80 \cdot 10^{-3}$

TABLE 4.9: Relative error e_r in the fully coupled enrichment, for the finer FE mesh (96 FE nodes). Note that the 96 MLPG verteces coincides with the 96 vertices of the FE

MLPG nodes	e_r^σ - FEM 34	e_r^σ - FEM 96
0	$2.41 \cdot 10^{-1}$	$1.15 \cdot 10^{-1}$
34	$2.29 \cdot 10^{-1}$	$2.08 \cdot 10^{-1}$
96	$1.50 \cdot 10^{-1}$	$1.53 \cdot 10^{-1}$
346	$5.50 \cdot 10^{-2}$	$5.50 \cdot 10^{-2}$
1209	$4.26 \cdot 10^{-2}$	$2.86 \cdot 10^{-2}$

TABLE 4.10: Relative error e_r^σ in the fully coupled enrichment

MLPG nodes	$\boldsymbol{\sigma}_{xx}^{peak}$ - FEM 34	$\boldsymbol{\sigma}_{xx}^{peak}$ - FEM 96
0	1.48	2.24
34	2.52	2.46
96	2.65	2.58
346	3.03	2.97
1209	3.03	3.01

TABLE 4.11: Peak stress $\boldsymbol{\sigma}_{xx}^{peak}$ in the fully coupled enrichment

4.5 Inverted Uncoupled Enrichment

It is worth noting that only in a global enrichment the meshless problem can also be solved first and independently, i.e., the following system can be solved:

$$\begin{cases} \mathbf{K}_{FE}\mathbf{u}_{FE} + \mathbf{K}_{MF}\mathbf{u}_{ML} &= \mathbf{b}_{FE} \\ \mathbf{K}_{ML}\mathbf{u}_{ML} &= \mathbf{b}_{ML} \end{cases} \tag{4.1}$$

This is very similar to the proposed uncoupled enrichment, only that now $\mathbf{K}_{FM}$ is neglected instead of $\mathbf{K}_{MF}$. The advantage of such an approach lies in the superior ability of the procedure to better reproduce the stress field, compared to the previous uncoupled enrichment already detailed. In this case, the "larger part" of the solution field $\mathbf{u}^h$ is calculated by MLPG, irrespective of the nodal density, while FEM enhances the solution. The discontinuities in the stress field are expected to be smaller. Apart from this remarkable difference, all of the previous considerations for the uncoupled enrichment apply here, too.
However, in this approach, both equations have to be solved again, if the density of MLPG nodes is repeatedly increased. In addition, the computation of the matrix $\mathbf{K}_{MF}$ is markedly more expensive than that of $\mathbf{K}_{FM}$, as the MLPG shape functions are involved in the computation. Further, if the enriched region does not extend until the boundary of the computational domain[9], this approach can no longer be used. For these reasons, this type of uncoupled enrichment, although capable of a stable improvement, is reported in this section and not elsewhere discussed in this Thesis.

MLPG nodes	e_r^u - FEM 34	e_r^u - FEM 96
0	$8.02 \cdot 10^{-2}$	$5.01 \cdot 10^{-2}$
34	$4.08 \cdot 10^{-2}$	$2.52 \cdot 10^{-2}$
96	$2.16 \cdot 10^{-2}$	$2.16 \cdot 10^{-2}$
346	$4.43 \cdot 10^{-3}$	$4.27 \cdot 10^{-3}$
1209	$3.12 \cdot 10^{-3}$	$1.08 \cdot 10^{-3}$

TABLE 4.12: Relative error e_r in the inverted uncoupled enrichment

[9] actually the local subdomains need to cover the whole computational area, as detailed before

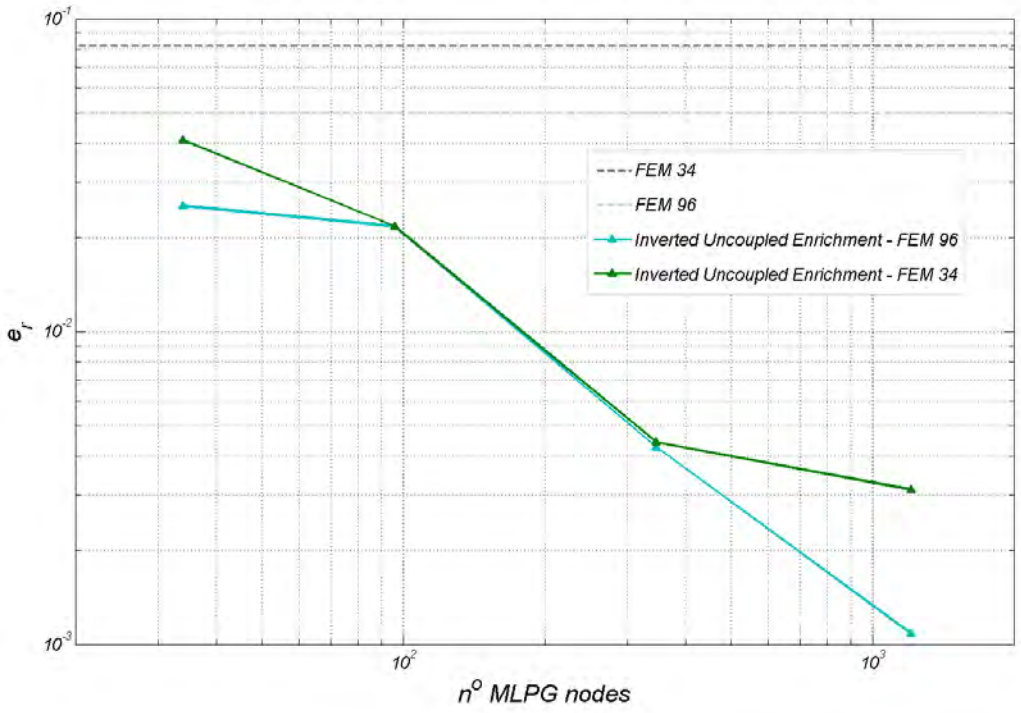

FIGURE 4.18: Convergence graph for displacement $\mathbf{u}$

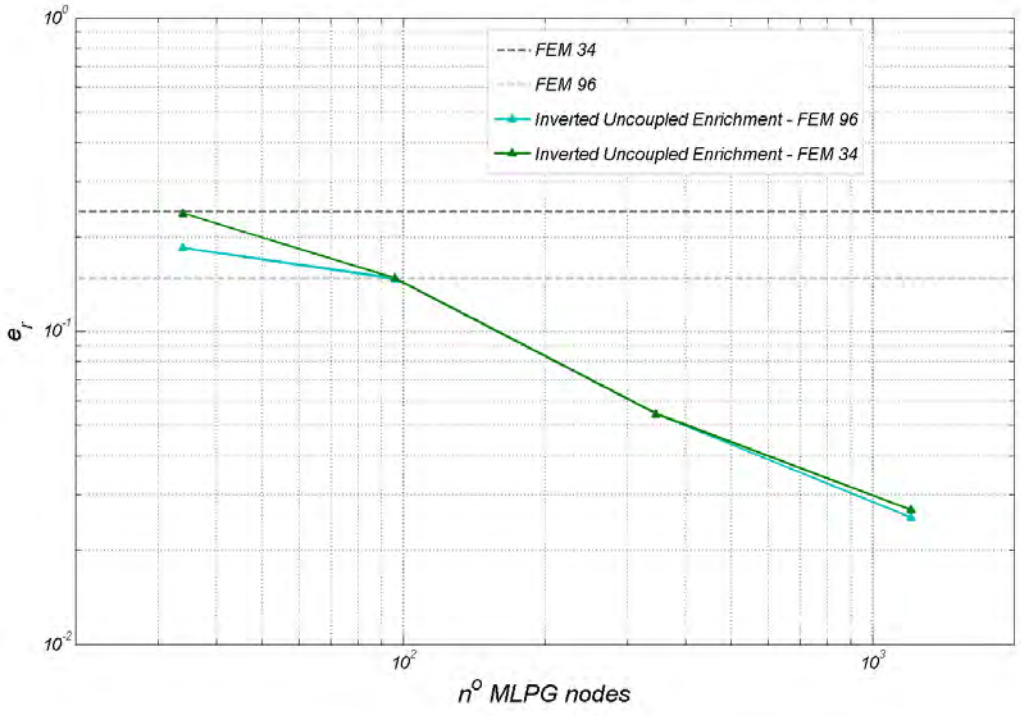

FIGURE 4.19: Convergence graph for stress $\boldsymbol{\sigma}$

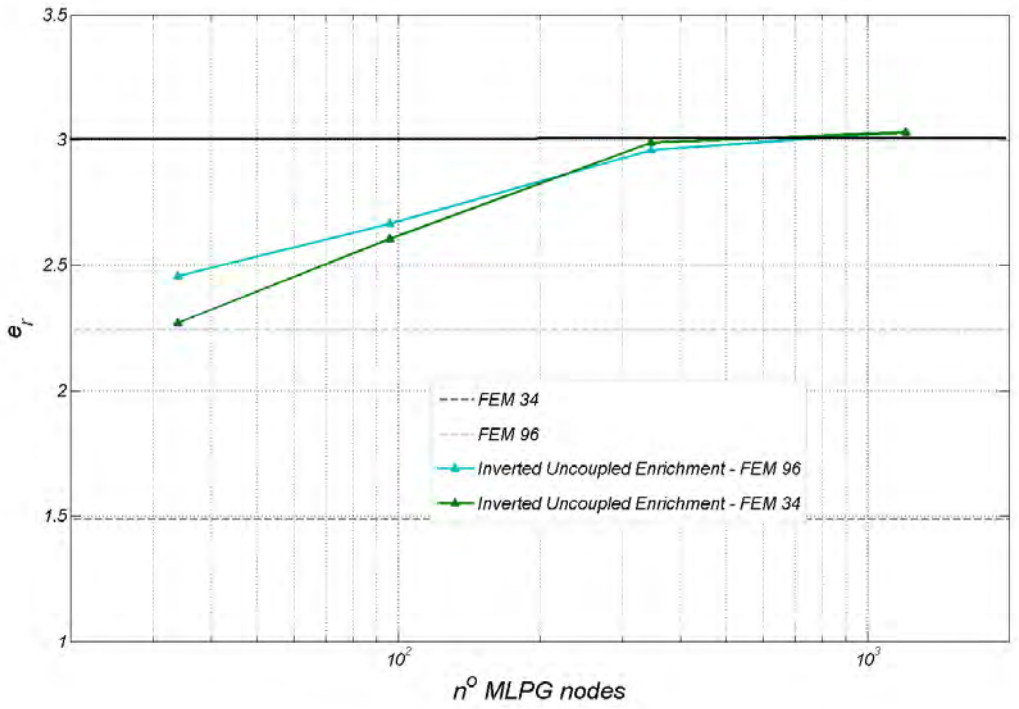

FIGURE 4.20: Peak stress $\boldsymbol{\sigma}_{xx}^{peak}$

MLPG nodes	e_r^{σ} - FEM 34	e_r^{σ} - FEM 96
0	$2.41 \cdot 10^{-1}$	$1.15 \cdot 10^{-1}$
34	$2.23 \cdot 10^{-1}$	$1.18 \cdot 10^{-1}$
96	$1.47 \cdot 10^{-1}$	$1.47 \cdot 10^{-1}$
346	$5.42 \cdot 10^{-2}$	$5.42 \cdot 10^{-2}$
1209	$2.68 \cdot 10^{-2}$	$2.53 \cdot 10^{-2}$

TABLE 4.13: Relative error e_r^{σ} in the inverted uncoupled enrichment

MLPG nodes	$\boldsymbol{\sigma}_{xx}^{peak}$ - FEM 34	$\boldsymbol{\sigma}_{xx}^{peak}$ - FEM 96
0	1.48	2.24
34	2.27	2.45
96	2.60	2.66
346	2.98	2.95
1209	3.03	3.03

TABLE 4.14: Peak stress $\boldsymbol{\sigma}_{xx}^{peak}$ in the inverted uncoupled enrichment

4.6 Influence of the Quadrature Scheme

The need for a proper quadrature scheme, in the computation of the stiffness matrix, which is ultimately reflected in a proper domain decomposition, has already been discussed. This section shows numerically the effect of quadrature schemes that does not meet the required accuracy.

The performance of the enrichment depends on the accuracy of the computation of the $\mathbf{K}_{ML}$ block. This Thesis will not deal with this aspect, which is well known in literature ([17]). This subsection only deals with the results of a simple integration scheme, to form the entries of the coupling blocks $\mathbf{K}_{FM}$ and $\mathbf{K}_{MF}$. This scheme maps 12 x 12 sample points from $[-1;1]^2 \subset \mathbb{R}^2$ to the circle Ω_{test} or Ω_{trial}, by the use of a polar coordinate transformation. As a result, the integrand is a discontinuous function. The quadrature scheme implemented in the rest of the Thesis, conversely, is highly accurate. Further increase in the number of quadrature points does not lead to any meaningful variation of the solution; hence, it will be used as a benchmark. The convergence graph gives numerical evidence to what was previously outlined in the "Critical Assessment". An integration over Ω_{test} and Ω_{trial} is far from being optimal. However, as the density of particles is increased, the limitation due to an inaccurate quadrature scheme seems to become less dramatic, in the uncoupled enrichment. Indeed, as the nodal density for MLPG is increased, Ω_{test} hardly ever intersects with element edges, and the integrand is no longer discontinuous. As a result, the integration is carried out with increasing numerical accuracy, as can be seen in Figure **??**. The low density of particles may be compensated, to some extent, by increasing the number of quadrature points, at the price of a slightly[10] higher computational cost. However, the situation is more problematic if the the density of MLPG is lower than that of FEM. In practice, anyway, the user should never be requested to take into account all these aspects to select the "proper" number of quadrature points; such a choice is, in general, problem-dependent.

Finally, it is noted that the radius of the Ω^{ML}_{trial} which is bigger than that of Ω^{ML}_{test} , and the already detailed complex feature of Φ_{ML}, do not lead to any acceptable results in the fully coupled enrichment, when the numerical errors associated with such a simpler quadrature scheme are overlooked, as can be seen in Figure 4.21

[10] recall that MLPG's shape functions are not involved in $\mathbf{K}_{FM}$

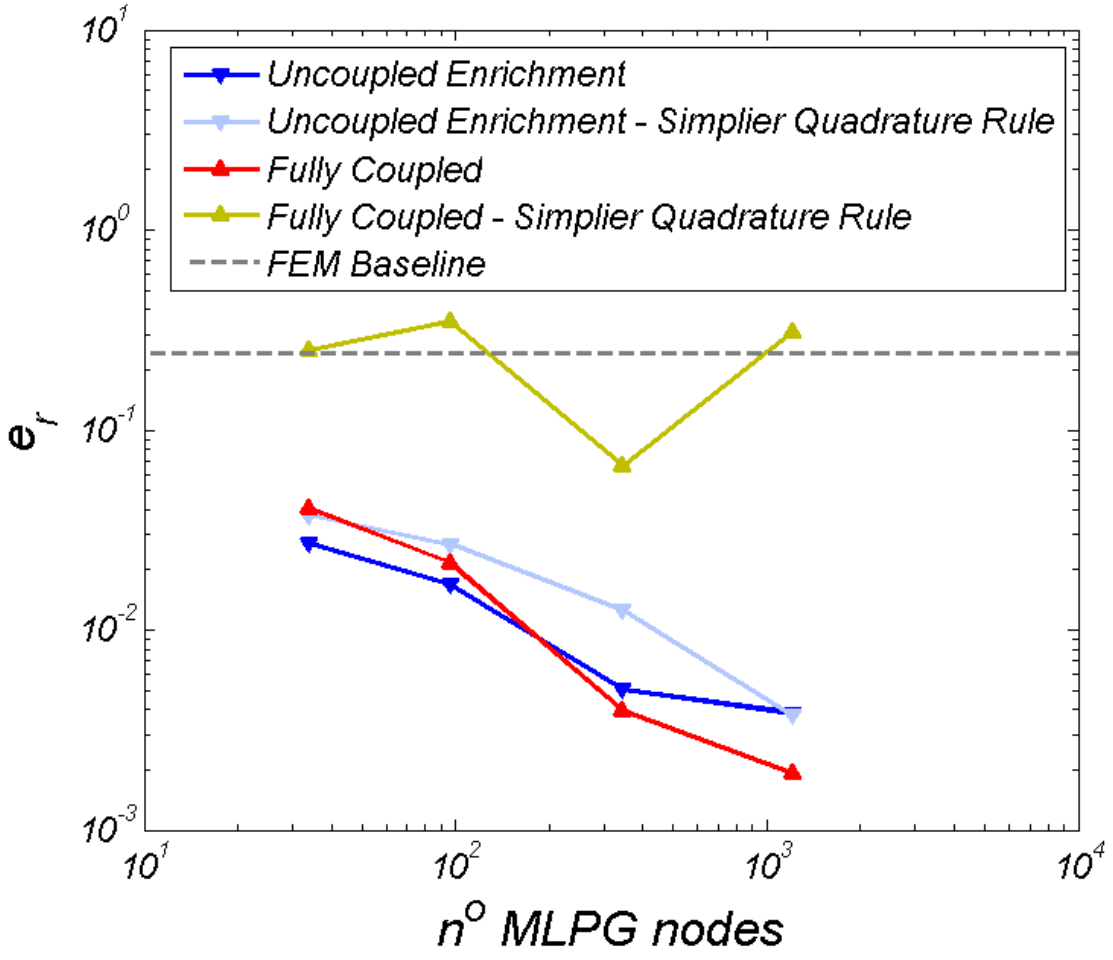

FIGURE 4.21: Comparison of the convergence graph for displacement **u** for the coarser FE mesh. The simpler quadrature rule uses 12x12 sample points

4.7 Local Enrichment

The idea of performing a local enrichment, to improve the solution where it is needed, has already been discussed. This section reports some numerical results of a local enrichment in the selected test case. The purpose, in this case, is to better reproduce the solution near the hole. To this aim, different nodal patterns are used, as shown in Figure 4.22.

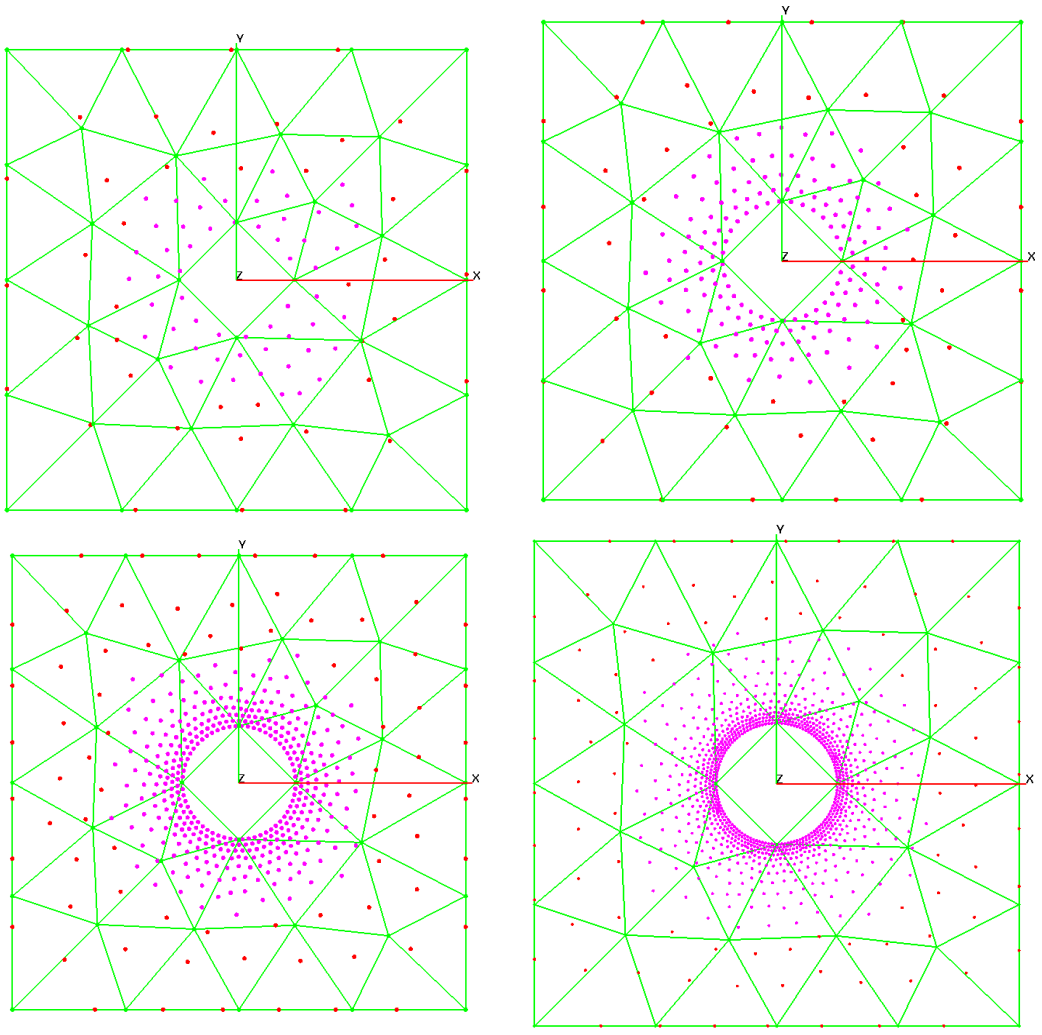

FIGURE 4.22: Nodal pattern for MLPG in the local enrichment. The red nodes have been imposed fictitious zero displacement, hence they do not take part in the computation. Note also that the enriched area is the greatest possible

Compatibility conditions are enforced at the boundaries of the enriched region, that may be defined as the greatest region for the which the MLS approximation is well defined. To tacitly avoid the geometrical difficulties due to this definition,

the outer nodes have been enforced to have fictitious zero displacement, thus ensuring the compatibility conditions between the two solution field, i.e., $\mathbf{u}^h_{ML} = \mathbf{u}^h_{FE}$. Note also, the enriched region, in this numerical experiment, extends as close as possible to the boundaries. It is seen that while the computation of the solution $\mathbf{u}$ suffers from the locality of the enrichment (see Table 4.15, 4.16 and Figure 4.23), the improvement in the stress field, and in the prediction of the peak stress, has proven to be more effective (see Table 4.18, 4.19 and Figures 4.24, 4.25). This happens because the greatest contribution to the error in the stress field stems from a region in the immediate vicinity of the hole, and hence it is a local effect. However, despite this improvement, it is necessary to extend the enriched region until the boundaries, to achieve full convergence of any value of interest. This is not a limitation of the method, rather, it appears to be a limitation of doing a local enrichment only.

As a concluding remark, an inexpensive way to enhance the prediction of the local stress field, by the use of an uncoupled enrichment, in a stable way, may be that of "nesting" the local MLPG problem in the FEM parent, global domain. The solution $\mathbf{u}^h_{FE}$, as calculated by the FEM, would serve as a boundary condition to the MLPG problem. In this case, since MLPG scheme solves "ex-novo" the elastostatics problem in the small area of interest, it is not difficult to envision that the discontinuities associated with the FEM solution are entirely avoided. Moreover, this approach will also avoid all of the integration problems associated with the computation of the coupling block; such an approach was, however, outside the scope of the present Thesis.

MLPG nodes	e^u_r - on FE-MLPG nodes	e^u_r - on FE nodes	e^u_r - on MLPG nodes
0	$8.02 \cdot 10^{-2}$	$8.02 \cdot 10^{-2}$	-
57	$7.95 \cdot 10^{-2}$	$3.88 \cdot 10^{-2}$	$1.11 \cdot 10^{-1}$
152	$9.44 \cdot 10^{-2}$	$3.99 \cdot 10^{-2}$	$1.11 \cdot 10^{-1}$
389	$9.19 \cdot 10^{-2}$	$3.68 \cdot 10^{-2}$	$9.88 \cdot 10^{-2}$
906	$6.94 \cdot 10^{-2}$	$2.82 \cdot 10^{-2}$	$7.16 \cdot 10^{-2}$

TABLE 4.15: Relative errors e_r in the uncoupled local enrichment.

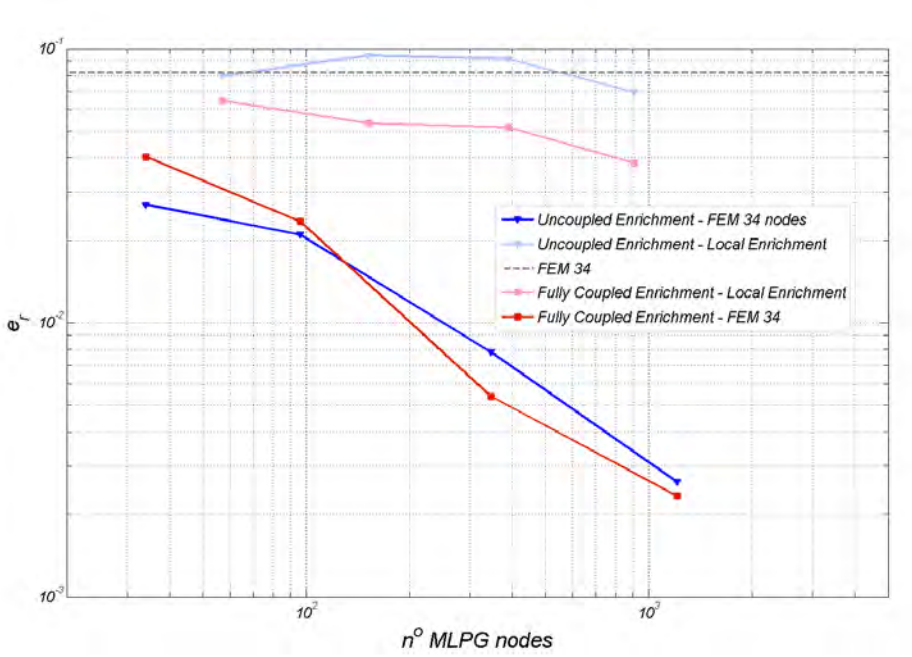

FIGURE 4.23: Convergence graph for displacement of a local fully coupled and uncoupled enrichment on the coarser FEM mesh.

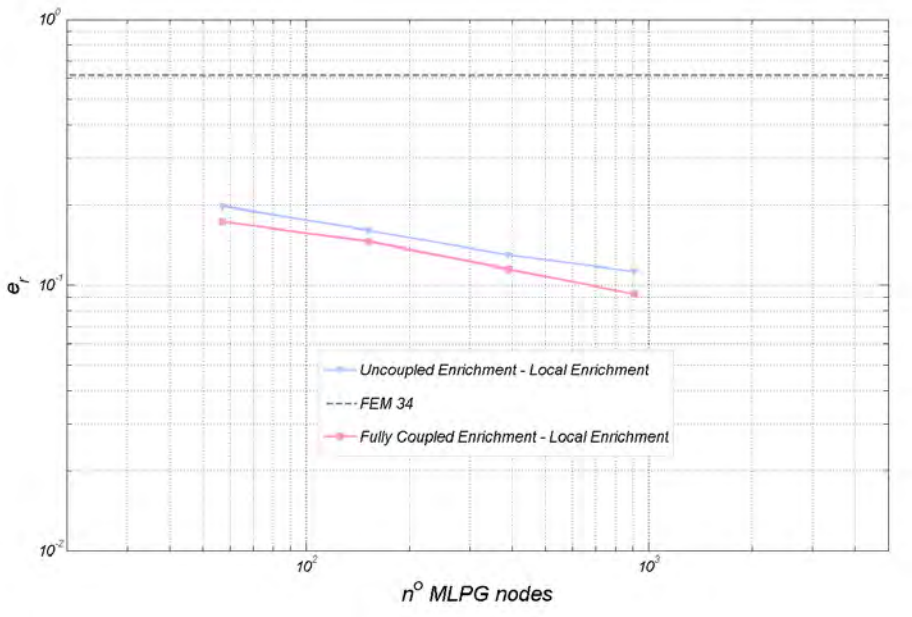

FIGURE 4.24: Convergence graph for stress of a local fully coupled and uncoupled enrichment on the coarser FEM mesh, here intentionally cal- culated on the finest nodal pattern of MLPG, as used in this local enrichment

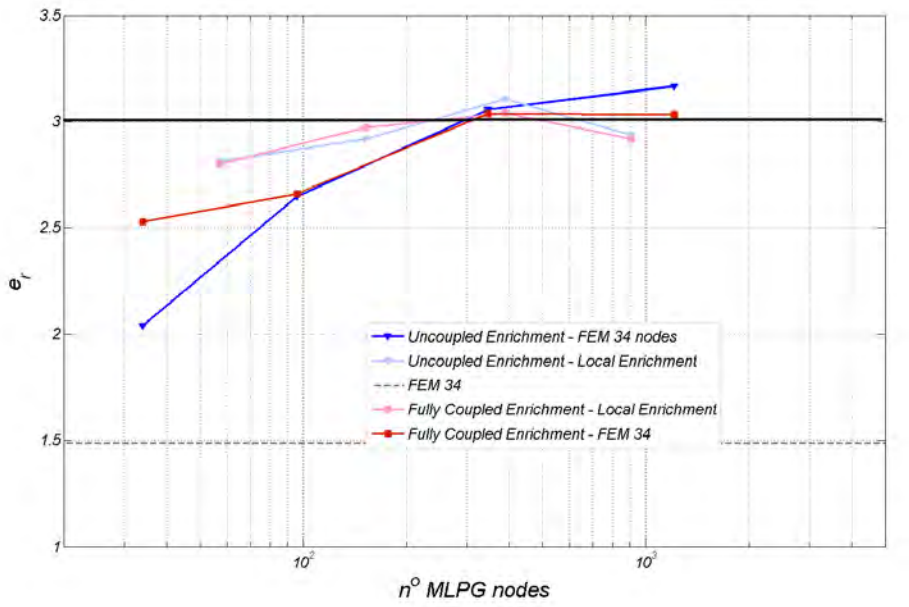

FIGURE 4.25: Peak stress for the local fully coupled and uncoupled enrichment on the coarser FEM mesh.

MLPG nodes	e_r^u - on FE-MLPG nodes	e_r^u - on FE nodes	e_r^u - on MLPG nodes
0	$8.02 \cdot 10^{-2}$	$8.02 \cdot 10^{-2}$	-
57	$6.45 \cdot 10^{-2}$	$2.99 \cdot 10^{-2}$	$9.13 \cdot 10^{-1}$
152	$5.33 \cdot 10^{-2}$	$2.17 \cdot 10^{-2}$	$6.28 \cdot 10^{-1}$
389	$5.15 \cdot 10^{-2}$	$1.95 \cdot 10^{-2}$	$5.55 \cdot 10^{-2}$
906	$3.82 \cdot 10^{-2}$	$1.35 \cdot 10^{-2}$	$3.95 \cdot 10^{-2}$

TABLE 4.16: Relative errors e_r in the fully coupled local enrichment. Since the MLPG nodes backwardly influence the FEM solution, the improvement is more effective than that of the uncoupled enrichment

MLPG nodes	e_r^u - uncoupled	e_r^u - fully coupled
0	$8.02 \cdot 10^{-2}$	$8.02 \cdot 10^{-2}$
57	$7.95 \cdot 10^{-2}$	$6.45 \cdot 10^{-2}$
152	$9.44 \cdot 10^{-2}$	$5.33 \cdot 10^{-2}$
389	$9.19 \cdot 10^{-2}$	$5.15 \cdot 10^{-2}$
906	$6.94 \cdot 10^{-2}$	$3.82 \cdot 10^{-2}$

TABLE 4.17: Comparison of relative errors e_r in the local enrichment, calculated on FE and MLPG nodes.

MLPG nodes	e_r^σ - uncoupled	e_r^σ - fully coupled
0	$6.16 \cdot 10^{-1}$	$6.16 \cdot 10^{-1}$
34	$1.97 \cdot 10^{-1}$	$1.72 \cdot 10^{-1}$
96	$1.60 \cdot 10^{-1}$	$1.45 \cdot 10^{-1}$
346	$1.29 \cdot 10^{-1}$	$1.11 \cdot 10^{-1}$
1209	$1.12 \cdot 10^{-1}$	$9.23 \cdot 10^{-2}$

TABLE 4.18: Relative error e_r^σ in the local enrichment, here intentionally calculated on the finest nodal pattern of MLPG, as used in this local enrichment

MLPG nodes	$\boldsymbol{\sigma}_{xx}^{peak}$ - uncoupled	$\boldsymbol{\sigma}_{xx}^{peak}$ - fully coupled
0	1.48	2.24
34	2.81	2.80
96	2.91	2.97
346	3.10	3.03
1209	2.93	2.99

TABLE 4.19: Peak stress comparison $\boldsymbol{\sigma}_{xx}^{peak}$ in the local enrichment

4.8 Actual Geometry versus Discretized Geometry

The Finite Element Method introduces a mesh that provides a partition of the computational domain Ω_{comp}, which is generally different from the domain Ω, as can be seen form Figure 4.26. In the present test case, the geometry of the hole is approximated by the use of triangles, used when computing the entries for the $\mathbf{K}_{FE}$ block. Hence, the discretization error occurs also in creation of the computational domain, and is reflected in the FEM test functions. Other approaches are also possible, such as using triangles with curved edges, but they are not considered in the present Thesis. As the functional space for FEM alone is increased, the geometry of the hole can be represented with increasing accuracy, by the use of a higher number of triangles that describes its geometry. This is different from refining only the initial computational domain Ω_{comp}, without changing the discretized geometry. In this latter case, convergence would be achieved towards a different problem, that has that different geometry as an actual domain Ω.
This suggest the need to account for the actual geometry of the computational domain, when the enrichment is carried out. Consider, for instance, the uncoupled enrichment. The FEM solution is calculated first on the computational domain provided by the FEM mesh. At a second stage, the MLPG problem is solved; in this case it is required that the integration for the computation of the $\mathbf{K}_{FM}$ block (and that of $\mathbf{K}_{ML}$ in the fully coupled enrichment) be done with respect to the actual domain Ω. That is, the second solution field has to be solved over a domain that accurately[11] represents the actual geometry. Indeed, as already highlighted in the "Critical Assessment", the solution field $\mathbf{u}_{FE}$, as provided by FEM, can be *any* continuous function. It will affect the accuracy obtained with a given number of particles, but not the ultimate ability of the method to converge to the right solution field.

A convergence graph is here reported to give numerical evidence; here $\mathbf{K}_{ML}$ and $\mathbf{K}_{FM}$ are calculated on the FEM geometry and on the actual geometry, for comparison, for the coarser FEM mesh.

[11] with respect to the number of nodes used

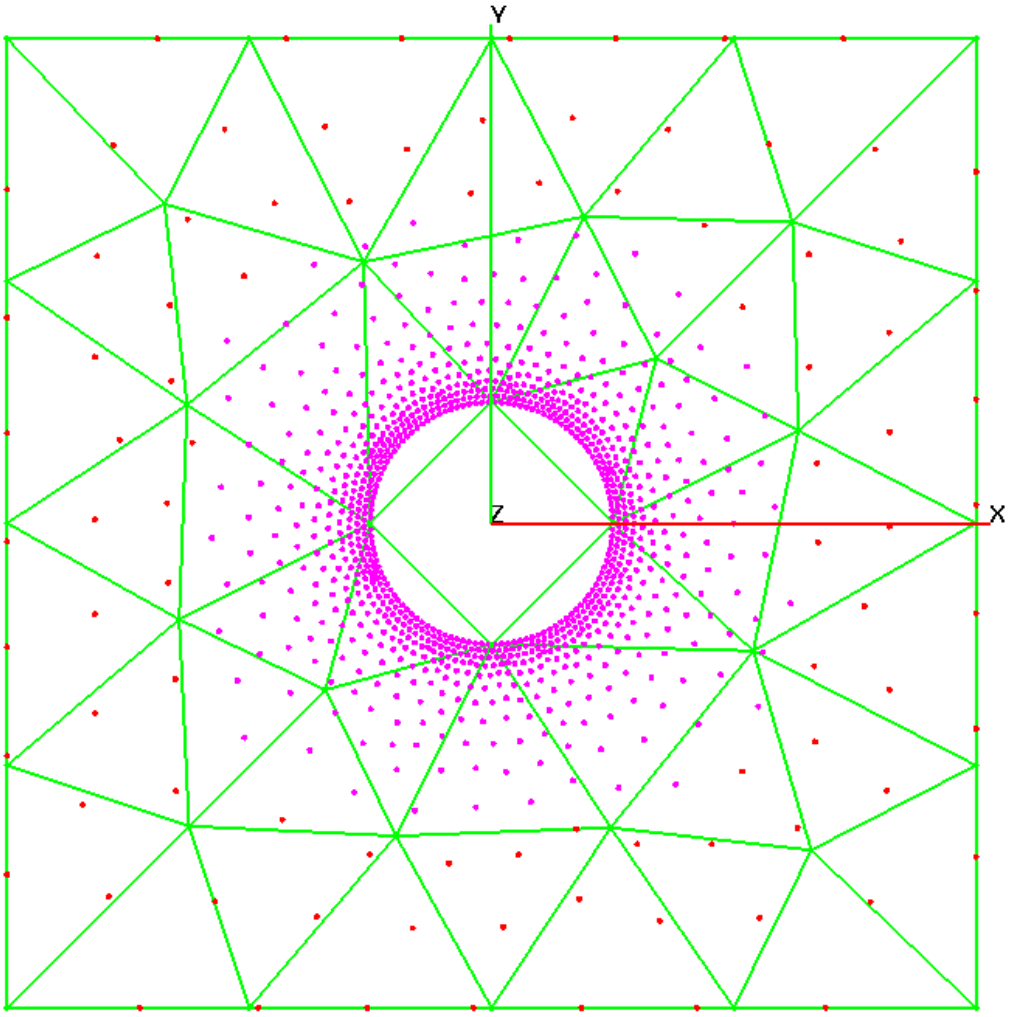

FIGURE 4.26: Note how the computational domain Ω_{comp}, for FEM, differs from the actual domain Ω (here in the local enrichment)

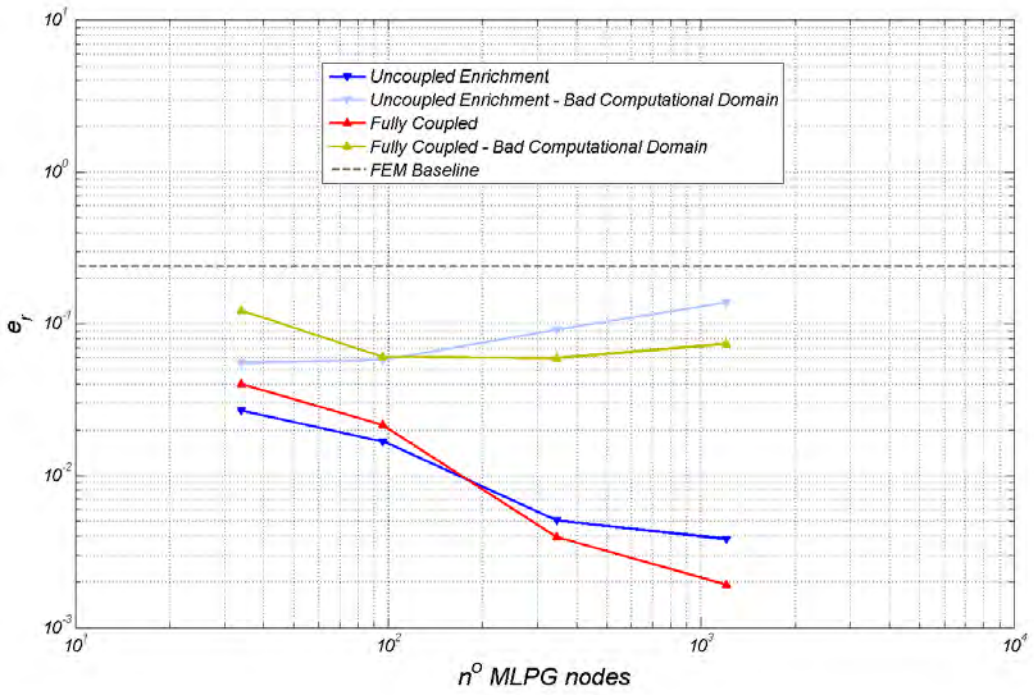

FIGURE 4.27: Comparison of the convergence graph for displacement **u** for the coarser FE mesh

4.9 Future Development

The topic discussed in the present Thesis appears to have a number of promising points that are to be analyzed in future works. Among them, we can mention:

- a performance analysis that take into account the actual computational cost of the enrichment
- the definition of some criterion regarding the selection of the shape functions and test functions radii in the enrichment
- the usefulness and performance of the enrichment with locking phenomena
- a detailed analysis of the quadrature rules for good results with the proposed strategy
- the performance of the enrichment where a singularity (e.g. a notch) exists
- the feasibility of a simpler quadrature scheme in the coupling block for a wider variety of situations.
- the accuracy and performance of a one way "nested" uncoupled enrichment, which should retain the MLPG full potential in the prediction of the stress, at a fraction of the cost of a fully coupled enrichment.

Chapter 5

Conclusion

The previous chapter has assessed numerically the quality of the proposed enrichment, in Elastostatics.
While it is well know that the performance of the MLPG scheme is highly dependent on some user specified parameters, in this Thesis such a "fine-tuning" of the model has been avoided, focusing on the potential of the enrichment. Rather, the aim here was to discuss a working method, that requires the minimum level of intervention by the user.
Both the uncoupled and the fully coupled enrichment have been investigated in a numerical experiment, which may also represent a case of interest, and their results are summarized in Figures 5.1, 5.2, 5.3.

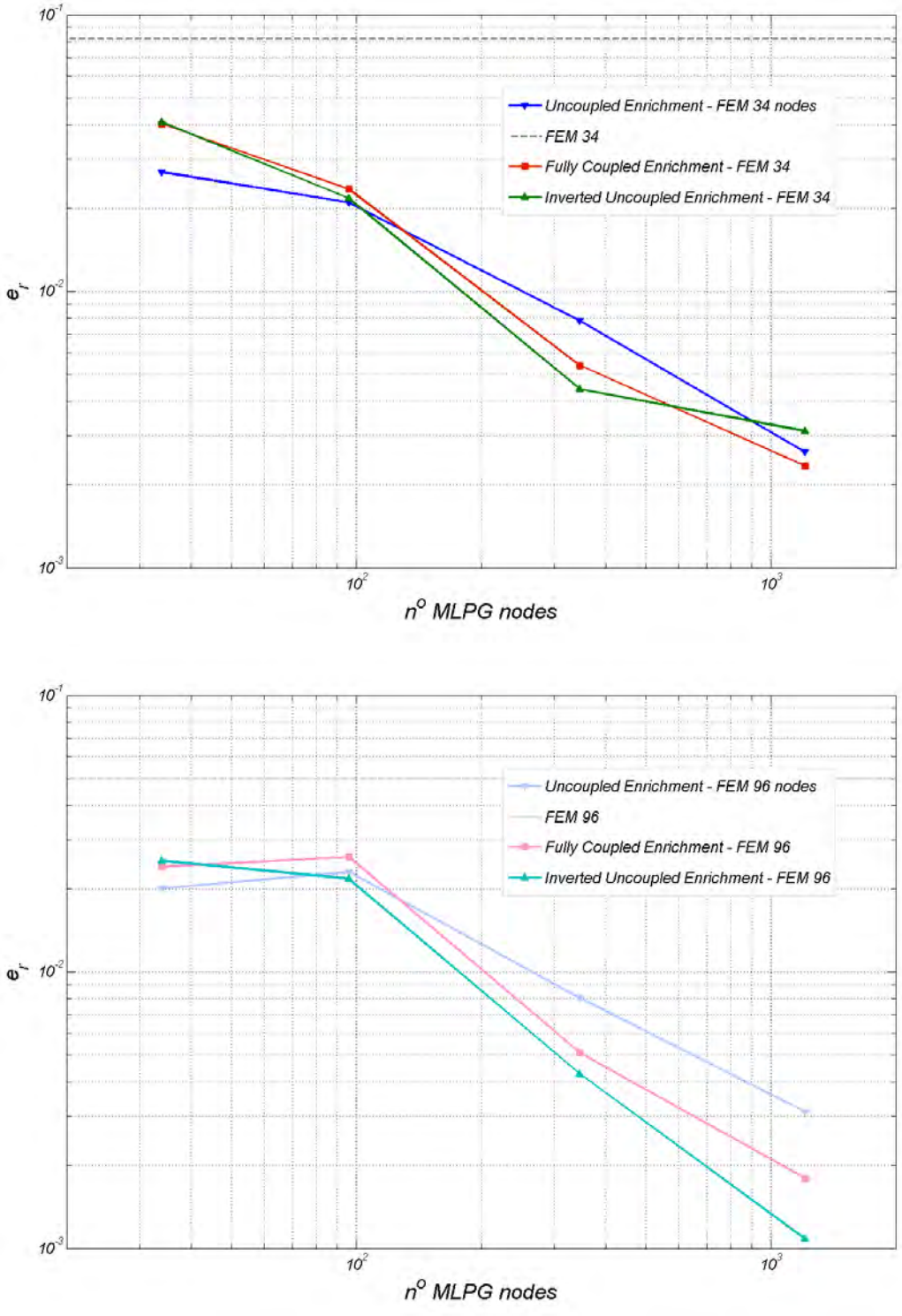

FIGURE 5.1: Comparison of the convergence graph for displacement **u** for the coarser and finer FE mesh

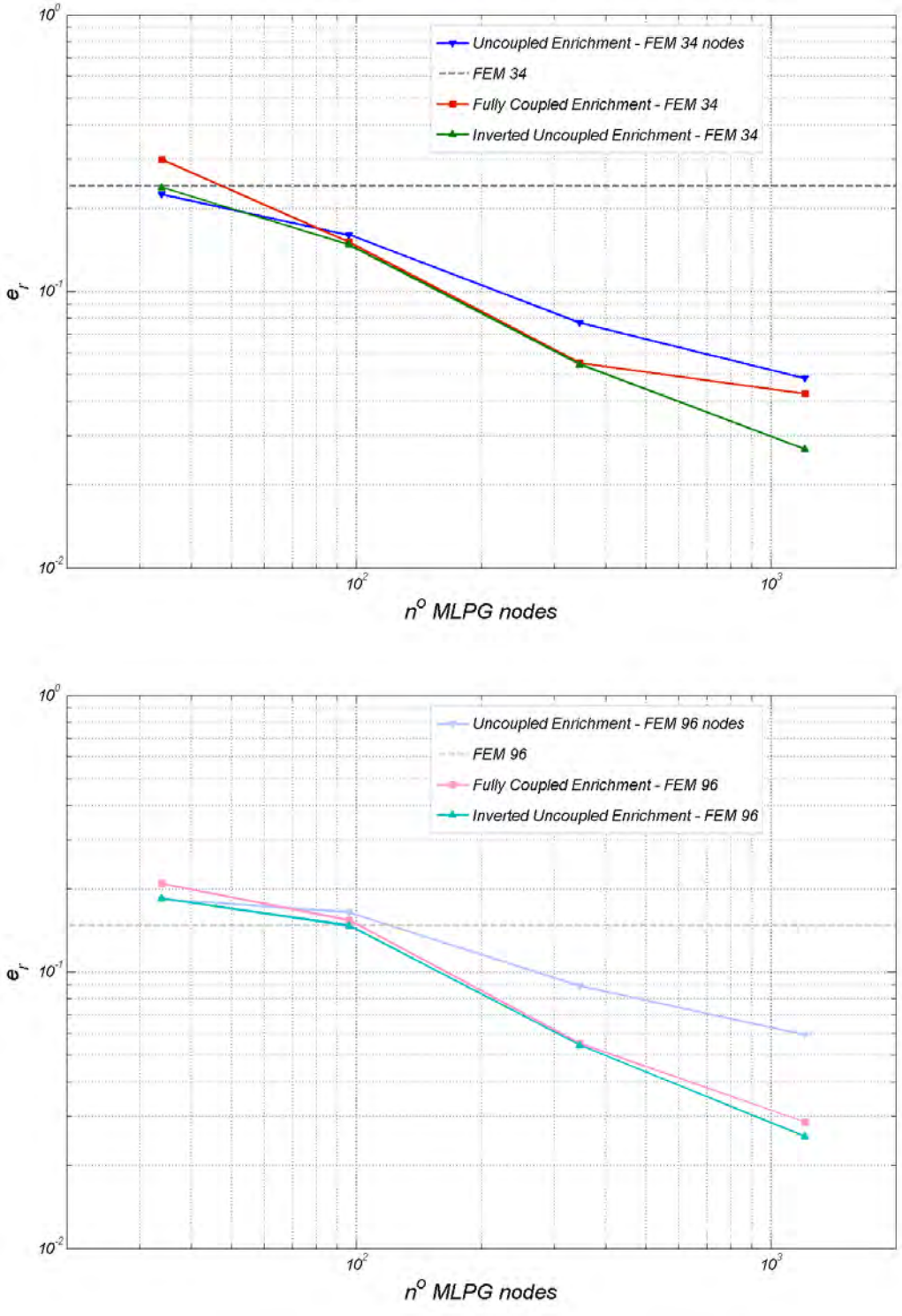

FIGURE 5.2: Comparison of the convergence graph for stress $\boldsymbol{\sigma}$ for the coarser and finer FE mesh

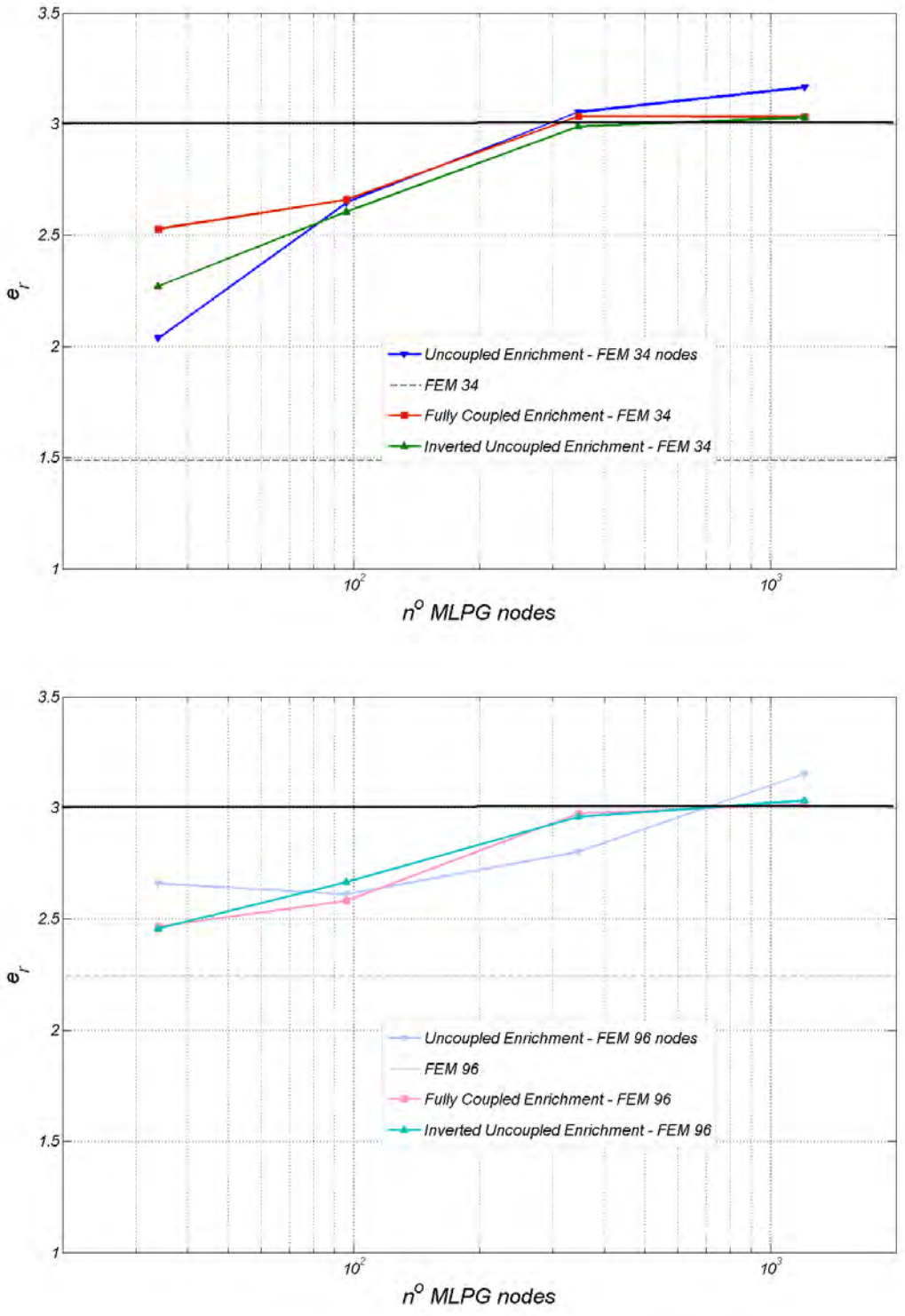

FIGURE 5.3: Comparison of the predicted peak stress $\boldsymbol{\sigma}_{xx}^{peak}$ for the coarser and finer FE mesh

The uncoupled enrichment is found to be a relatively inexpensive way to improve the accuracy of the displacement field $\mathbf{u}^h$ when needed. The MLPG nodes need not be placed on any particular way; on the contrary, even when the same pattern of nodes of the FEM is adopted, the enhancement is substantial. The uncoupled enrichment is capable of delivering an improvement comparable to that of a fully coupled approach, but at a fraction of the cost. Additionally, the computation of the entries in the coupling block $\mathbf{K}_{ML}$ was found to be not too sensitive to the integration scheme.

The stress field $\boldsymbol{\sigma}^h$ can suffer from the initial, non-smooth solution field, as supplied by linear FEM. Hence, this approach may deliver spurious stress peaks across element edges, that may only be partially compensated by adding more particles. If the stress $\boldsymbol{\sigma}$ is of main concern, the use of a fully coupled approach is recommended.

The fully coupled enrichment has proven to be a more robust approach for a general improvement of both the solution field along with its derived quantities, in Elastostatics. Moreover, the peak stress is accurately predicted.

The poor discretization of the actual domain, as operated by the FEM, which is reflected in the entries of the FEM stiffness matrix, need not be modified when adding particles. This ultimately simplifies the implementation of an enriching procedure, when the actual geometry is not well represented by the FEM discretized domain. Further, a quadrature rule that simply disregard those sample points outside the actual domain Ω, when making the entries for $\mathbf{K}_{MF}$ and $\mathbf{K}_{FM}$, is found to deliver satisfactory results. Despite these approximations, the enrichment appears not to be affected by such limitations.

On the contrary, the effect of a simpler integration scheme should be avoided if at all possible, since a working strategy has already been presented in this Thesis. This is especially true in the case of a fully coupled enrichment, which involves the computation of the $\mathbf{K}_{MF}$ matrix.

A second type of uncoupled enrichment, which solves the meshless problem first, has been investigated. Such a method enhances both the displacement field and the stress field. However, the need for a global enriched area $\Omega_{enr} = \Omega$ limits the range of its practical applicability.

Finally, the effect of a local enrichment has been investigated. It has been shown how a local enrichment may not converge to the right solution. However, a local effect, such as a steep gradient of stress, may be accurately resolved by such a local refinement. A simpler approach for a local, uncoupled enrichment is left as

a future work.
In short, the uncoupled enrichment appears to be well suited for those situations that need to have the displacement field enhanced quickly and inexpensively. The fully coupled enrichment, conversely, is a more reliable technique for improving the prediction of the derived quantities, i.e., stress. A local enrichment, whichever its nature, may fail to improve the displacement field everywhere, because of the nature of the elliptic PDEs of Elastostatics. On the contrary, very satisfactory results have been obtained by a local enrichment in the prediction of the local stress field and of the peak stress.

In essence, the present method appears to possess a great potential for improving an existing FE solution, with no remeshing cost, especially in those problems with a local, steep gradient of stress.

Bibliography

[1] Antonio Huerta and Sonia Fernandez-Mendez, *Enrichment and coupling of the finite element and meshless methods*, 1999

[2] Andrew Nealen, *An As-Short-As-Possible Introduction to the Least Squares, Weighted Least Squares and Moving Least Squares Methods for Scattered Data Approximation and Interpolation*

[3] N.Sukumar, J.Dolbow, A.Devan, J.Yvonnet, F.Chinesta D. Ryckelynck, P. Lorong I. Alfaro, M. A. Martinez E. Cueto, M. Doblare', *Meshless Methods and Partition of Unity Finite Elements*, 2005

[4] Michael Metcalf, Malcolm Cohen *Modern Fortran Explained*, 2011

[5] Elbridge Z. Stowell *Stress and strain concentration at a circular hole in an infinite plate*, 1950

[6] G. H. Paulino, I. F. M. Menezes, J. B. Cavalcante Neto, L. F. Martha *A methodology for adaptive finite element analysis: Towards an integrated computational environment*, 1999

[7] Satya N. Atluri, Shengping Shen, *The Basis of Meshless Domain Discretization: The Meshless Local Petrov Galerkin (MLPG) Method*, 2003

[8] S. N. Atluri, T.-L. Zhu, *The meshless local Petrov-Galerkin (MLPG) approach for solving problems in elasto-statics*, 2003

[9] Robert Schaback, *Why does MLPG work?*, 2006

[10] T. Belytschko, D. Organ, Y. Krongauz, *A coupled finite element-element-free Galerkin method*, 1995

[11] G. R. Liu and Y. T. Gu, *Meshless Local Petrov-Galerkin (MLPG) method in combination with finite element and boundary element approaches*, 2000

[12] E. Stagnaro, *Geometria*, 2002

[13] Salsa, Vegni, Zaretti, Zunino *A Primer on PDEs*, 2012

[14] Jonson, *Numerical Methods for Partial Differential Equations*, 2009

[15] A. Adams, *Calcolo Differenziale 2*, 2003

[16] S. N. Atluri, T. Zhu, *A new Meshless Local Petrov-Galerkin (MLPG) approach in computational mechanics*, 1999

[17] S. N. Atluri, H.-G. Kim, J. Y. Cho, *A critical assessment of the truly Meshless Local Petrov-Galerkin (MLPG), and Local Boundary Integral Equation (LBIE) methods*, 1999

[18] G. Gambolati, *Metodi Numerici per l'Ingegneria*, 2003